Toward High Data Rate CubeSat Telecommunication

by

Nicholas Hansen

Submitted in partial fulfilment of the requirements
for the degree of Master of Applied Science

at

Dalhousie University
Halifax, Nova Scotia
November 2019

Dedicated to my parents

For giving me a heart and a brain

And teaching me to use both

Table of Contents

List of Tables

List of Figures

Abstract

This thesis contains the analysis and design for high-performance digital telecommunication sub-systems for use in small low earth orbit satellites. Additional details are given concerning Dalhousie University's first CubeSat, LORIS. To further high-performance satellite communications this paper provides analysis of the low earth orbital motion of the satellite and the effect on the channel capacity. It is found that the channel capacity is time varying and to utilize this resource fully a dynamic and adaptive modulation coding scheme must be employed. Additionally, several designs for CubeSat S-band rectangular patch antenna arrays are presented and evaluated. It is found that polarization loss can be mitigated by 90% by using a sequentially rotated feed network to achieve polarization diversity. Various other topics are covered which provide a practical look into CubeSat design considerations and background on radio system design. The radio link budget is described, and a working example is given. It is also found that high performance direct conversion architecture radios are commercially available and could be leveraged in S-band systems at a low cost.

List of Abbreviations and Symbols Used

AC – Alternating Current

AWGN – Additive White Gaussian Noise

COTS – Commercial off the shelf

CP – Circular polarization

ε_r – Relative permittivity

E_b/N_0 – Bit energy to noise power spectral density ratio

EM – Electromagnetic

FEC – Forward Error Correction

GMSK – Gaussian Minimum Shift Keying

GFSK – Gaussian Frequency Shift Keying

IEEE - Institute of Electrical and Electronics Engineers

ISM – Industrial Scientific Medical

ITU – International Telecommunication Union

ISS – International Space Station

IF – Intermediate Frequency

LO – Local Oscillator

LORA – Long Range

LORIS – Low Earth Orbit Reconnaissance and Imaging Satellite

LHCP – Left hand circular polarization

LEO – Low Earth Orbit

LOS – Line of Sight

MCS – Modulation Coding Scheme

MSK – Minimum Shift Keying

OBC – Onboard computer

OS – Operating system

OOK – On Off Keying

PSRF – Partial Sequentially Rotated Feed

PLL – Phase Locked Loop

RF – Radio Frequency

RHCP – Right hand circular polarization

STK – Satellite Tool Kit

SNR – Signal to Noise Ratio

SRF – Sequentially Rotated Feed

UHF – Ultra High Frequency

VHF – Very High Frequency

VSWR – Voltage Standing Wave Ratio

Acknowledgements

First and foremost, I thank God for showing mercy and grace to me in my life. I also would like to thank my family for their unending encouragement and support. I thank my parents for pushing me and encouraging me to pursue higher education, and for their steady and unwavering belief in my ability. I thank my wife for her joyful companionship during my graduate level education. I am also grateful to the members of my committee for their helpful advice and availability to make this possible. Specifically, I thank my supervisor Dr. Zhizhang Chen for giving me this opportunity and working with me to make it reality. I would like to thank the ECE department administrators for their tremendous kindness and patience. I would like to thank our graduate advisor Dr. Dmitry Trukhachev for his excellent knowledgeable advice and teaching. I would like to thank my fellow graduate students for their help, feedback, and friendship. Each of your involvements in my life has made it a fuller, better experience and it is only by your many supportive influences that I have been able to reach this point.

Chapter 1.0 Introduction

In the mid 1990s the first containerized micro-satellite was designed by a student team from Stanford University [1]. This could be considered to be the first instance of a Cube Satellite (CubeSat) mission. This type of small satellite has rapidly become a popular platform for LEO research, earth observation, and telecommunication. Several satellite launch providers have adopted the Cube Satellite standard, making CubeSats cheaper and encouraging the market to offer standard off-the-shelf components compatible to this shape. Since year 2000 nearly 1000 CubeSat missions conducted and <90% are 3U or less [2]. Figure 1 shows the size and dimensions of this type of satellite.

Figure 1 - CubeSat Dimensions [3]

Because of the constraints of having small surface area and volume, these satellites have typically adopted mission objectives which require little power. A small surface area limits the amount of harvestable solar power and launch providers may impose limits on the battery capacity due to safety regulations [4]. In the realm of digital RF communications, power is directly linked to bit energy to noise power spectral density ratio (E_b/N_0) and consequently the achievable bit rate. A survey by [5] reports that 75% of CubeSats prior to 2010 achieved a typical bit rate of 9600 baud or less. However, many CubeSats can generate much more data from their scientific payload and would be severely limited by such a low bit rate [6]. Therefore, the design of an affordable, efficient and capable RF communication system would enhance the scientific value of small satellite research missions.

The practical motivation of this work was an opportunity to build and operate a 2U CubeSat. The opportunity came from the Canadian CubeSat Project, announced by the CSA in 2017. As part of the team at Dalhousie University, I facilitated the design and implementation of the satellite as technical lead on the RF communication subsystem. The field of digital satellite communications is technologically mature but low-cost solutions are inherently uncommon in the aerospace industry. CubeSat equipment vendors stand to profit from the sale of their solutions, making this option is unrealistic for many projects, including ours. In addition, aerospace is tightly regulated on a number of fronts, including telecommunications regulations and material safety regulations to avoid mission risk for the launch shuttle or the satellite itself. Large satellites are not suitable for first time technological demonstration nor applications with short duration. Small missions mitigate some of the issue because less complexity and fewer components shortens the design, analysis, and testing of the spacecraft. Thus, the goal of CubeSat projects in general is to produce a disposable satellite at lower cost and shorter project

timeline compared to regular satellites. For telecommunications, this goal can be achieved by adapting terrestrial radio equipment for use in space, and by employing techniques to improve performance without necessarily driving up cost, size, and complexity. In order to facilitate an orderly discussion, the outline of the paper is now presented.

Before discussing the satellite design, the general problem of establishing radio link with a LEO satellite is described in Chapter 2. The name of Dalhousie's first satellite is LORIS (Low Orbit Reconnaissance and Imaging Satellite), and its purpose and goals are discussed in Chapter 3. The RF system design for the LORIS is described in Chapter 4. Finally, in Chapter 5, I consider the analysis and design and verification of antennas for high performance S band CubeSat radio systems. To improve readability some equations appear in a larger font size where necessary.

Chapter 2.0 Radio Link Conditions

In this section we approach the design of CubeSats by methodically considering the general conditions for telecommunication that we may encounter. Line of sight between a ground station and a satellite is typically required for radio link to be established. In some cases, even LOS can be insufficient, however LOS analysis can at least provide an upper bound on total communication time. Based on a line of sight condition in open space we can assume an AWGN channel. Depending on the orbital motion of the satellite and the geographic location of the ground station(s) LOS time[1] may vary. An orbit can be characterized by the inclination and period. Orbital inclination is the angle between the orbital plane and the equatorial plane depicted in Figure 2 [7].

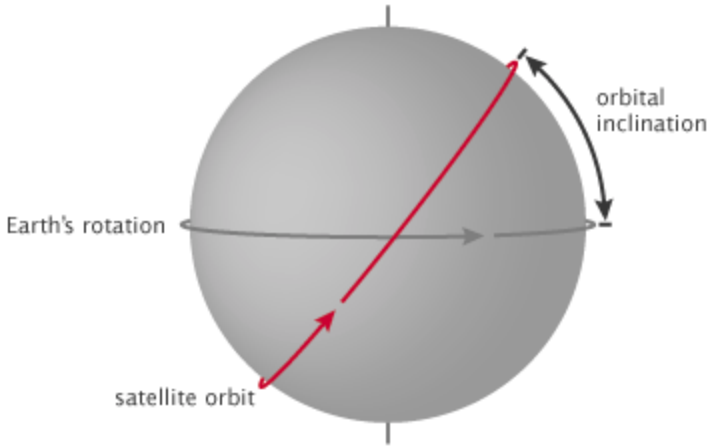

Figure 2 - Depiction of Orbital Plane

Orbital period is the length of time it takes for the satellite to travel around the earth once. By limiting ourselves to those orbits with inclination 0^{o}-90^{o} and with period less than 128 minutes, we may now examine three types of LEO for comparison: polar orbit, inclined orbit, and

[1] "LOS time" and "Radio link time" are used to mean "amount of time with line of sight between the satellite and ground station" and the same for radio link.

equatorial orbit. Most LEO CubeSats purposed for research and communication will have orbital dynamics within this range. In the case of retrograde LEO orbits the conditions for communication would mirror this analysis. Figure 3 shows the characteristics of these orbits.

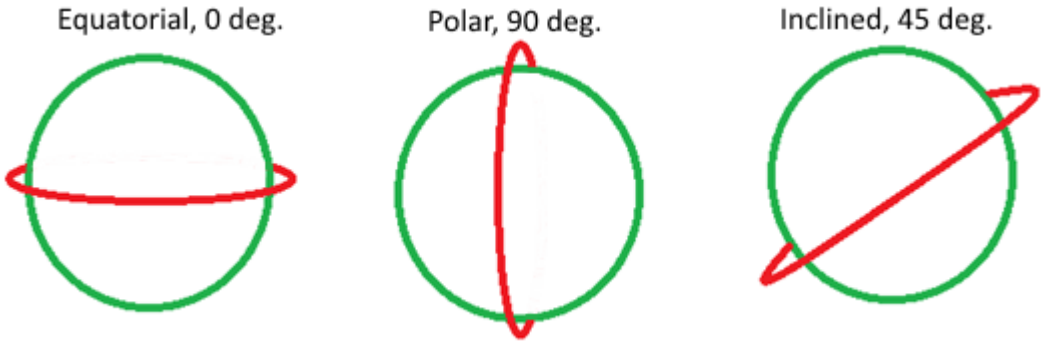

Figure 3 - Orbits of Varying Inclination

2.1 LOS Time

With three ground stations placed at 0, 45, and 90 latitude the LOS access time per day is computed for three satellites at the inclinations described in Figure 3. Although the earth is an irregularly shaped geoid a spheroidal approximation is typically used for modelling. WGS 84 is the most accepted global geodetic reference system [8]. Analytical Graphics Inc. makes their STK software available online and it can perform LOS access analysis using the WGS 84 earth model. The daily average in [minutes / day] given by this software are compared to values from a VBA application produced by Maarten Meerman Astro-Training in Table 1.

Units are min/day	Groundstation 90º latitude	Groundstation 45º latitude	Groundstation 0º latitude
Polar Orbit STK	144.6	31.6	21.8
Inclined Orbit STK	0	50.2	33.3
Equatorial Orbit STK	0	0	148.8
Polar Orbit MM	155.5	36	22.5
Inclined Orbit MM	0	58.5	35
Equatorial Orbit MM	0	0	154.5

Table 1 - Comparison of LOS Estimates

A few observations can be made on the LOS analysis made using these two programs.

- If the inclination of the satellite orbit is less than the latitude of the ground station, no communications will be possible.
- When the inclination of the satellite orbit is similar in magnitude to the latitude of the ground station, more communications windows will be available.

- The two simulations used give estimates within 15% of each other.

In general, the orbit of the satellite and the placement of the ground station are not very flexible parameters for a CubeSat mission. A CubeSat is usually secondary payload to some other more important mission, making it cheaper to put them in orbit but restricting the ability to be selective about the orbit. Ground stations for CubeSats will typically be placed near or in cities, where it is convenient to operate and maintain the equipment. Cities are usually not located at extreme latitude. Because of these reasons most CubeSat missions will have LOS time nearing 40 minutes per day for a single ground station and single satellite. This is a relatively small amount of time, so taking the step to multiple ground stations or multiple satellites is a natural one for missions requiring high data throughput. Transferring large amounts of data from low earth orbit is inherently impeded because of the orbital motion of the satellite. Obviously, it is preferable to determine precise LOS access time using STK, but the 40-60 minute LOS rule of thumb given is useful for building intuition and approaching the RF system design.

2.1.1 Case Study: Halifax and ISS

LORIS is anticipated to be deployed from the ISS, giving the satellite a very similar orbit. Since there are ISS resupply shuttles every quarter year, this would be a common type of orbit for a CubeSat. The orbital period is 92 minutes, making 15.5 trips around the earth per day at a speed of 7.7 [km/s]. The altitude is on average 410km above the surface of the earth. Each orbit shifts to the west by approximately 22.9^{o} of longitude. [9] Each day the ground track shifts only 6^{o}, thus the weekly average is fairly constant. Based on MM and STK analysis, Halifax and LORIS will have approximately 1 hour of LOS time each day. In section 2.5 we will deal with the question of "How much of this LOS time is practically usable for radio link time?" Figure 4 and

5 show the graphical interface of AGI STK software and Maarten Meerman Astro Training software to help visualize the situation.

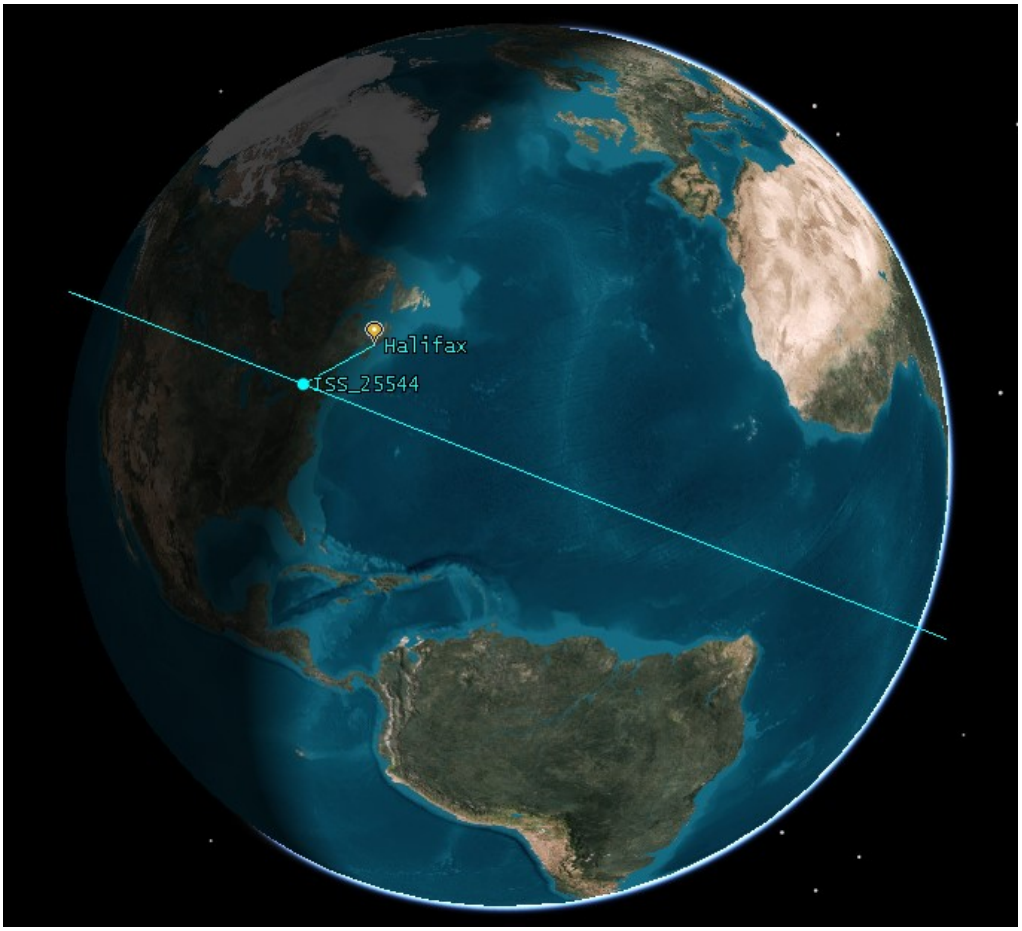

Figure 4 - AGI STK Graphical View of Earth in the Window of the Application

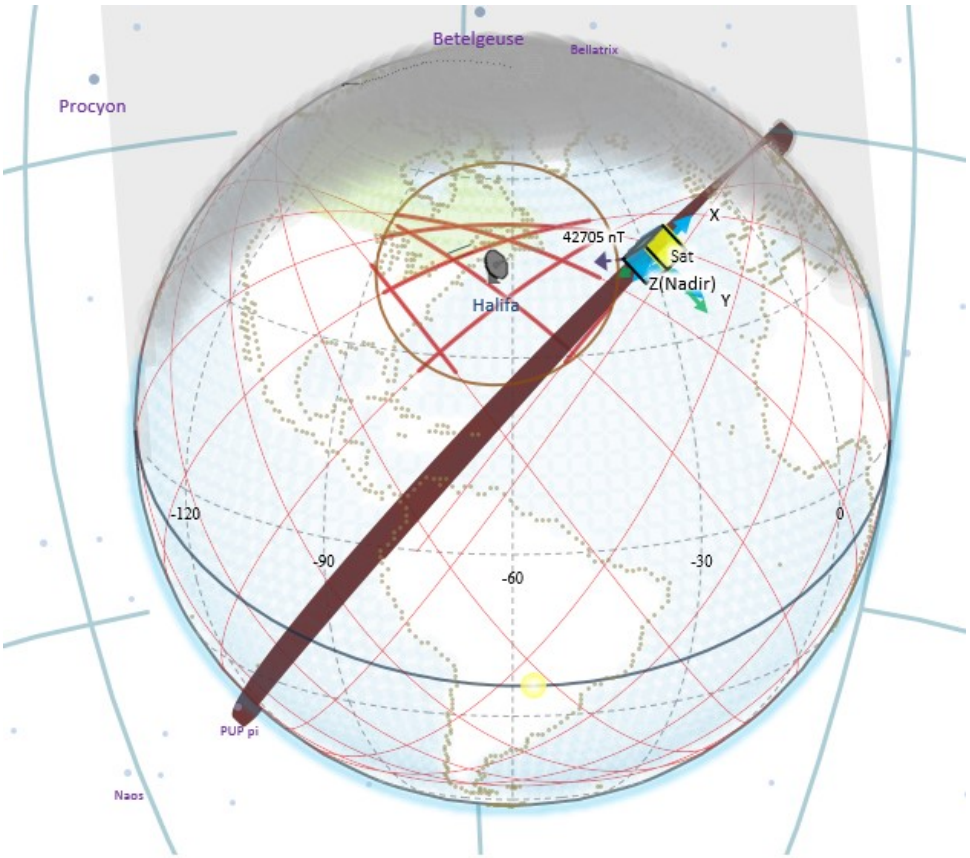

Figure 5 - MMAT Graphical View of Earth in the Window of the Application

2.2 Doppler Shift

Due to the high speed of the satellite relative to the receiver on the ground there is a significant doppler shift. Doppler shift varies the uplink and downlink frequencies during satellite pass. You have probably experienced doppler shift when being passed by an ambulance or firetruck with the siren on. The same effect causes a shift in the center frequency of the transmission from the satellite. While the satellite is approaching the ground station, the frequencies will be higher than the designed center frequency. After the satellite reaches halfway through a pass it will be moving away from the ground station and the frequencies will be lower than normal. Doppler shifts are well understood and can be corrected if the antenna and transceiver are sufficiently

wideband and therefore can send and receive signals over higher and lower frequencies. Either the ground station or satellite can compensate for the doppler shift, but it simpler to do compensation at the ground station. Where no automatic means are available, a tunable radio can even be manually adjusted during the satellite pass. Amateur radio operators contact the astronauts living on the ISS on a semi-regular basis and use this method to maintain communication while the ISS travels in its orbit. Doppler shift for RF can be calculated using equation (1) for the relevant frequency.

$$f_r = f_t \left(\frac{c+v}{c-v}\right); \tag{1}$$

For the roughly approximate geometry of a satellite moving directly toward the receiver at 7.7 [km/s] transmitting at 436 MHz, the doppler shift is ±11 KHz. This is the maximum doppler possible since the radial velocity of the satellite is always less. The satellite is never travelling directly toward the receiver so the radial velocity relative to the receiver is always multiplied by cos(θ) where θ is the angle between the direction of the transmitted signal and the direction of flight of the satellite. The shape of the doppler shift function can be seen in Figure 6. Doppler shift can not be calculated with the free license of AGI STK, which would account for differences caused by the curvature of the earth and the true relative motion of the satellite and ground station. The use of feedback control for frequency locking can mitigate the issue of doppler shifted signals. For example, the Costas loop as a type of phase locked loop can recover a doppler shifted carrier.

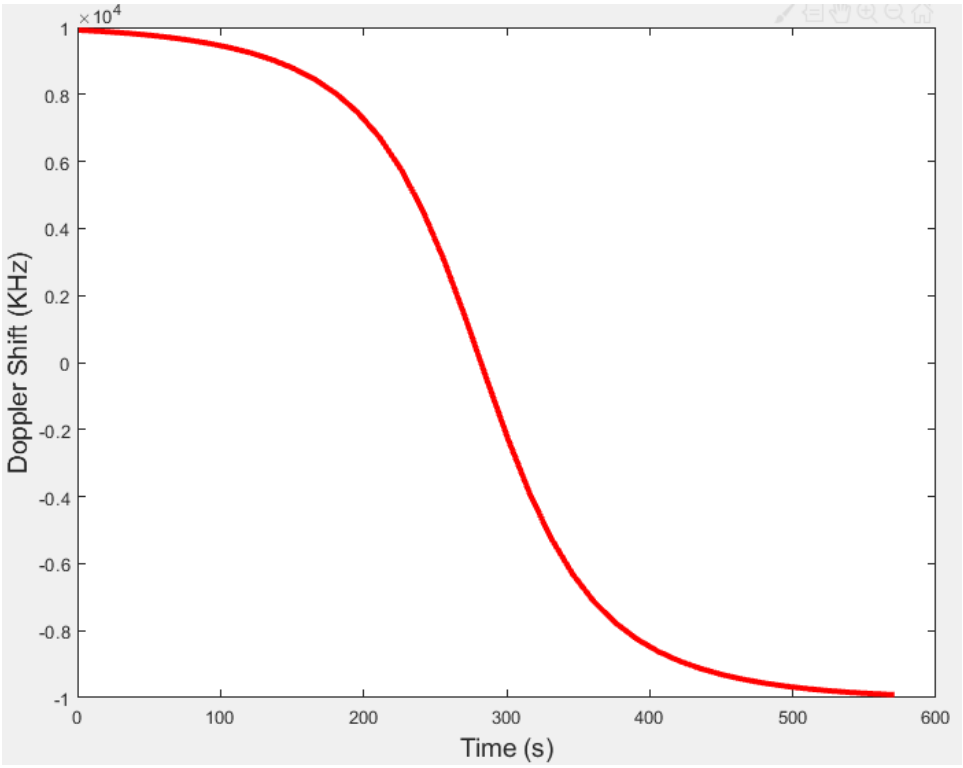

Figure 6 - Doppler Shift of a VHF LEO Satellite

2.3 Free Space Loss or Spreading Loss

Radio waves propagate at the speed of light in vacuum, and in the absence of obstacles travel in straight lines. In the near field the effect of the antenna radiation pattern is dominant, but in the far field the energy may be approximated as a plane wave [25]. As we travel farther from the source, the plane wave approximation becomes more valid and the RF energy is spread more thinly. This spreading loss is usually called free space loss[2] and is inherent to RF wave propagation. The effects of other disturbances such as attenuation due to atmosphere are not included by this function but can be modeled later in the link budget.

[2] "Free space loss" could be considered a misnomer since the loss is from the geometrical spreading of energy, not attenuation of the wave caused by the medium.

Free Space Loss is given by equation (2).

$$FSL_{dB} = 32.45 + 20\log_{10}(D_{km}) + 20\log_{10}(F_{MHz}); \quad (2)$$

The point to point distance between a LEO satellite and a ground station is constantly changing due to the orbital motion of the satellite. Figure 7 shows a simple diagram of the situation, where the satellite is moving left, and the slant range is decreasing while the elevation angle is increasing. When the satellite is on the horizon, it is at maximum range. When the satellite is directly overhead, it is at minimum range.

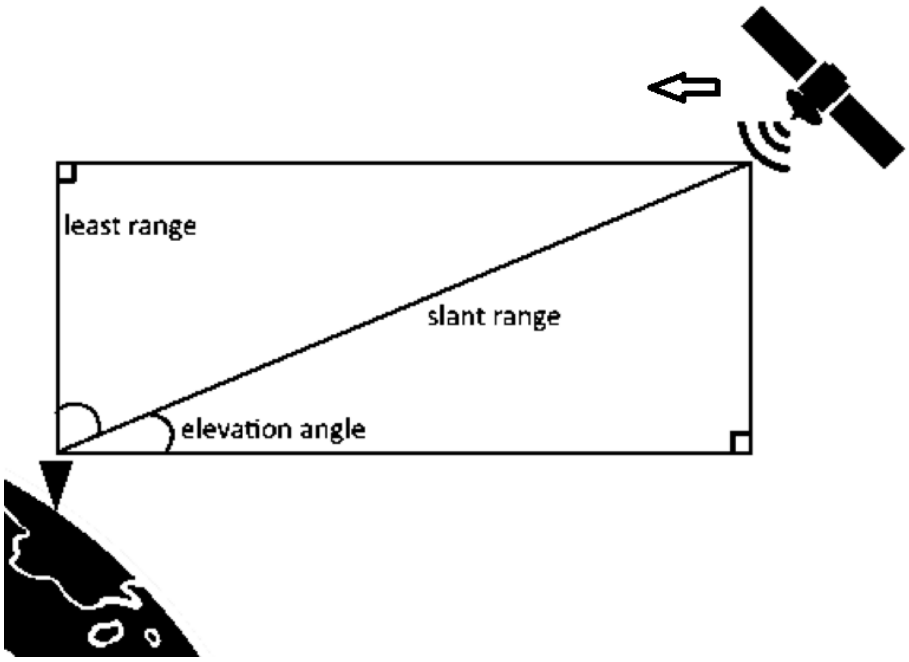

Figure 7 - Simple diagram of slant range

The change in the slant range can be seen for a LEO overhead satellite pass in Figure 8. The effect on the FSL can be seen in Figure 9.

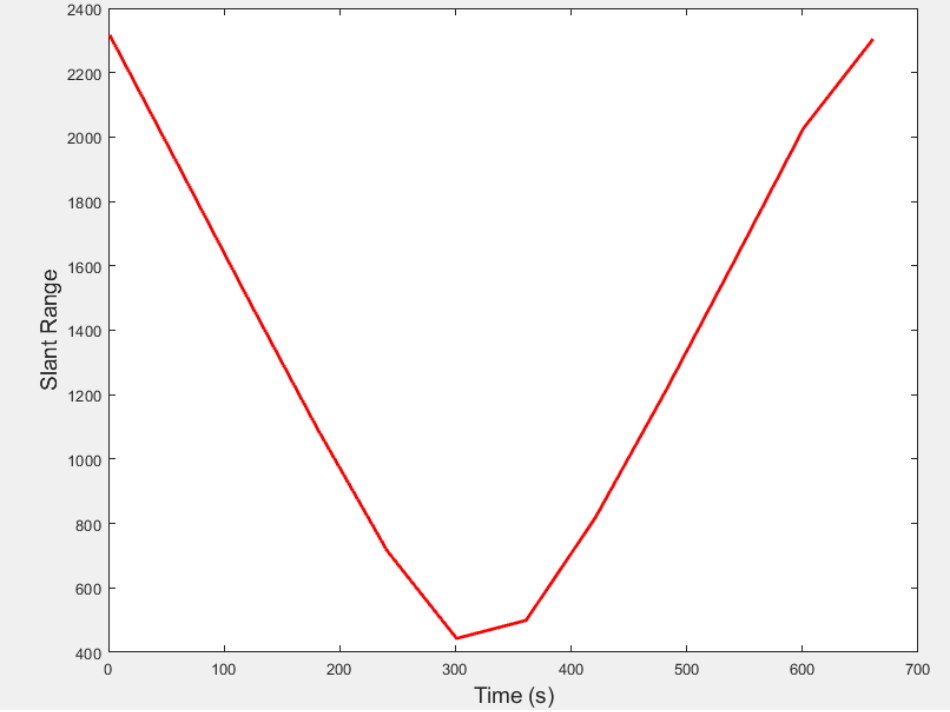

Figure 8 - LEO Slant Range (km) over Time

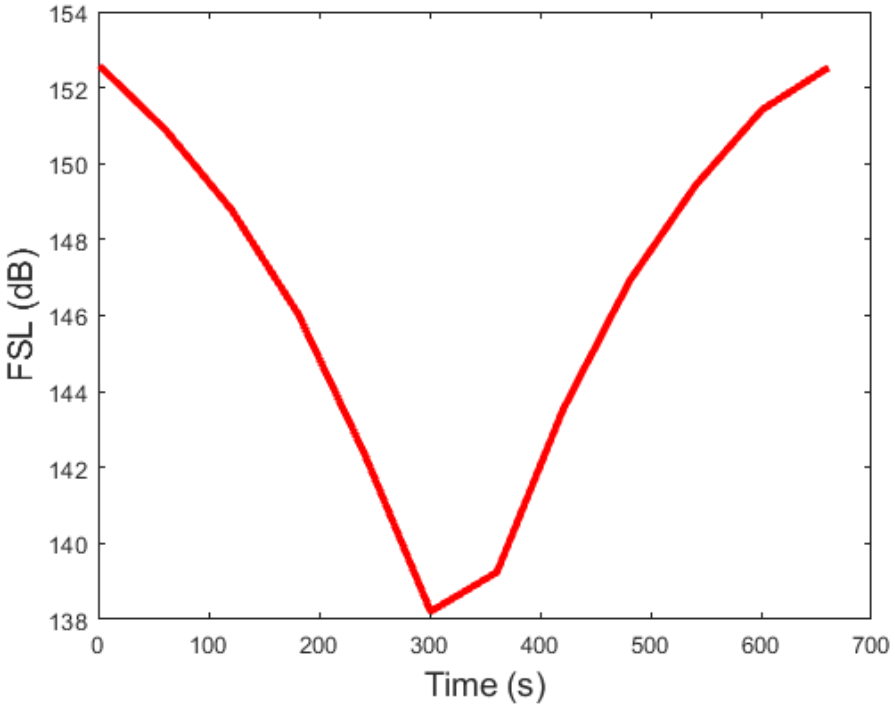

Figure 9 - FSL of LEO Satellite over time

A good rule of thumb to keep in mind is that each 200-300 Km results in nearly 3db (half) power loss, and each increase in 200-300 MHz results in 3db power loss, shown in Table 2.

Distance Frequency	500 km	710 km	1000 km	1300 km
430 MHz	139 dB	142 dB	145 dB	147.3 dB
610 MHz	142 dB	145 dB	148 dB	150.4 dB
860 MHz	145 dB	148 dB	151 dB	153.3 dB
2400 MHz	154 dB	157 dB	160 dB	162.3 dB
3400 MHz	157 dB	160 dB	163 dB	165.4 dB

Table 2 - Tabulation of the 3dB FSL per 200 Approximation

2.4 Link Budget

Link budget analysis uses the physical model to predict hypothetical system performance. Key parameters are transmitted power, antenna gain, and system noise. Any amount of impairments may be modeled in the link budget and a common practice is to over engineer the system by adding a performance margin in proportion to the expected impairment. This can account for equipment degradation over time and occasional extreme weather events, thus minimizing communication outages. The link budget informs telecommunication system designers on system behaviour quickly and without experimental cost. A link budget can be used as a requirements engineering tool to determine what system performance is needed for a given situation, or as a system design tool to evaluate the viability of certain hardware. Link budgets use decibels to allow simple tabular addition and subtraction. This originates from the need to perform calculations by hand quickly and without error, possibly on a survey trip or construction site. The link budget is most practical for situations where both ends of the link are stationary, and this is where the method originates. Terrestrial point to point radio links are the prime example of a

static radio link, but these also exist in satellite communications. For example, meteorological satellites often occupy a geostationary orbit. A typical geostationary orbit has an altitude near 35 784 km and the astronomical position of the satellite, from a ground station, is unchanging [10]. Thus, only minor antenna tracking and pointing would be required. However, supposing such a satellite transmitted 50W from a dipole antenna and the signal is received directly below the satellite. Receiving with another dipole antenna 20,000 km away, at 1.5 GHz, the receive power becomes very small. Using the Friis Transmission equation (3) the received power can be calculated for a receiver with the same dipole antenna [11].

$$P_R = \frac{P_T G_T G_R \lambda^2}{(4\pi R)^2}; \tag{3}$$

With the parameters described the formula yields 1.26e-16 or 0.000000000000000126. Clearly, because of the great distance involved, the satellite signal is weakly received and consequently the potential data rate is low. The low earth orbit presents several advantages and one significant disadvantage compared to geostationary orbit. Advantages include less latency and much less free space attenuation, while the main disadvantage is that the satellite is always in fast motion compared to the ground station [10]. As a result, high gain antennas must utilize azimuth and elevation (AZ/EL) tracking systems and the ground station complexity and cost are increased. In addition, any obstructions such as tall buildings, hills, and trees may impede the radio link, although the same may be said for radio links with geostationary satellites. Latency is given by equation (4) which is the round-trip time plus any overhead processing time (C) introduced by the communication hardware. If the end user is communicating through a complex network with many hops, interacting with several datacenters, the value of C becomes dominant.

$$L = 2d/v + C; \tag{4}$$

The speed of radio waves in vacuum is equal to the velocity of light, however within atmosphere the speed is nominally less at 299,750 [km/s]. For a satellite in LEO latency is two orders of magnitude less than a satellite in GSO. If automatic repeat request (ARQ) type data transfer protocol is employed the latency can have a significant negative impact on overall throughput, especially if the radio link experiences fading or unrecoverable bit errors. In the event of a lost packet a satellite in LEO could retransmit 100 times sooner than a satellite in GSO. For the reasons discussed the upcoming Starlink constellation from SpaceX providing global low latency broadband internet occupies an operational altitude of 550 km [12]. More importantly, the number of hops in the network must be kept to a minimum for low latency to be possible.

The RF link budget for the LORIS project is presented in the following section. Equations for this section are also presented in figure 10 so that they may be run directly in MATLAB (2018b). Values of the variables must be defined before running these computations. Beginning with input parameters of slant range equal to 1000 km (corresponding to 20º elevation angle) and a frequency of 438 MHz, the free space loss is computed with equation 5 as 145.28dB.

$$FSL_{dB} = 32.45 + 20\log_{10} D_{km} + 20\log_{10} F_{MHz}; \quad (5)$$

Assuming the satellite is capable of 2W transmit power using a dipole antenna with 2 dB of gain, and line loss of 1 dB the Effective Isotropic Radiated Power is 4dBW.

$$EIRP_{dB} = 10\log_{10} P_{tx,W} + G_{tx} - L_{tx}; \quad (6)$$

Adding a margin of 6dB for losses such as gaseous absorption loss, antenna pointing loss, and polarization loss the Isotropic Receive Level is -148.27dBW.

$$IRL = EIRP_{dB} - FSL_{dB} - gaseous - pointing - polarization; \quad (7)$$

Using the assumption of a ground control antenna with 11dB directivity and 0dB line loss the Received Signal Level is -137.27dBW. Losses in the receive direction can be eliminated in the ground station by using a low noise amplifier at the antenna.

$$RSL_{dB} = IRL + G_{rx} - L_{rx}; \tag{8}$$

Having determined the strength of the signal at the receiver, we must determine if the signal is stronger than the noise floor of the device. Assuming a receiver Noise Figure of 8dB the thermal noise level in 25 KHz bandwidth at room temperature can be calculated as -152dBW.

$$P_{T,dBW} = -204 + 10\log_{10} 25000 + NF_{dB}; \tag{9}$$

The receiver itself contributes the majority of thermal noise in the system. A high gain antenna pointed at the sky would not have a high antenna noise temperature unless it is pointed at the sun or detecting interference. To account for antenna noise the Noise Figure of the receiver can be converted to Effective System Noise Temperature.

$$T_e = 290(10^{(NF_{dB}/10)} - 1); \tag{10}$$

An antenna pointed at the sky might have 60K noise temperature. The total noise per Hz can be computed with the sum of receiver and antenna noise temperature. This is equal to -195dBW/Hz.

$$N_{0,dBW/Hz} = -228.6 + 10\log_{10}(T_e + T_{ant}); \tag{11}$$

In 25 KHz of bandwidth the total system noise level is -151.99dBW.

$$N_{0,dBW} = N_{0,dBW/Hz} + 10\log_{10}(25000); \tag{12}$$

Another way to express the noise calculation is with multiplication of the factors followed by conversion to decibels. This yields roughly the same result of -152.58dBW. This is because the effective thermal noise temperature of the receiver is much larger than the antenna.

$$N_{receiver} = (1.38 \times 10^{-23})(T_e + T_{ant})(25000); \quad (13)$$

$$N_{receiver,dB} = 10\log_{10}(N_{receiver}); \quad (14)$$

The carrier to noise ratio is simple to calculate by subtracting signal power from noise power. It is 15.3dB.

$$C_{N,dB} = RSL_{dB} - N_{0,dBW}; \quad (15)$$

Energy per bit can be calculated by calculating the signal power per bit and subtracting noise power per bit. For spectral efficiency near 1 this will not differ much from carrier to noise ratio. From E_b/N_0 the BER can be predicted based on channel models and the required system link margin can be assessed. Here the noise figure is assumed at 8dB, which is more noise than a typical modern receiver, thus some extra noise margin is built into this link budget.

$$E_{b,dB} = RSL_{dB} - 10\log_{10}(19200); \quad (16)$$

$$N_{0,dB} = -204 + NF_{dB}; \quad (17)$$

$$N_{0,dB,bitrate} = N_0 + 10\log_{10}(19200); \quad (18)$$

$$\frac{E_b}{N_0} = E_b - N_{0,dB,bitrate}; \quad (19)$$

Such a link budget can be used to verify that a radio link can be closed under the conditions specified. The example values used in this description are appropriate for a CubeSat mission, and

table 3 on the following page shows the link budget for the LORIS project. The full link budget is provided in MATLAB code for the readers' convenience. For further information on link budgets I would recommend [10].

LORIS Project Link Budget		Downlink		Uplink
	Unit	GMSK Telemetry	Payload	GMSK Command
Orbit Altitude	km	410	410	410
Distance of Elevation Angle at 20 deg	km	1000	1000	1000
Frequency	MHz	438	438	438
Bandwidth	Hz	25000	25000	25000
Emission Type		F1D	F1D	F1D
Transmitter				
Tx Power Output	W	2	2	20
	dBW	3	3	13
	dBm	33	33	43
Transmission Line Losses	dB	1	1	3
Antenna Gain	dBi	2	2	11
Effective Isotropic Radiated Power	dBW	4	4	21
Path				
Free Space Loss (1000 km)	dB	145.28	145.28	145.28
Antenna Polarization Loss	dB	3	3	3
Atmospheric loss	dB	1	1	1
Antenna Pointing Loss	dB	3	3	3
Isotropic receive level	dB	-148.27	-148.27	-131.27
Receiver				
Antenna Gain	dBi	11	11	2
Line Loss (Using LNA)	dB	0	0	1
Received Signal Level	dBW	-137.27	-137.27	-130.27
Noise at the receiver				
Receiver Noise Figure	dB	8	8	
Effective thermal noise temperature	K	1540	1540	
Boltzman's Constant	dBJ/K	-228.6	-228.6	-228.6
	W/HzK	1.38E-23	1.38E-23	1.38E-23
Antenna Noise Temperature	K	60.00	60.00	290.00
Noise power in 25000 Hz, N0	dBW	-152.6	-152.6	
Signal Strength				
Carrier to noise ratio C/N0	dB	15.3	15.3	
Desired symbol rate	baud	19200	19200	19200
Bit energy to noise ratio Eb/N0		15.9	15.9	
Required Eb/N0		10	10	
Receiver Sensitivity	dBm	-	-	-110
	dBW	-	-	-140
System Link Margin	dB	5.9	5.9	9.73

Table 3 - LORIS Link Budget

```
%in dB, MHz and KM
D_km = 1000; %range between station and satellite, 20 deg
F_MHz = 438;
ss_gain = 2;%space station gain
gt_gain = 11;%ground station gain
FSL_db = 32.45 + 20*log10(D_km) + 20*log10(F_MHz);
%For a 2W system in space
p0_W = 2;
Gain_tx = ss_gain;%space station antenna, dipole, well matched
LineLoss_tx = 1;%estimate, short line in the sat.
EIRP_dB = 10*log10(p0_W) + Gain_tx - LineLoss_tx;
%For a 20W system on the ground
p0_W_GND = 20;
Gain_tx_GND = gt_gain;%ground station antenna, YAGI
LineLoss_tx_GND = 3;%long run from roof
EIRP_dB_GND = 10*log10(p0_W_GND) + Gain_tx_GND - LineLoss_tx_GND; %2.6
%assuming some gaseous absorbtion loss
GasLoss = 1;
Antenna_pointing_loss = 3;%within hpbw
polar_loss = 3;%loss due to antenna polarization
%space station receiving from ground side
IRL = EIRP_dB_GND - FSL_db - GasLoss - Antenna_pointing_loss - polar_loss;
%ground station receiving from space station
IRL_GND = EIRP_dB - FSL_db - GasLoss - Antenna_pointing_loss - polar_loss;
%For reception at the space station
Gain_rx = ss_gain;
LineLoss_rx = 1;%no LNA in Space station
RSL_dB = IRL + Gain_rx - LineLoss_rx;
%for reception at the ground station
Gain_rx_GND = gt_gain;
LineLoss_rx_GND = 0; %using an LNA to compensate for line loss
RSL_dB_GND = IRL_GND + Gain_rx_GND - LineLoss_rx_GND;
%Thermal noise level / Thermal noise threshold
%for room temperature, assuming BW of 25KHz,
%NF not always given in datasheet... 8dB typ
NF_db = 8;
Pt_dBW = -204 + 10*log10(25000) + NF_db; %Freeman page 60
%effective system noise temperature Freeman 6.21
Te = 290*(10^(NF_db/10)-1)  ; %1539 K for Room temperature, 1450 for 0 C
%pointed at the earth
Tant = 290;
Tant_2 = 60; %pointed at the sky / noisy sky
%noise level, 6.25 (noise density in 1 Hz of BW)
N0_dBwpHz = -228.6 + 10*log10(Te+Tant);
N0_dBwpHz_2 = -228.6 + 10*log10(Te+Tant_2);
%noise power in 25 kHz
N0_dBw = N0_dBwpHz + 10*log10(25000);
N0_dBw_GND = N0_dBwpHz_2 + 10*log10(25000);
noise_floor = (1.38*10^-23) * (Te+Tant_2) * 25000;
noise_floor_dB = 10*log10(noise_floor);%another way to get noise power
%carrier to noise ratio, 6.26 and 6.24
CN_db_downlink = RSL_dB_GND - N0_dBw_GND;%downlink
CN_db_uplink = RSL_dB - N0_dBw;%uplink
%downlink, Freeman eqn 3.1-3.4
bit_rate = 19200;
%energy per bit
E_b = RSL_dB_GND - 10*log10(bit_rate);
N_0 = -204 + NF_db; %noise
bit_N0 = N_0 + 10*log10(25000);
Eb_N0 = E_b - N_0; % 3.4
```

Figure 10 - MATLAB Link Budget Script

2.5 Radio Link Time

Achieving radio link between two points requires transmitted RF waves to be detectable at the receiver. Signal to noise ratio can be predicted through the link budget as seen previously. While there is unobstructed LOS between transmitter and receiver the condition for establishing radio link is ideal. For elevation angle less than 5, atmospheric effects caused by the troposphere and other obstructions such as buildings and hills may interfere. The geometry causes the radio wave to travel through more atmosphere in order to reach the receiver. The effect of the atmospheric refractivity index as a function of altitude is also a function of frequency. Frequencies above 10 GHz face serious attenuation due to absorption and scattering [13]. Thus, communication between ground station and satellite at low elevation angle may experience fading. The possibility for establishing radio communications at low elevation angles depends on the fading margin and the situation of the ground station.

An ideal good ground station location should have no obstructions to the horizon in all directions. This ideal site would take advantage of all the LOS time and more. However, it may be impractical to assume this possibility. Alternatively, the ground station engineer must perform site evaluation and consider the effect of obstacles. In a city, the top of a tall building can be a suitable site. In rural areas, the top of a hill could provide clearance over forests, terrain and buildings. Typical prograde orbits as described in Section 2.1 will result in satellite passes at all possible AZ/EL coordinates. Therefore, any pointing system must be capable of the full $360^{o}/180^{o}$ range of motion in each degree of freedom. Achievable slant range ultimately depends on the size of the ground station antenna. Being agnostic, at this point, of the RF system design, the total radio link time should carry an arbitrary margin of reduction from the LOS time for the

purpose of mission planning. Although LOS conditions are met other conditions will prevent radio link. For example:

- Severe weather (wind, rain, snow, and ice) may cause fading or degrade the ground station performance by icing the antenna.
- In the case of manually triggered downlink, a ground station operator may not be available during a satellite pass (the pass may occur in the middle of the night).
- In the case of scheduled downlink, the satellite and the ground station may have temporal or spatial alignment errors.
- Although infrequent, space weather and solar activity can disrupt communications.
- Equipment degradation onboard the satellite will gradually reduce the performance of all systems.
- If the ground station site has obstructions to the horizon, the possibility for communication will be occasionally limited by those obstructions.

In the example given in Section 2.2, the total LOS time is 1 hour per day between Halifax and the ISS. Therefore, total radio link time may be taken as 70% of this number, which is 46 minutes per day. Using this number and the data rate of the radio system, the overall data downlink capacity for the entire mission can be calculated.

2.6 Performance Upper Bound

The user of a radio system is typically only interested in one specification: the data rate. Data rate is well understood and can be calculated if the radio system is sufficiently well defined in the design. In order to derive the upper bound of possible performance a link budget is required to determine the SNR. The Shannon channel capacity for an AWGN channel shows the

maximum data rate for a band limited channel as a function of SNR. The formula is given below in equation (20).

$$C = Wlog_2\left(1 + \frac{S}{N}\right)\ [bits/s]; \tag{20}$$

Where the channel capacity C is a function of the channel bandwidth W in Hz and the signal to noise ratio. Since the use of RF bandwidth is a regulatory and licensing issue more than a technical one, channel capacity per Hz may be used. Spectrum availability and choice is discussed in the next section. An interesting result of Shannon's formula is the notion that a very wide bandwidth with very low SNR may still theoretically be used to transfer data. Since 1948 the non-constructive proof has been validated by the rise of spread spectrum techniques, which has become a common technology. Plotting channel capacity as a function of bandwidth, seen in Figure 11 below from [13], two regimes of telecommunication are revealed. Here $P/N^o = 10^6$.

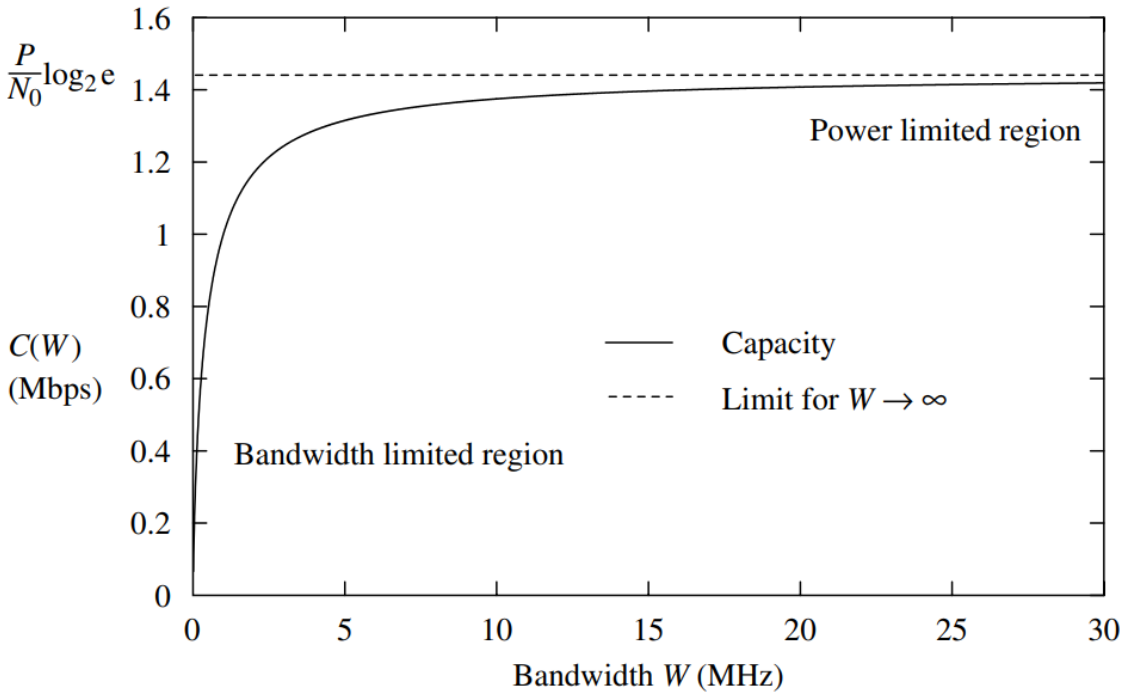

Figure 11 - Plot of Channel Capacity vs Bandwidth

In a wideband or spread spectrum situation where bandwidth is plentiful but energy per Hz is low, the communication regime is power limited and increasing the bandwidth further yields diminishing return. The average power per bit is low. On the other side, when the received power is strong within a band limited channel, the communication regime is bandwidth limited and increasing the SNR further yields diminishing return. The average power per bit is high. Supposing that spectrum and power are equally valued resources, one could design systems to operate at the knee of the curve in Figure 11. Often times power is more precious because a device is battery dependent, such as a mobile phone, walkie talkie, or CubeSat. Signals of 2-10W provide adequate SNR for sensitive ground station receiver equipment. Once again knowing channel capacity does not tell us how to implement a system which can achieve channel capacity. A typical RF system with fair performance can achieve 1 [bit/s/Hz], while advanced RF systems can achieve higher spectral efficiency. Due to the FSL curve seen in Figure 9, the channel of a LEO satellite is not simply AWGN but also time varying. The SNR will always vary with FSL as the satellite passes overhead and the channel capacity will vary proportionally. Based on Figure 9 and the data from STK, the SNR varies by 14 dB during a direct overhead pass. In Figure 12 below the effect on a 25 KHz band limited channel is shown. This assumes that the received signal level is 0 when the satellite is on the horizon. Integrating this curve yields 43.23 Mbit, while a realistic constant rate of 19.2 kbps for 661 seconds is 12.6 Mbit.

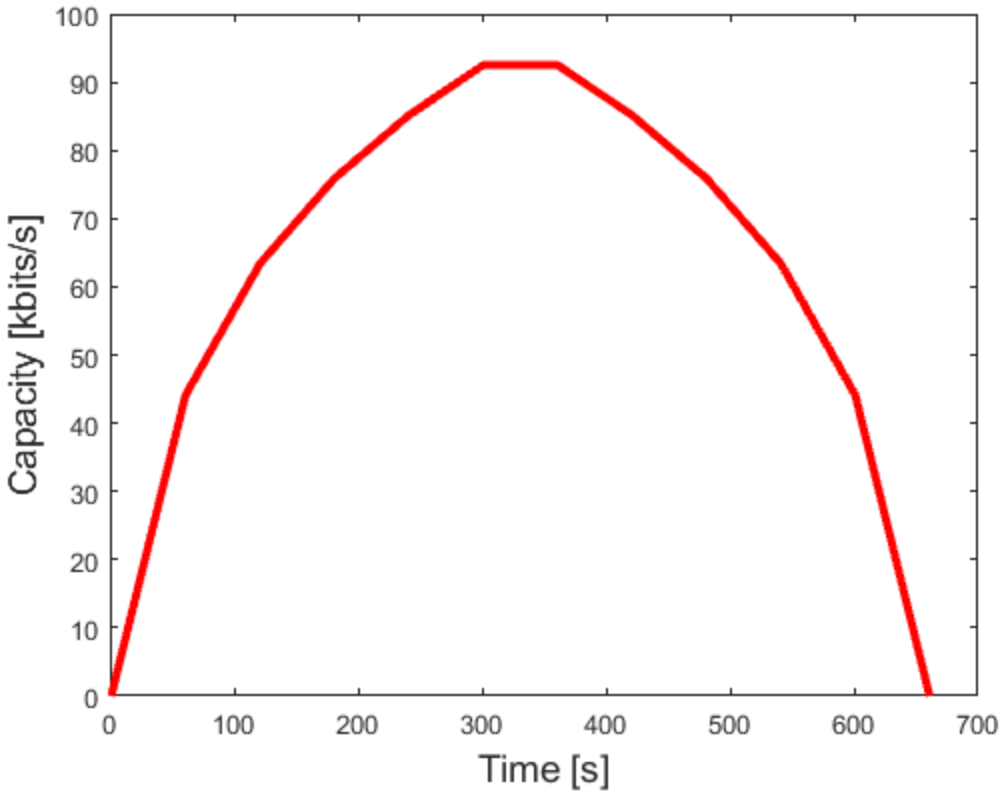

Figure 12 - Time Varying Channel Capacity in a 25 KHz Channel

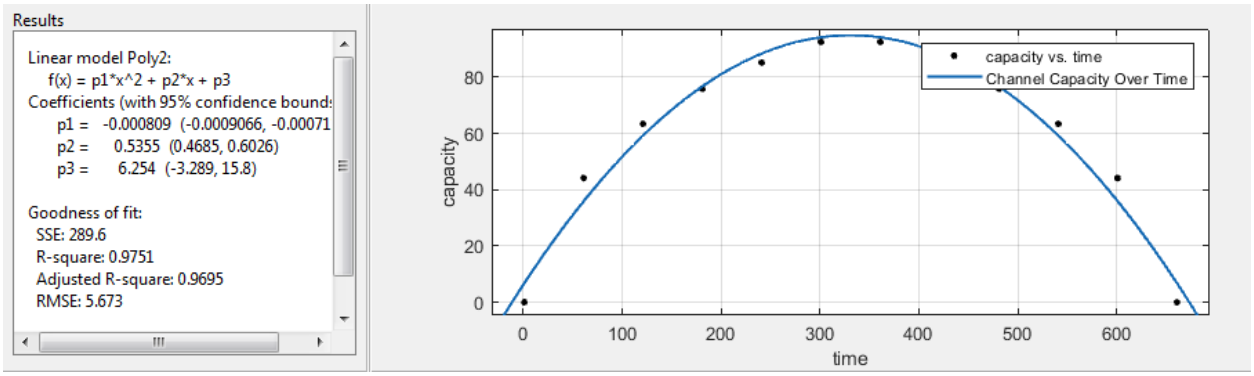

Figure 13 - Curve fitted to time varying capacity

In order to take full advantage of such a time varying channel capacity, dynamic modulation and FEC encoding should be utilized. Otherwise the RF system will be fundamentally impaired. The modulation coding scheme (MCS) for modern 802.11ac standard is an example of a

communication scheme employing multiple modulation levels and multiple code rates. The MCS table for 802.11ac is shown in Table 4 to illustrate the benefits of a sophisticated MCS [14].

Modulation Coding Scheme and Forward Error Correction Rate for 802.11ac						
MCS	Modulation	FEC Rate	Data Rate			
			20 MHz (Mbps)	40 MHz (Mbps)	80 MHz (Mbps)	160 MHz (Mbps)
0	BPSK	1/2	7.2	15.0	32.5	65.0
1	QPSK	1/2	14.4	30.0	65.0	130.0
2	QPSK	3/4	21.7	45.0	97.5	195.0
3	16QAM	1/2	28.9	60.0	130.0	260.0
4	16QAM	3/4	43.3	90.0	195.0	390.0
5	64QAM	2/3	57.8	120.0	260.0	525.0
6	64QAM	3/4	65.0	135.0	292.5	585.0
7	64QAM	5/6	72.2	150.0	325.0	650.0
8	256QAM	3/4	86.7	180.0	390.0	780.0
9	256QAM	5/6	N/A	200.0	433.3	866.7

Table 4 - Example Modulation Coding Scheme from WLAN

If we could use this MCS scheme it would proceed as follows. At the beginning of the satellite pass, where the satellite is at a low elevation angle, MCS level 0 is used. A simple binary phase shift constellation is used for modulation, while a very aggressive code rate of ½ is used. In Figure 14 below the satellite is in position 1. Because of the MCS level, the communication link is extremely robust and can handle low SNR. At position two in the middle of the satellite pass the SNR will improve to the maximum as the slant range reaches the minimum. During that precious window in time a dense modulation constellation alongside a low forward error correction code rate could utilize the channel more efficiently, such as MCS level 9. At position 3 the satellite is once again far away and the MCS level must be reduced to maintain an acceptable bit error rate. With the ability to change modulation scheme and coding rate throughout the pass of a LEO satellite the channel capacity could be more fully utilized.

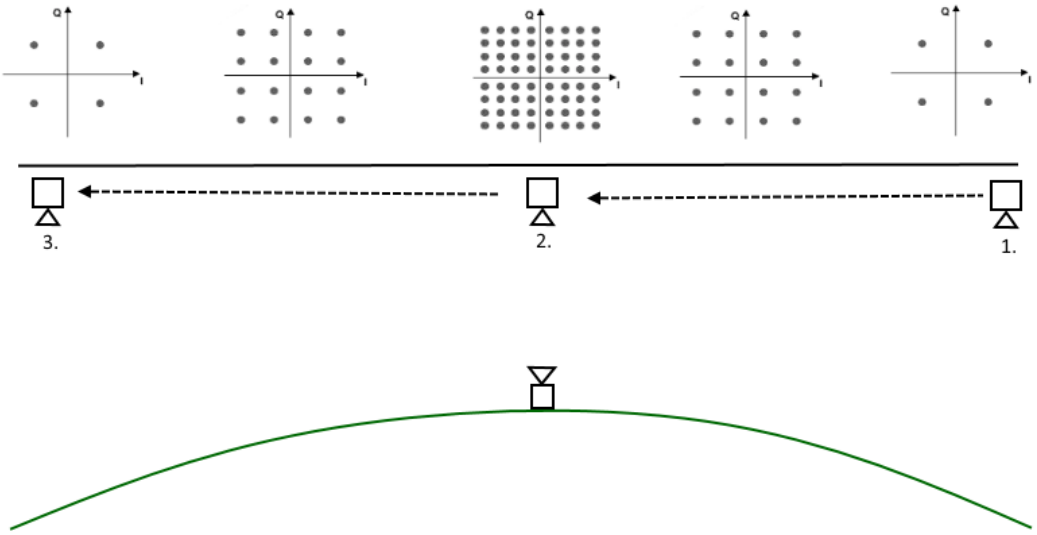

Figure 14 – Diagram of Dynamic Modulation Schemes During LEO Satellite Pass

2.6: Effects of High Frequency

According to Figure 15 on the following page, specific attenuation caused by atmospheric effects increases in proportion with frequency. Therefore, a band with frequency less than 10 GHz is recommended for CubeSat missions due to energy limitations on board the satellite. Because of wavelength decreasing proportional to increasing frequency, the antenna size decreases substantially when communicating on higher frequency bands. For example, in the V band one wavelength is ~2m, while in the C band one wavelength is ~60mm. Available bandwidth also tends to increase at higher frequency. For Amateur Satellite Service, in the V band only 4MHz is available, where in the C band 40 MHz is available. Thus, high frequency spectrum comes with the benefits of smaller antenna size and wider bandwidth availability. These benefits make higher frequency bands appear to be attractive options because of high bandwidth availability and small antenna size.

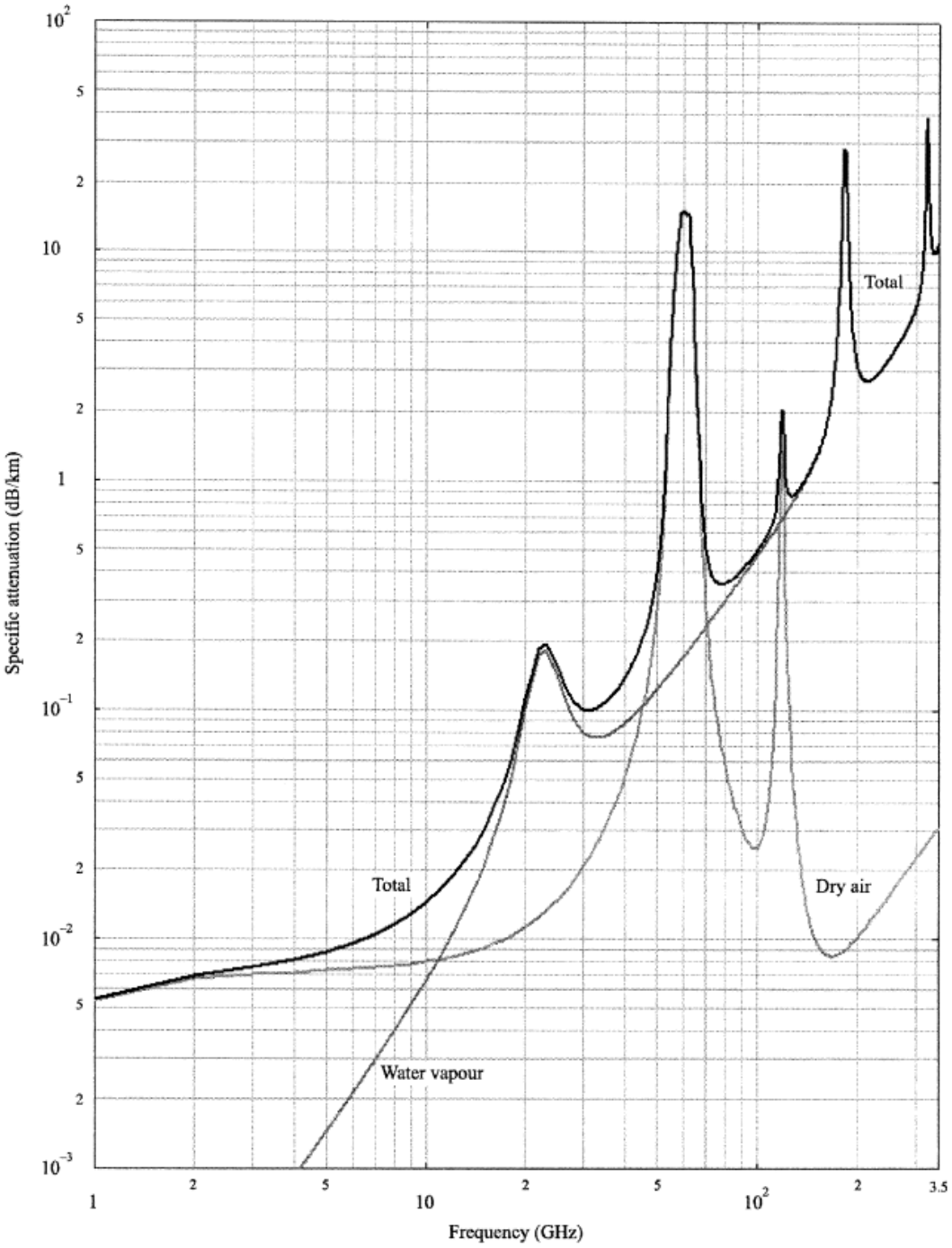

Figure 15 – Attenuation Due to Atmosphere vs Frequency [10]

However, increasing frequency increases the free space loss proportional to the increase of frequency, discussed in section 2.3. Power is a major consideration for CubeSats because of their small size. Thus, lower frequencies are actually more desirable unless the need for more bandwidth is a primary constraint. Small antenna size can be beneficial alongside certain antenna design techniques, which is discussed later in chapter 5. The 70 cm band balances the need for bandwidth, reasonable antenna size, and very importantly it does not reflect off the ionosphere since it is above the highest critical frequency. Many amateur satellites occupy this band, including many CubeSats. Future generations of CubeSats and amateur satellites will increasingly use the S and S2 bands due to the congestion of the U band and the decreasing cost of high frequency RF equipment. Another lateral strategy is to simply increase the number of ground stations to receive more data on the same band limited channel. More ground stations create more windows of communication. Satellite networks in LEO can also dramatically improve data throughput compared to that of a single satellite. Big players can reach an economy of scale not available to individual CubeSat missions.

2.7 Chapter 2 Conclusions

There are several inherent impairments to LEO satellite communication including limited communication window, long distance propagation, and spectrum availability. Because of the orbital motion of the satellite the radio link is mostly unavailable. Using a single ground station can make approximately 1 hour of radio link possible per day, if its geographic location is suitable for the satellite orbit. When LOS and thus radio link is available, the time varying slant range will inherently vary the capacity of the channel. For an ideal system able utilize the variable channel capacity, approximately 43.23 Mbit could theoretically be transmitted during an 11-minute direct overhead pass. This is in a 25 KHz band limited channel which is equivalent to

2.61 bits/s/Hz while the satellite is in range. With a static rate such as 19.2 Kbps, which can still operate at long distances with low SNR, only 12.6 Mbit could be transmitted. Depending on the needs of the mission, even a modest amount of spectrum bandwidth and infrastructure could theoretically yield high throughput. For missions requiring high data rates in the order of millions of bits per second, more bandwidth would be required and moving to S band would be appropriate. Capacity achieving RF systems are not realizable, nevertheless the analysis and model prediction shows the upper limit. Knowing this upper limit enables a better approach to solving the problem of implementing a digital satellite communication system.

Chapter 3.0 Mission Requirements

3.1 Mission Objective

The LORIS (Low Orbit Reconnaissance and Imaging Satellite) mission involves the design and operation of a CubeSat based on the efforts of students at Dalhousie and facilitated by the support of the Canadian Space Agency. The main objective of the LORIS satellite is the technological demonstration of the system, while the main objective of the project as a whole is educational outreach. Secondary mission objectives include successfully taking a picture with the camera payload and recovering it through radio downlink and recovering telemetry data from the satellite. Considering the state of the aerospace industry in general, instances of advanced satellite networks such as the Iridium communication constellation and Planet Labs earth imaging constellation are technologically advanced utilizing mature technology. CubeSats do not generally represent the state-of-the-art as a whole, but rather as platforms for affordable research and development. The benefit of small containerized satellites is to reduce the project scope and cost compared to traditional efforts. These small satellites also serve to help first time developers learn the processes and regulations required of satellite designers. Several CubeSats have become the first national satellite of their countries, for example LitSAT-1 was the first Lithuanian satellite [15]. LORIS is classified as an amateur satellite because the designers are students learning from the process of making it and have no pecuniary interest from the operation of either ground station or satellite station. The purpose of the satellite itself is to operate the payload, which is two high definition cameras. ITU regulation 22.2 mandates that any non geostationary satellite has limited rights and shall not cause interference to other services [16], therefore radio emissions should be treated with caution.

3.2 Size Constraint

The size and geometry of the CubeSat chassis places size constraints on the equipment. Components inside the satellite must fit within the 100mm square bus with 8.5mm square notched corners, shown in Figure 16. The four 8.5mm minimum structural columns in the four corners interface with the CubeSat launcher. The satellite slides along these rails as a spring launches the contents of the pod out of the deployer. There are multiple CubeSat launch providers and the deployment pod may differ slightly. The specification of the corners is 8.5mm minimum for the purpose of ensuring that there is enough surface for the CubeSat to safely slide out of the deployment pod.

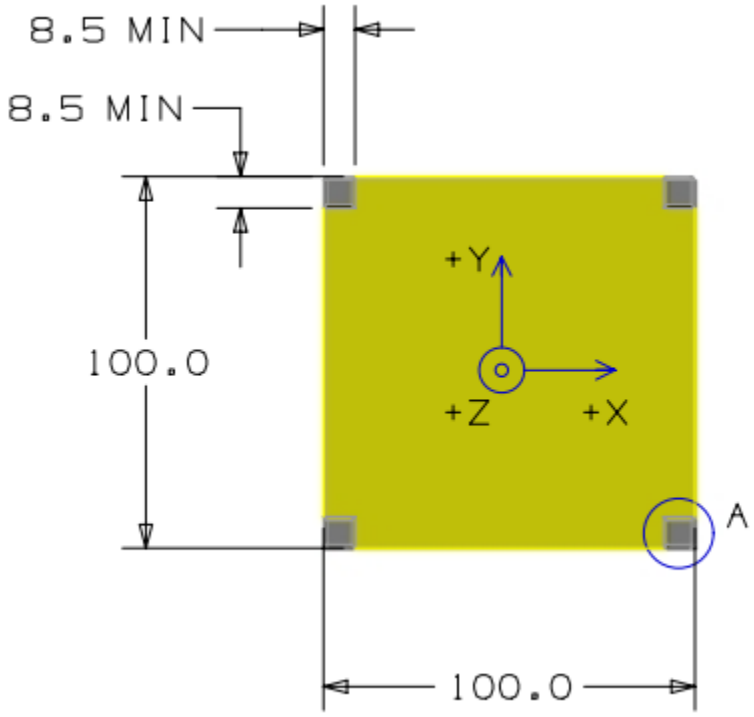

Figure 16 - X and Y Dimensions of a CubeSat [17]

The Nano Racks CubeSat Deployer is shown in a schematic cross section in Figure 17. The corner rails of the CubeSat are to slide along the 2.5 mm rails of the deployer. The deployer has rails centered on the CubeSat minimum specification of 8.5mm, maximizing the contact area of the solid metal. Unfortunately, this system reduces to usable space inside the CubeSat. Furthermore, due to the four deployable solar panels LORIS has only 85 mm^2 available for hardware components. For the LORIS mission the RF subsystem is allocated one 'slice' consisting of 85 mm^2 with and 2 cm in height, with additional routing space for the antenna.

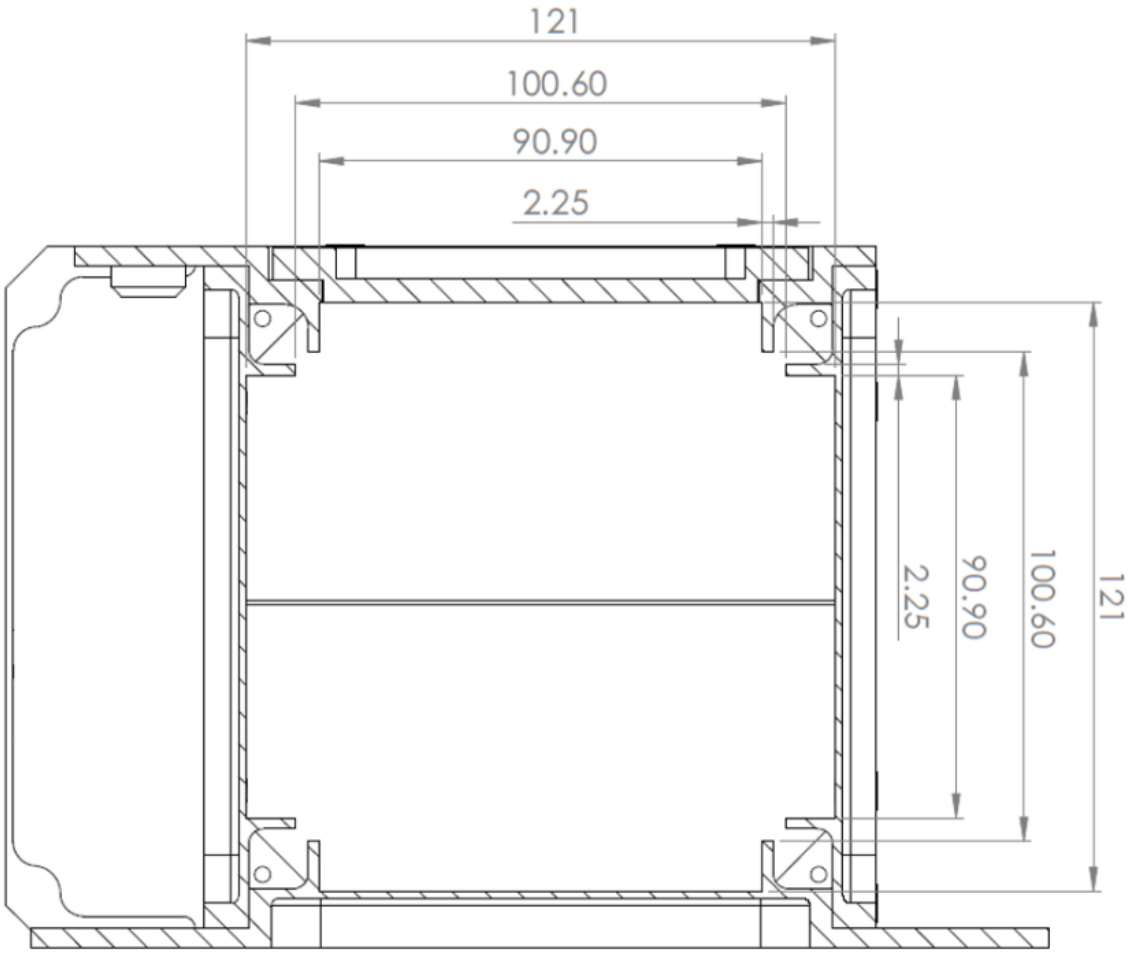

Figure 17 - Schematic of NanoRacks CubeSat Deployer [4]

3.3 Antenna Location and Deployment

In order to avoid impairments to radiating and receiving RF energy from the antenna it is preferable to mount it outside the chassis. Most antenna systems for CubeSats are deployable using burnwire mechanism. A burnwire mechanism is typically nylon or silk thread tied around the deployable and a resistor. To deploy, a current is applied to the resistor creating enough heat to burn the thread. For LORIS, each 2U face is deployable giving more space to mount solar panels. On the underside of these deployable panels would be a good place for a patch antenna. The operating frequency would need to be sufficiently high to make the patch antenna small enough. Alternatively, an antenna could be stowed underneath the panels removing the need for additional burnwire deployment mechanisms. Figure 18 is an exploded diagram of the structure which depicts the situation with the deployable wings [19].

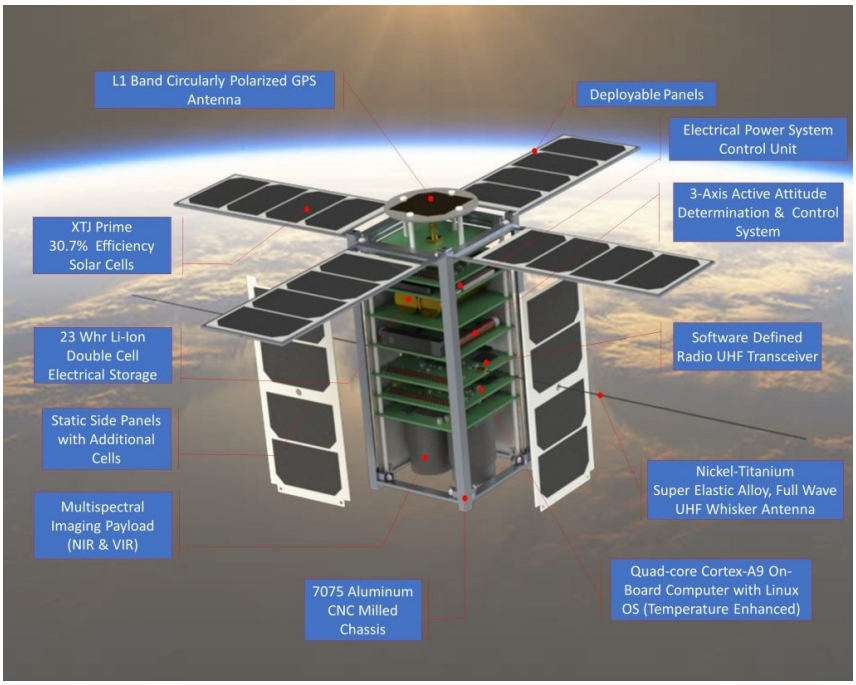

Figure 18 - CubeSat with Panels Deployed

Initially these panels are stowed, and the satellite is a rectangular prism. After the satellite is launched from the ISS it tumbles for 30 minutes, after which the satellite can wake up and deploy the solar panels. There is an attitude determination and control system on the satellite which allows LORIS to point the camera toward earth. In addition, attitude control allows the use of directional antennas. Directional antennas can greatly improve performance because power is not wasted radiating RF waves into space rather than toward earth.

3.4 Power Constraint

The power subsystem of LORIS operates on a budget of solar power income versus expenditures in the various subsystems. During the part of the orbit when the sun is eclipsed by the earth, the satellite must operate solely on battery power. These factors place limits on how much power the RF system can consume. Peak power consumption will occur when the downlink is established, and a picture is being transmitted to the ground station. This is a relatively small duration compared to the time waiting for LOS conditions to be available, however the receiver will be on all the time unless the satellite enters safe hold mode. The power budget for LORIS allows 3.3V or 5V supply consuming up to 2W for receiving and up to 5W for transmitting.

3.5 Data Volume

The LORIS team made it a design goal to be able to recover at least 1 image from space each day the satellite is in operation. Each picture will consist of 8 MB of data before compression and less than 1 MB after compression. Each data packet will also have overhead from headers, parity checks, telemetry, and FEC encoding. For the moment assuming a 1MB picture requires 2 MB to transmit, the amount of time to transmit one payload message can be calculated. At a rate of 19.2kbps a message of 2MB of data will take 105 seconds to transmit assuming no bit errors. In chapter 1 it was shown that 12 MB could be transmitted with one good satellite pass, which

occurs 4-5 times per day. Thus, a radio capable of 19.2 kbps would be enable LORIS to capture and downlink several images per day with ease. It is possible to generate far more images than the RF system could handle. Creating videos is also a possibility, which would quickly exceed the data transfer capabilities. To achieve better data volume a bigger channel must be legally obtained, and an RF system must be implemented to take advantage of it. Perhaps in the next generation of Dalhousie CubeSat missions this will become a goal, at which point the material in Chapter 2 and 5 would be useful. For this project a simple RF system will meet the performance requirements, and neither S band nor MCS scheme is needful.

3.6 Spectrum Considerations

Permission to transmit data over the wireless channel is managed differently in each country. Internationally the ITU coordinates spectrum use and makes recommendations for the laws internal to each nation. In general RF spectrum is regarded as a natural resource and the use of it incurs some fees. Application must be made both to the ITU and the local governing body, both of which may also incur some fees. The exception to the fee structure is amateur radio which has a definition in the ITU radio regulations [16]. Because the radio frequency spectrum is coordinated both national and internationally, the Canadian Government and the ITU have legal power over who can use the spectrum to communicate. The cost to obtain and maintain a conventional spectrum license is prohibitive for this project. In addition, our project has no real need for a dedicated channel. Beyond educational efforts and technological demonstration, there is no real scientific value to the camera data, nor is the satellite hardware particularly advanced compared to others. Amateur satellite licenses do not carry the same costs as a commercial license. Therefore, qualifying and using amateur satellite service is an important part of the LORIS project. The satellite needs a license application and each ground station needs a license

application and a certified amateur radio operator. Amateur satellite radio has allocations in the bands indicated by Table 5.

Designator	H	A	V	U	L	S	S2	C	X	K	R
Band	15 m	10 m	2 m	70 cm	23 cm	13 cm	9 cm	5 cm	3 cm	1.2 cm	6 mm
Frequency (General)	21 MHz	29 MHz	145 MHz	435 MHz	1.2 GHz	2.4 GHz	3.4 GHz	5 GHz	10 GHz	24 GHz	47 GHz

Table 5 - Available Spectrum for Amateur Satellite Service

Many CubeSat missions have historically used spectrum allocated for amateur use, although this is possibly encroachment. In order to qualify as an amateur satellite, it must fulfil the mandate set by the ITU. This includes the "self-training, intercommunication, and technical investigations carried out by amateurs" meaning that it is not difficult to qualify for universities and educational institutions. The licence holder must also be a licenced amateur radio operator, and the satellite should offer some service for amateur radio operators. A more definitive requirement for amateur satellites is that the controllers and users of the amateur satellite (or any radio operating in amateur allocated spectrum) may not have any pecuniary interest in the use of the spectrum. Even indirect exchanges of money may disqualify the mission from using amateur spectrum. If the mission definition is appropriate and amateur satellite spectrum can be licensed, the choice of frequency band is still a nuanced decision. Higher frequencies incur higher free space loss but have more usable bandwidth. VHF and UHF are appropriate for low data rate applications such as voice transponders and repeaters, as well as low data rate science missions. Recently more CubeSats have been moving to S band communication systems in order to achieve a higher data throughput. S band usage requires more ground station infrastructure to make up for the extra loss due to higher frequency. The LORIS mission does not merit the extra cost and resources required to develop an S band RF system. However, as S band COTS equipment becomes more

available and cost-effective future systems will require appropriate antenna designs to complete the RF system.

Chapter 4.0 System Design

4.1 System Characteristics

The radio communication system is responsible for relaying data from the satellite to the ground and vice versa. Data may include telemetry, pictures, diagnostics, and commands to the satellite. Communication is critical to the success of the mission; therefore, the system must meet a high standard of robust operation.

4.2 High Level Design

The system as a whole must have a transceiver in the ground station and in the satellite station. Figure 19 shows the top-level system diagram.

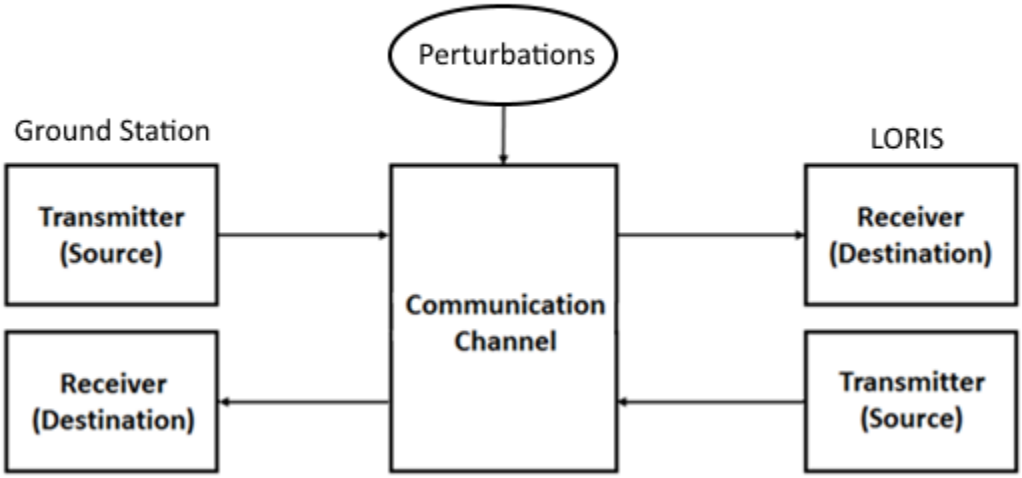

Figure 19 - Generic Two-Way Communication System

This document primarily considers the implementation of satellite downlink. Satellite uplink can be considered as the same problem except with drastically relaxed constraints. A ground control station can support larger equipment and consume more power, but otherwise requires the same

features as the satellite counterpart. Figure 20 depicts a generic functional block diagram of a one-way digital communication system with added detail.

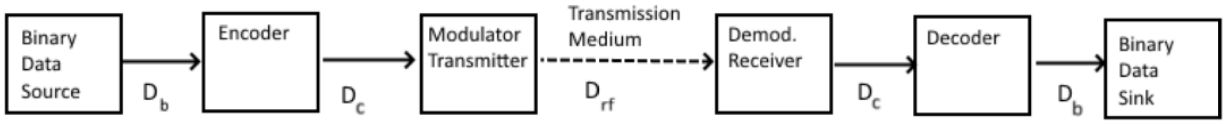

Figure 20 - One-Way Digital Communication System

4.3 Receiver Theory and Selection

Today there are many COTS radio transceivers and receivers available ranging from turn-key solutions to RF front ends ready for PCB component level integration. Notably the major semiconductor companies such as Analog Devices, Maxim Integrated, Texas Instruments, Silicon Labs, Quorvo, and Semtech all offer a variety of competitive RF products. Receivers in general must satisfy the level of sensitivity required in the application. Thermal noise represents a fundamental limit on receiver sensitivity through the Boltzmann constant. At standard temperature the thermal noise power (P) is:

$$P = kTB = (1.38 \times 10^{-23})(290)(1) = -174\ dBm/Hz; \quad (21)$$

Where k is the Boltzmann constant, T is the temperature in Kelvin, and B is the bandwidth [20]. Thus, a noiseless receiver would still have a fundamental noise floor of -174dBm/Hz at standard temperature. When the Noise Factor (F) or Noise Figure (NF) specification is given by the manufacturer it is a measure of how much noise the receiver adds to the signal, given by (22):

$$F = \frac{(GP+N_R)}{GP}; \quad (22)$$

And (23)

$$NF = 10log_{10}(F); \tag{23}$$

Where G is the receiver gain, P is the thermal noise power, and N_R is the noise added by the receiver. The Noise Figure is simply Noise Factor expressed in decibels. Thus, a receiver device in a network degrades the signal to noise ratio by contributing noise N_R, while the thermal noise power in the incoming signal is accounted for in P. Noise in the incoming signal is amplified by the gain of the device, but that is not part of the noise factor of the device itself. Rather the noise factor is the ratio of total noise power output to the part that is due to input noise. Figure 21 shows a block diagram displaying the effect of a device adding noise to a signal chain. Receiver noise figure is defined as the ratio in equation (22) and in essence it considers the receiver noise against the input noise and shows that an amplifier never reduces noise, and in multistage amplification noise adds up quickly.

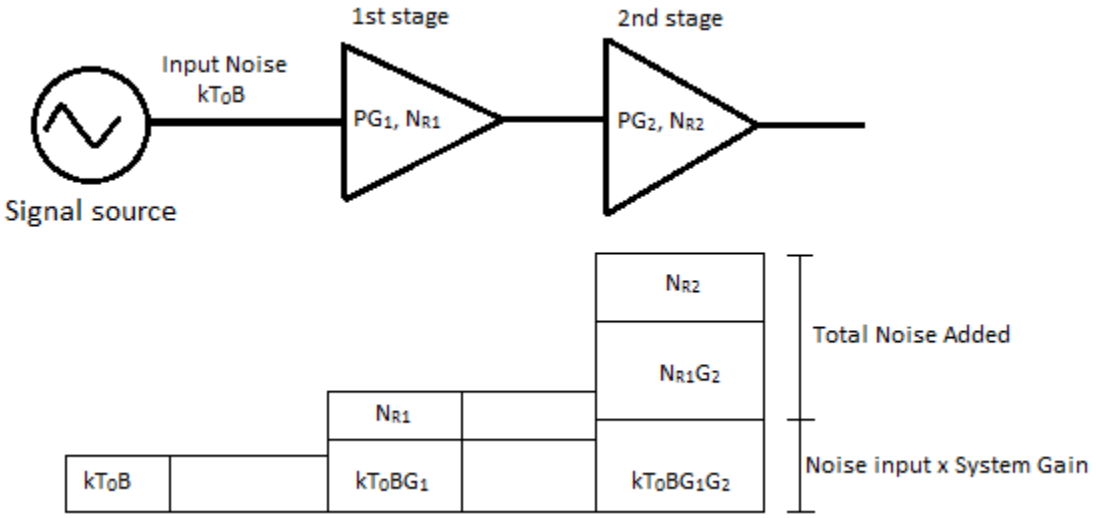

Figure 21 - Noise accumulation in signal processing

Practical implementations of receivers can be modelled as a network of components, even if the receiver is implemented on a single die (especially if it is a multistage receiver). Noise Figure can be extended to cascaded components using (24):

$$NF_{Total} = 10\log\left[\left(F_1 + \frac{F_2 - 1}{G_1}\right) + \left(\frac{F_3 - 1}{G_1 G_2}\right) \ldots + \left(\frac{F_n - 1}{G_1 G_2 \ldots G_{n-1}}\right)\right]; \quad (24)$$

Where F is the Noise Factor of the nth stage, and G is the gain of the nth stage. Here we can observe that the overall Noise Factor is minimized with a low Noise Factor and high gain in the first stage. For this reason, having a good LNA as close to the antenna as possible is important. A typical receiver signal chain is presented in Figure 22 [22].

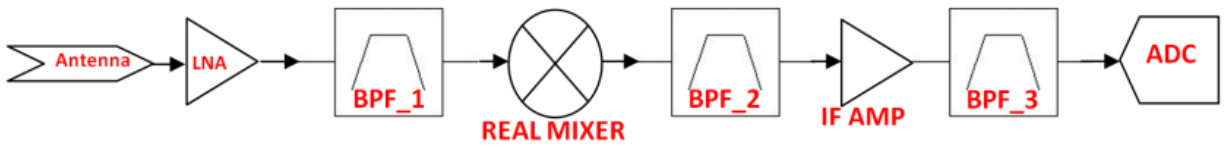

Figure 22 - RF Receiver Chain

We may consider some techniques used to implement radio receivers beginning with direct conversion. A direct conversion or homodyne receiver converts the target RF signal to a baseband signal in one stage [20]. This type of receiver also goes by the name zero-IF receiver [23]. Because only one local oscillator (LO) is required to convert the RF signal to baseband, these receivers can be smaller, less complex, and with a lower cost. Another strategy is to convert the high frequency RF signal down to low frequency base band in multiple steps. In the first stage the signal is processed the same as direct conversion, except that the LO is chosen to produce an intermediate frequency (IF) rather than baseband. The IF signal is then filtered and amplified before continuing to either the demodulator or additional downmixing stages. A super-heterodyne receiver can generally achieve higher frequency operation because they can leverage multiple down-conversion stages. On the other hand, a direct conversion receiver can achieve wider bandwidth and lower power consumption. Both techniques rely on the frequency shift property of the Fourier transform known as the modulation theorem shown in (25). This property

states that when a time domain function x(t) is multiplied with a sinusoid whose frequency is f_c the result is two copies of ½ amplitude and shifted by ± f_c [23].

$$F\{x(t)[\frac{e^{j2pif_ct}+e^{-j2pif_ct}}{2}] = \frac{1}{2}[X(f-f_c)+X(f+f_c)]; \qquad (25)$$

It is not difficult to find ready made radio equipment on the consumer market. Sub-GHz transceivers are easier to find and cheaper than S band equipment. For S band communication the AD9364 is a high performing radio front end from Analog Devices. Products such as the USRP B200 mini-i from Ettus Research provide powerful wideband and flexible RF transceivers. The transceiver uses direct conversion since the AD9364 uses adjustable PLLs to perform complex demodulation, after which the signal is sampled and passed to the supporting hardware. Because this radio is software defined it is also capable of a sophisticated MCS as described in chapter 2. The tunable frequency range is 70MHz-6GHz, and the instantaneous bandwidth is 56 MHz. This hardware also comes with disadvantages such as low transmit power and no support for a low power standby. Complex MCS schemes are possible since the SDR is wideband and could be programmed to use additional techniques such as spread spectrum. Many other COTS products exist based on the AD9364 which could fill the need for S band radio hardware in a small package. To handle the high sampling rate coming from the AD9364 most designs use an FPGA. Software defined radios leave the demodulation and decision making up to a CPU rather than accomplishing those tasks in hardware. There are numerous other RF transceiver front ends available with varying degrees of cost, completeness, and performance. For LORIS which is targeting the UHF band offerings such as Semtech's SX1276 are more suitable. That family of transceiver devices can perform LORA, GMSK, MSK, GFSK, and OOK modulation and demodulation. Companies such as Enhanced Radio provide breakout boards and

integrate power electronics. For this project we selected a more complete product with the nL400 from Microhard, a Canadian company based in Alberta. The nL400 meets the performance requirements of the project:

- 19.2 kbps link rate
- Serial communication to controller
- 410-480 MHz operation
- 0.1-2W transmit power
- -110dBm sensitivity
- GMSK modulation
- 25 KHz bandwidth occupation
- 3.3V supply

4.4 Antenna Simulation

Using HFSS simulation software from ANSYS we can check the theoretical behaviour of the antenna configuration. By using a half wave dipole with one parasitic reflector element the radiation pattern becomes directional. This is based on the widely used Yagi-Uda antenna configuration which originated from the publications of Uda and Yagi in 1927 and 1928 respectively [26]. The presence of a reflector and thus an earth pointing radiation pattern is desirable since the satellite will always be pointed nadir (directly down) in order to take pictures. On the following pages a series of figures present the simulation geometry and resultant radiation pattern. Figures 23-25 show the CubeSat with the driven dipole below and the parasitic reflector element above. These wire antennas can be implemented using Nitinol (nickel titanium alloy) wire, which can deform under stress and return to the straight position when released. This

allows the antennas to be stowed underneath the solar panels without requiring an additional burn wire deployment mechanism.

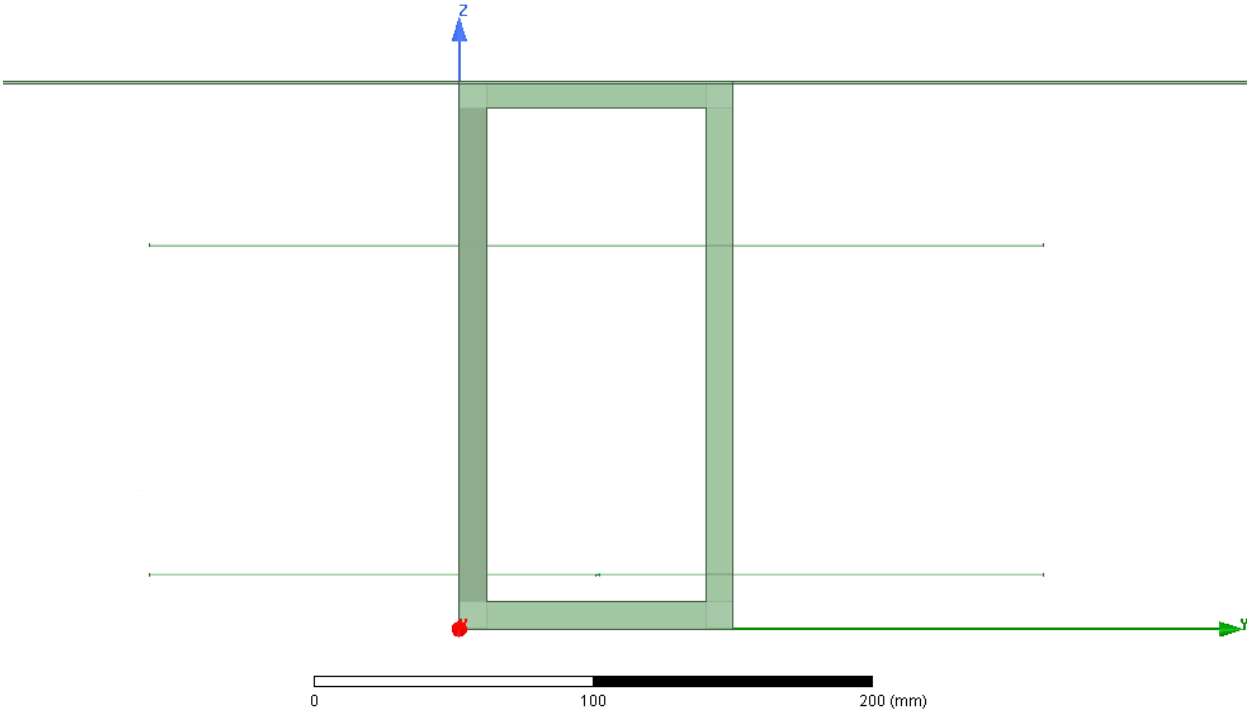

Figure 23 - CubeSat Simulation Geometry in Front View

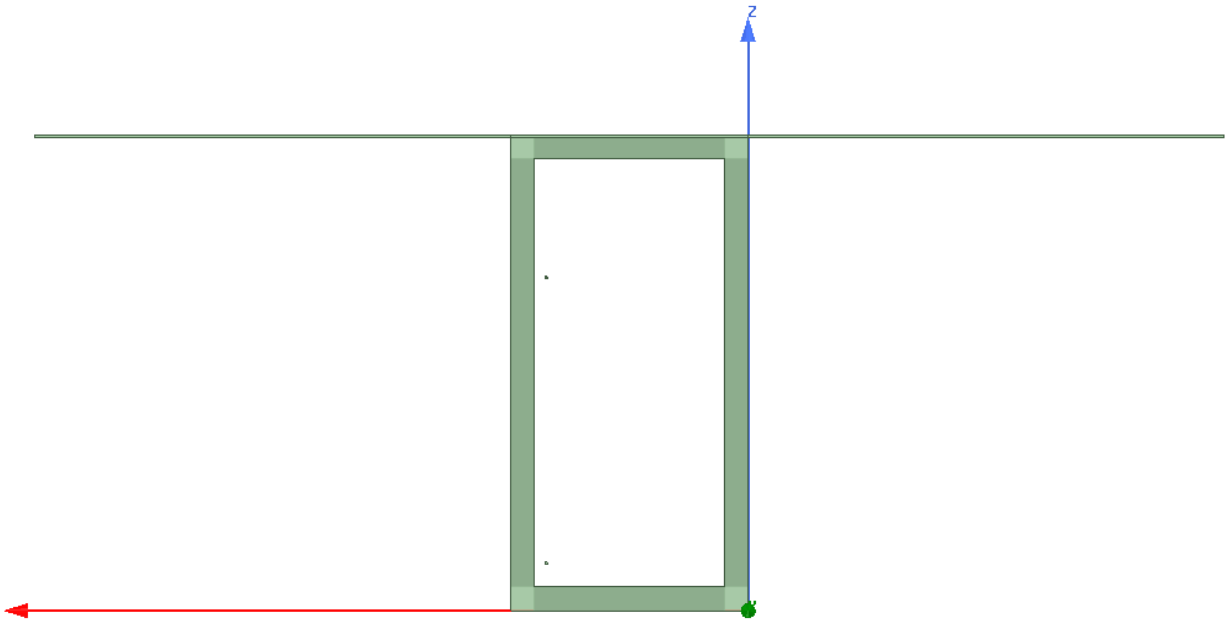

Figure 24 - CubeSat Simulation Geometry in Side View

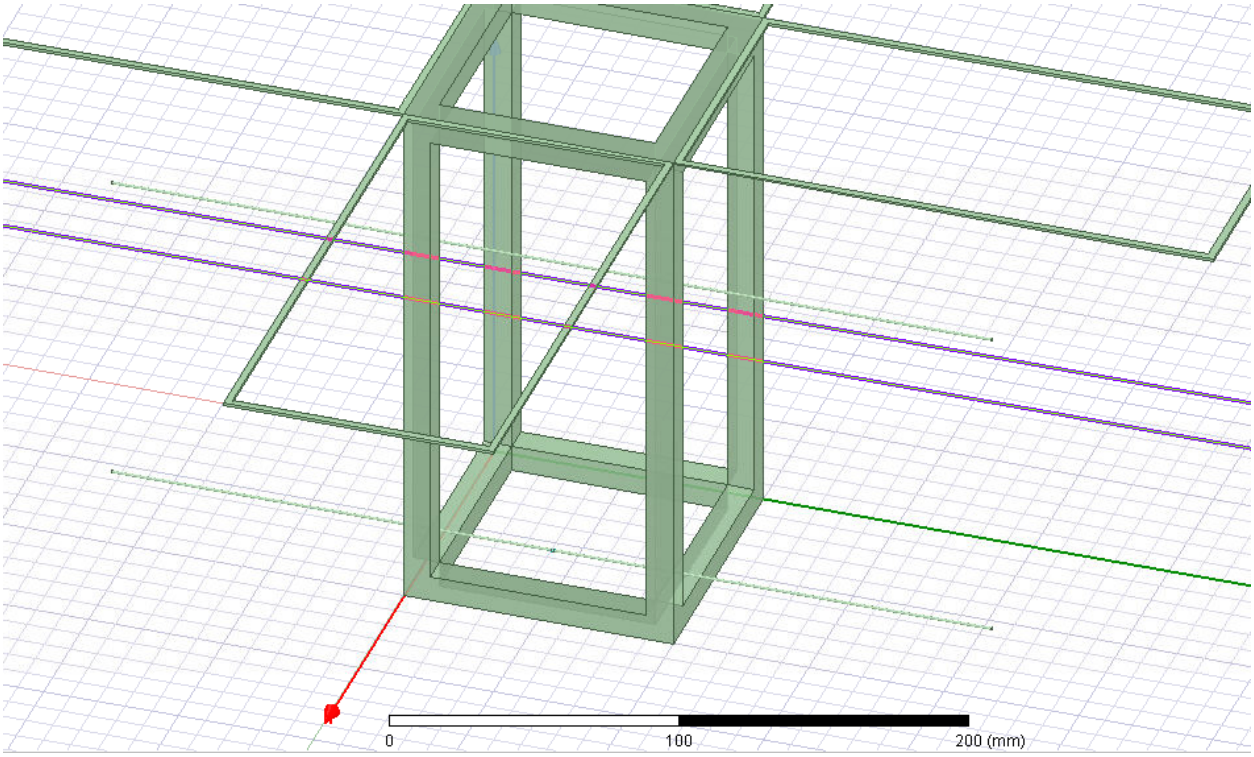

Figure 25 - CubeSat Simulation Geometry in Trimetric View

Figures 26-28 show the simulated radiation pattern for this configuration. On the 90° Phi axis, or the narrow axis, the radiation pattern reaches the 3dB point at 148°. This means that the half power beam width of the radiation pattern is 64° wide. On the 0° Phi axis, or the wide axis, the radiation pattern is 160° wide. The orientation of the satellite will affect the satellite footprint which is the area on the earth where there is RF coverage from the satellite. To improve the communication window duration the attitude control system can rotate LORIS so that the Y positive axis is pointing north. Alternatively, a ground station with more gain and sensitivity could be established to compensate for the antenna pointing loss.

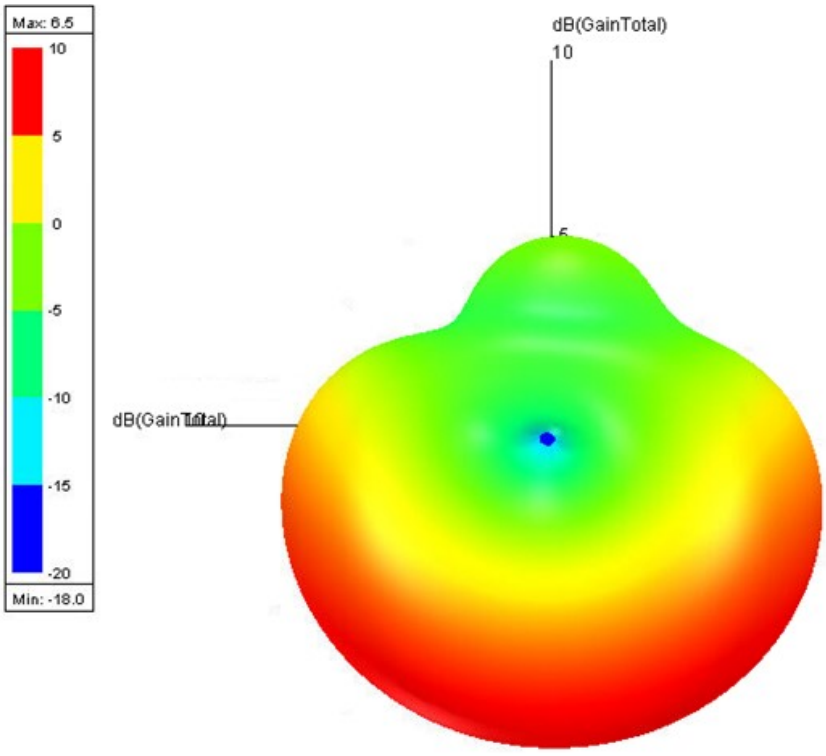

Figure 26 - Dipole with Reflector Radiation Pattern Front View

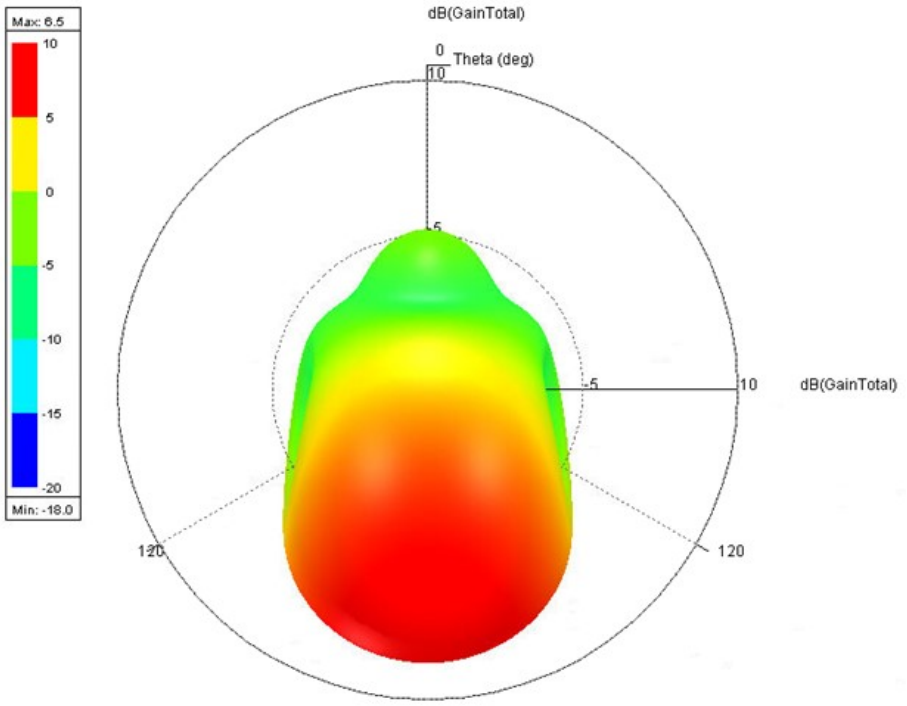

Figure 27 - Dipole with Reflector Radiation Pattern Side View

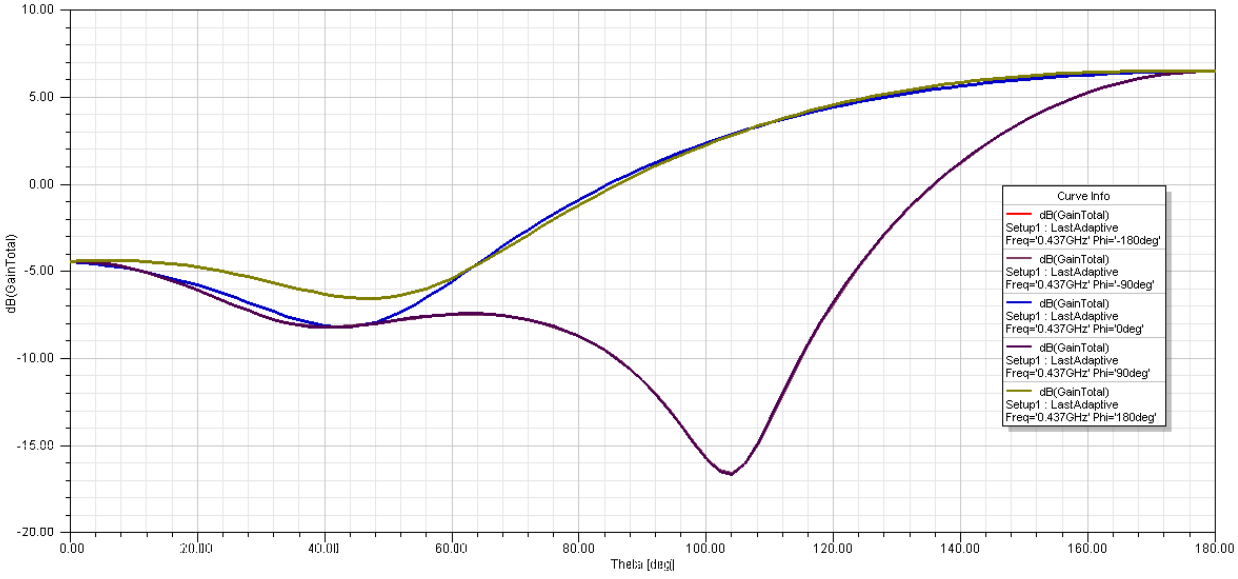

Figure 28 - Dipole with Reflector Radiation Pattern Stacked Rectangular Plot

4.5 System Design Summary

The satellite telemetry and data link radio subsystem consists of:

- One GMSK transceiver
    - Model name is nL400 from Microhard Systems Inc.
    - 410-480 MHz operational range
    - 2W transmit capability
    - Full Duplex capable
- One driven antenna element
    - Straight half wave dipole element, Nitinol wire
- One parasitic antenna element (reflector)
    - Straight half wave dipole element, Nitinol wire
- One short RF coaxial cable selected for
    - Low attenuation at 435 MHz
    - Mil-C-17 Specification
    - A balun connector will be required to mate to the antenna

This system is to operate in the amateur satellite radio service in 435-438 MHz. This simple design is sufficient for the needs of the first-time LORIS satellite project. In chapter 5 higher performance is pursued through the antenna design for an S band system.

Chapter 5.0 Patch Antenna Design

In order to optimize the performance of any RF system, a suitable antenna must be used in the design. Characteristics such as directivity, impedance, and polarization will impact the overall system performance. In this chapter a 3.4 GHz antenna design for S band CubeSat to earth communication is presented. It is shown that patch antennas can be configured in arrays to provide suitable characteristics. In addition, a low cost and ease of fabrication is maintained.

5.1 Antenna Background

The antenna is the component of an RF system which interfaces EM energy between the electrical conductor and the wireless channel. The antenna is an integral part of the system, it can not be dispensed with or compromised, and the characteristics of the antenna have a dramatic impact on the system performance. Antennas exhibit reciprocity for sending and receiving EM energy, thus a good antenna can be used for both [27]. All antennas operate as AC devices because they are driven to emit RF waves by the RF currents travelling in the antenna. Thus, AC circuit and transmission line theory are fundamental to antenna design. Additionally, as the EM waves propagate through space they spread and in the far field approximately resemble a plane wave [27]. Far field behaviour can differ from near field behaviour because of the spreading effect, and antenna radiation patterns impact performance differently depending on distance between radios.

Antenna directivity is measured based on the definition of the hypothetical isotropic source. An isotropic antenna is one which radiates uniformly in all directions. Such an antenna would have 0dB gain[3]. Figure 29 demonstrates radiation patterns and their relation to antenna gain.

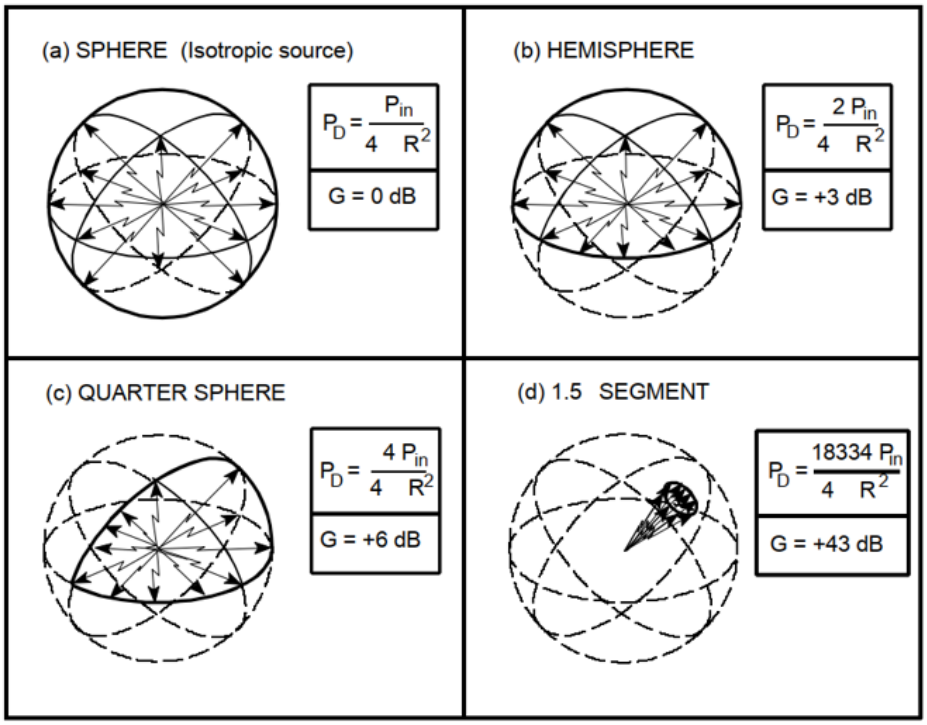

Figure 29 – Diagrammatic Explanation of Antenna Gain [28]

[3] The term "gain" is misleading because antennas are passive, unlike amplifiers which also use the term gain. Directivity would be the preferred term, where gain is formally defined as directivity multiplied by efficiency. A passive antenna always has efficiency less than one. Active antennas may in fact have both amplifier gain and antenna directivity gain, which is why the mixed terminology is undesirable.

Transmissions lines transport electrical power through space, ideally without consuming power or radiating radio waves. Unfortunately, no transmission lines are ideal and to minimize wasted power the designer must ensure impedance matching. For best performance the characteristic impedance of the transmission line must match that of the load. The model for transmission line is an endless parade of connected capacitors and inductors, shown in Figure 30. The transmission line may impede AC transmission because of the characteristic impedance. This is not related to the DC resistance of the line or power dissipation. The real impedance is so small it is often neglected, but it is always non-zero. The best case for transferring power is for the source, line, and load to all have matched impedance. In radio systems the antenna is the load.

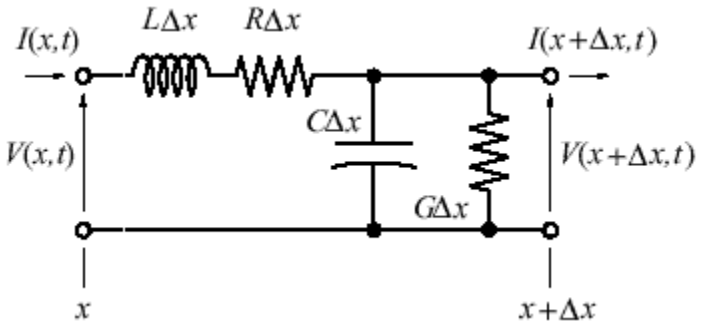

Figure 30 - Transmission Line Equivalent Circuit

Obtaining a matching impedance between source, transmission line, and load is important for implementing a good antenna. When the impedance is matching across the system, the antenna can radiate with good efficiency. A poor impedance match results in voltage reflections within the antenna, and little radiated RF energy. Voltage standing wave ratio (VSWR) is given by the equation (26):

$$VSWR = \frac{1+|\Gamma|}{1-|\Gamma|}; \quad (26)$$

Where Γ is the reflection coefficient, also called S11 parameter or return loss [29].

5.2 Antenna Arrays

When identical antennas are located near each other their radiation patterns are superimposed and an antenna array is formed. Antenna arrays result in more directivity (and sensitivity) due to the constructive interference of superimposed waves. Unwanted sidelobes may arise or be suppressed due to the spacing of the array elements. The main-lobe angle may be steered if the array permits control over the phase in each array element. Alternately the main-lobe angle may be fixed at an angle by adjusting the spacing of the array elements.

5.3 Planar Antenna Design

Planar antennas are a class of antenna with at least two distinct advantages: compatibility with conventional PCB manufacturing, and support for sophisticated geometries on the planar surface. Sometimes the flat profile and conformability of planar antennas are also advantageous. Many antenna designs can be implemented in a planar form. Most simple patch geometries have been investigated, such as squares and circles. New designs and novel improvements are constantly being proposed. Figure 31 shows an example of a planar antenna integrated directly onto a silicon substrate.

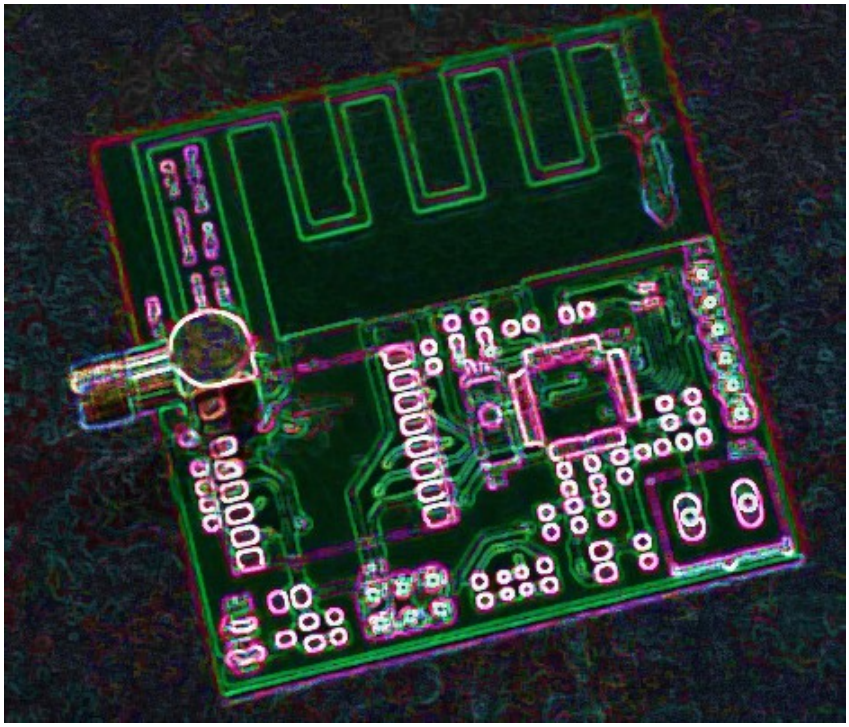

Figure 31 - PCB Trace Antenna

5.4 Substrate

The properties of the substrate are very important for planar antenna design. Different substrates will change the properties of the antenna. The key parameter of the material is relative dielectric constant (ε_r), recently (and more accurately) called relative permittivity. This is a measure of how much the electric field is attenuated when the material is the dielectric of a capacitor. Thick substrates and low values of relative permittivity are desired for patch antennas [30]. The laminate branded as RT/Duroid 5870 from Rogers Corporation has a $\varepsilon_r = 2.33$. I used their thickest standard stock laminate.

5.5 Microstrip Transmission Line

Some patch antennas are probe fed or stripline fed, both of which detract from the flatness and ease of manufacture of the antenna. For applications where flatness and simple fabrication is desirable microstrip transmission line is appropriate. Section 3.2 shows why flatness is desirable for a patch antenna mounting to the bottom of a deployable CubeSat solar panel. Microstrip transmission line takes away from the available surface area that could be occupied by antennas, and in some cases the microstrip itself may radiate. The design choice is a trade off, and the choice is application dependant. Microstrip transmission are inherently lossy and imperfect not only due to the inherent copper losses of the transmission medium, but also because no perfectly homogenous substrate exists. With Microstrip transmission lines part of the EM field is in the air and part of the field is between the conductor and ground. We have traction on the problem of knowing microstrip impedance through physical understanding and detailed EM simulations. Formulas such as effective dielectric constant (28) are available based on curve fitting to the results of simulations as mentioned in [31].

5.6 Impedance Matching

Every small change to the geometry of a planar antenna also changes the complex impedance characteristics of the antenna. In order to maximize the simplicity of the design, the antenna can be tuned to the desired frequency using only microstrip and patch geometries. This approach avoids the need for additional components such as passive capacitors and inductors to create an impedance matching network. However, if there are manufacturing defects in the patch antenna geometry then the impedance match will be disturbed.

The most impactful parameters are those of the patch itself. In this design we are using rectangular patches. For rectangular patch, length and width can be calculated using equations 27 to 31 [30]. These equations result in dimensions for an antenna as shown in figure 32.

$$W = \frac{c}{2f_o\sqrt{\frac{(\varepsilon_r + 1)}{2}}} \; ; \tag{27}$$

$$\varepsilon_{eff} = \frac{\varepsilon_r + 1}{2} + \frac{\varepsilon_r - 1}{2}\left[1 + 12\frac{h}{W}\right]^{-\frac{1}{2}} ; \tag{28}$$

$$L_{eff} = \frac{c}{2f_o\sqrt{\varepsilon_{eff}}} \; ; \tag{29}$$

$$\Delta L = 0.412h\frac{\left(\varepsilon_{eff} + 0.3\right)\left(\frac{W}{h} + 0.264\right)}{\left(\varepsilon_{eff} - 0.258\right)\left(\frac{W}{h} + 0.8\right)} \; ; \tag{30}$$

$$L = L_{eff} - 2\Delta L \; ; \tag{31}$$

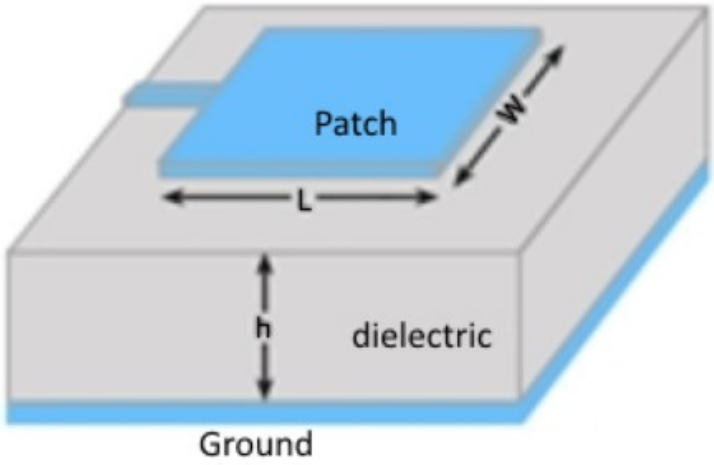

Figure 32 - Basic patch antenna diagram

The width of the patch is less critical than the length and dielectric thickness. Rectangular patch width affects radiation resistance (and therefore radiation efficiency) and impedance and can be used to tune the antenna [30]. For a rectangular patch the feed point affects impedance according to equation 32 [30].

$$R_{in} = R_r cos^2(\frac{\pi x_f}{L}); \quad (32)$$

Where x_f is the inset distance from the radiating edge, L is patch length, and R_r is the input impedance if the patch was fed at the edge. Noting that L is comparable to a half wavelength, for R=L/4 we can see that an eighth wavelength inset feed reduces the input impedance by 50%. Once the patch dimensions are determined, the microstrip transmission line must be designed to feed the patch. The microstrip can be connected to the patch using inset feed. The width and length of the inset affect the impedance. Figure 33 shows an example of inset feed.

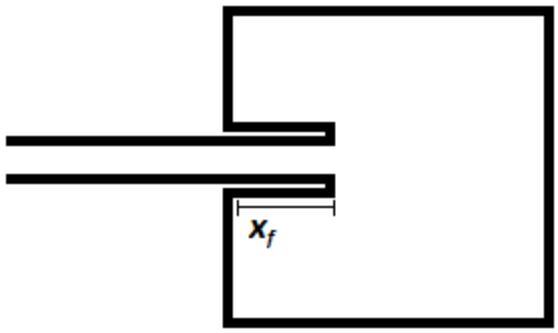

Figure 33 - Inset feed of a patch antenna.

The width of microstrip transmission line is an extremely sensitive parameter. Low impedance lines are wide, while high impedance lines are narrow. Depending on the substrate thickness and the electric permittivity of the substrate the trace width will have a different impedance. Narrow microstrip line is delicate and detracts from the robustness of the antenna feed network because the antenna becomes vulnerable to mechanical or chemical wear. A microstrip trace cross section is shown in figure 34.

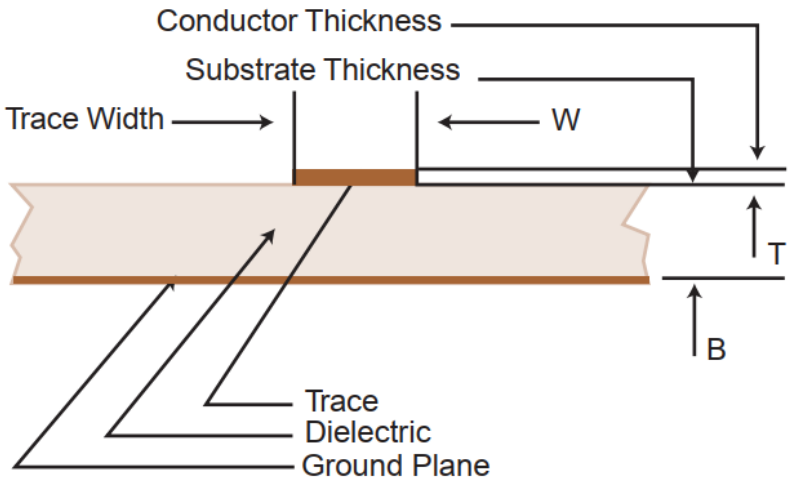

Figure 34 - Microstrip Trace Cross Section (Credit to Rogers Corporation)

To calculate the characteristic impedance of a microstrip transmission line, follow the following steps [32]:

1. Calculate width according to thickness for a homogeneous medium. Here U is the ratio of trace width to substrate thickness, e is the base of the natural logarithm, and T is the ratio of conductor thickness to substrate thickness.

$$U_1 = U + \frac{T \ln[1+\frac{4e}{T}\tan^2((6.517U)^{0.5})]}{\pi}; \quad (33)$$

2. Calculate width corrected for a mixed media

$$U_r = U + \frac{(U_1-U)(1+\frac{1}{\cosh((\varepsilon_r-1)^{0.5})})}{2}; \quad (34)$$

3. Calculate intermediate value Y,

$$Y = \frac{\varepsilon_r+1}{2} + \frac{\varepsilon_r-1}{2}(1+\frac{10}{U_r})^{-(A_u \cdot B_{er})}; \quad (35)$$

$$A_u = 1 + \frac{\ln(\frac{{U_r}^4+\frac{{U_r}^2}{2704}}{{U_r}^4+0.432})}{49} + \frac{\ln((\frac{U_r}{18.1})^3+1)}{18.7}; \quad (36)$$

$$B_{er} = 0.564(\frac{\varepsilon_r-0.9}{\varepsilon_r+3})^{0.053}; \quad (37)$$

4. Calculate characteristic impedance at 0 frequency Z_0. Here η_0 is 376.73

$$Z_0 = \frac{Z_\alpha(U_r)}{Y^{0.5}}; \quad (38)$$

$$Z_\alpha(x_{arg}) = \frac{\eta_0 \ln\left(\frac{\left(6+(2\pi-6)e^{-\left(\frac{30.666}{x_{arg}}\right)^{0.7528}}\right)}{x_{arg}} + \left(\frac{4}{x_{arg}^2}+1\right)^{0.5}\right)}{2\pi}; \quad (39)$$

5. Calculate effective permittivity at 0 frequency

$$\varepsilon_{eff,0} = Y\left(\frac{Z_\alpha(U_1)}{Z_\alpha(U_r)}\right)^2; \quad (40)$$

6. Calculate filling factor P. Here T_{mm} is the substrate thickness in mm.

$$P_1 = 0.27488 + U[0.6315 + 0.525(0.0157 f_{GHz} T_{mm} + 1)^{-20}] - 0.065683 e^{8.7513U}; \quad (41)$$

$$P_2 = 0.33622\left(1 - e^{-0.03442\varepsilon_r}\right); \quad (42)$$

$$P_3 = 0.0363 e^{-4.6U}\left(1 - e^{-\left(\frac{f_{GHz} T_{mm}}{38.7}\right)^{4.97}}\right); \quad (43)$$

$$P_4 = 2.751\left(1 - e^{-\left(\frac{\varepsilon_r}{15.916}\right)^8}\right) + 1; \quad (44)$$

$$P = P_1 P_2 [f_{GHz} T_{mm}(0.1844 + P_3 P_4)]^{1.5763}; \quad (45)$$

7. Use P to calculate the effective permittivity at frequency f

$$\varepsilon_{eff,f} = \varepsilon_r - \frac{\varepsilon_r - \varepsilon_{eff,0}}{1+P}; \quad (46)$$

8. Use the result from 7 to calculate characteristic impedance at frequency f

$$Z_{0,f} = Z_0 \left(\frac{\varepsilon_{eff,0}}{\varepsilon_{eff,f}}\right)^{0.5} \left(\frac{\varepsilon_{eff,f}-1}{\varepsilon_{eff,0}-1}\right); \quad (47)$$

5.7 Patch Antenna

Based on the available area on the underside of the satellite (described in chapter 3) and the orbital motion (described in chapter 2) a patch antenna is designed and subsequently evaluated for performance. The design process is iterative and follows a natural evolution. Beginning with requirements imposed on the design, a single patch is created and evaluated. Based on the first iteration more complex designs are created using patch antenna arrays. These designs are novel because of the design requirements set as goals before creating them. Many patch antennas use multiple layers of copper clad laminate to use probe or stripline or aperture feed, all of which detract from the goal of producing a very thin antenna that can conform to the underside of a CubeSat panel. Additionally, the overall dimension is such that the antenna can fit on a 2U CubeSat deployable panel.

5.7.1 Design Requirements

- The antenna shall be naturally impedance matched to 50 Ohms without the use of a matching network.
    - This simplifies the difficulty of fabrication and testing and brings a reduction of the final complexity and weight. The absence of SMT components also maintains the flat profile.
- The antenna shall be constructed of a single layer of RT/duroid 5870
    - This microfibre reinforced PTFE laminate is appropriate for usage in space.
    - It is intended for microstrip and stripline applications
    - Ease of fabrication and lightweight solution
    - Substrate is useful up to Ku-band [33]
- The patch shall be fed using inset microstrip line

    - Due to the geometry of the satellite the antenna will conform better with a fully planar configuration
- The antenna shall not exceed the dimensions of 90 mm in width and 190mm in length
    - This is reasonable for a 2U or 3U CubeSat
- The antenna shall support circular polarization (CP) to minimize polarization loss factor
    - Due to the motion and orientation of the satellite relative to the ground station it is difficult to ensure the alignment of linearly polarized antennas. Therefore, it is common to use CP antennas for aerospace applications.

5.7.2 Anechoic Chamber Test Equipment

The anechoic chamber consists of two antenna mounts which are motorized and a chamber with RF energy absorbing foam. The basic setup is shown in figure 35.

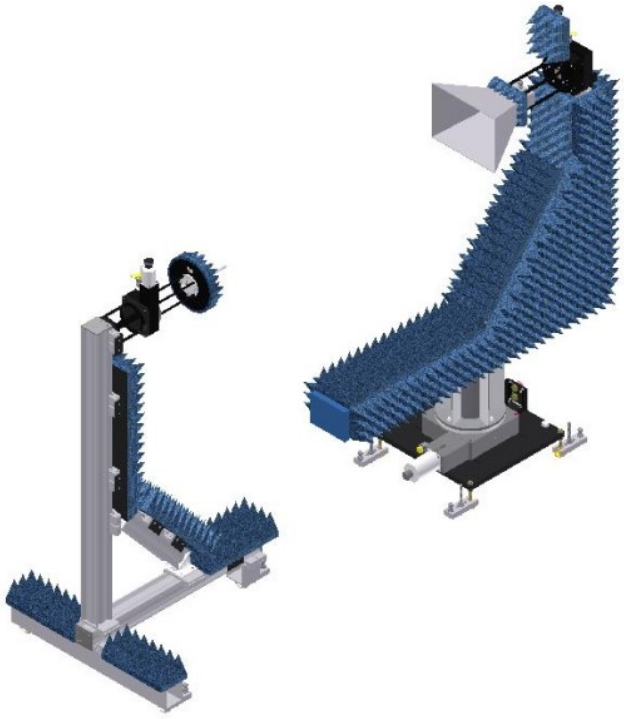

Figure 35 - NSI RF Anechoic Test Chamber Setup

Both antenna masts can rotate the antenna around the Phi axis. Only the mast for the antenna under test (AUT) can rotate around the Theta axis. The Phi and Theta axis are shown in figure 36.

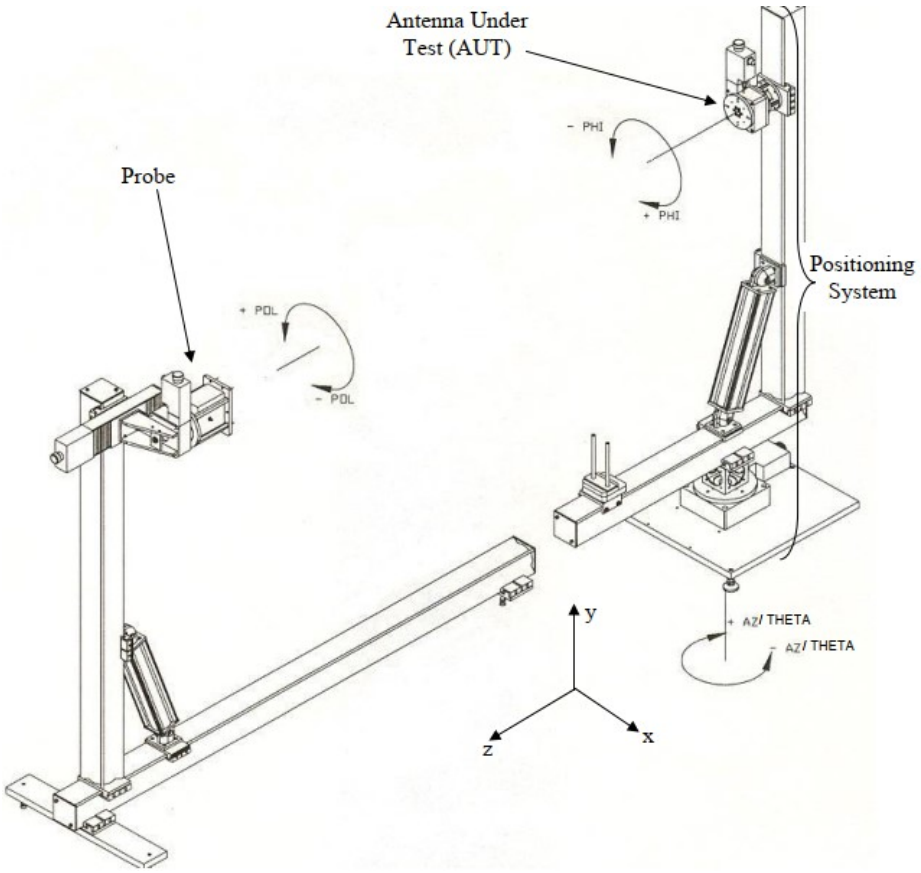

Figure 36 - Anechoic Chamber Axes of Rotation. Credit to NSI-MI.

The anechoic chamber is suitable for tests above 1 GHz based on the size of the chamber and the specification of the manufacturer. The distance between antenna mounts is 280 cm. For low frequency tests below 400 MHz a larger chamber and different probe is required to avoid reflections polluting the measurements. In addition, the proprietary software from NSI Inc. builds the antenna radiation pattern based on near field assumptions which may not hold below a certain frequency. The spikey foam material exists to help suppress RF reflections. Figure 37 shows the situation where scattering effects could distort the measurement.

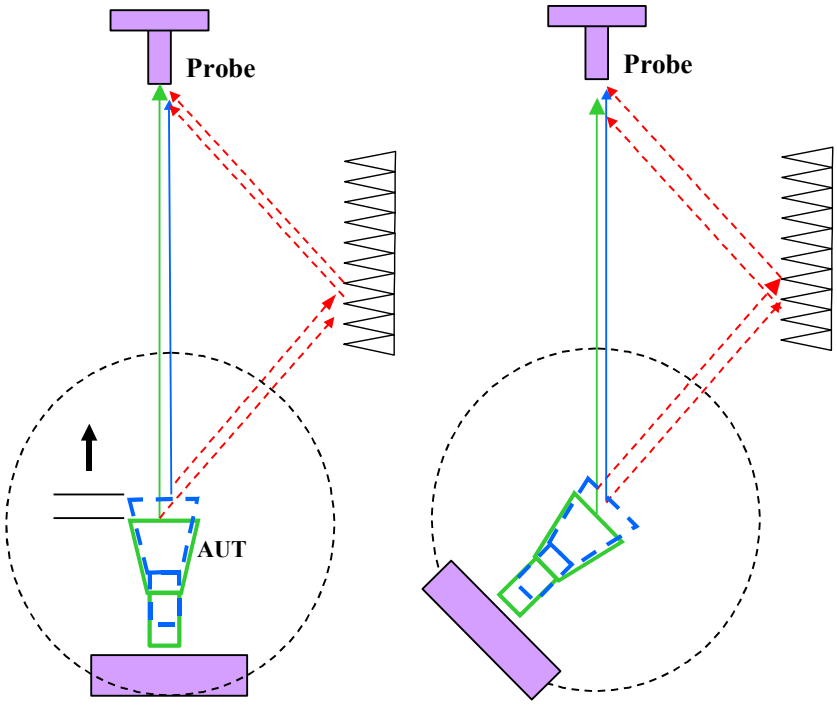

Figure 37 - RF Reflections and Suppression Material

During a period of renovations in 2015-2016 some parts of the system were disconnected and moved to another building. In addition, the system is over 15 years old, and although it still works in some respects it requires calibration and retrofit. As such the Phi axis of rotation does not move for the full range of motion. The chamber may still be used to partially measure the radiation pattern and characteristics of an antenna. The anechoic chamber system is capable of calibrating the stepper motors by indexing across the range of movement. The chamber must be indexed before and after each test.

5.7.3 Design and Test of a Single Patch

A single element patch antenna with microstrip inset feed was designed and fabricated. The outline of the antenna is shown in figure 38.

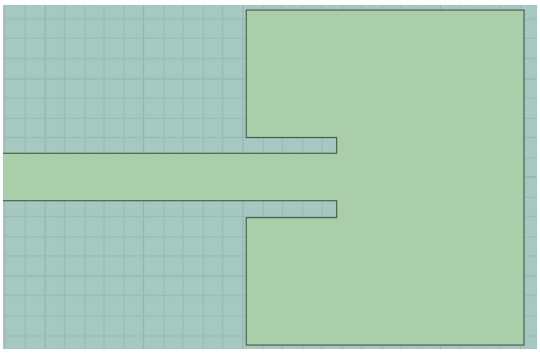

Figure 38 - Single Patch Antenna

This antenna design serves as a baseline for realizable performance and as a basic confidence building exercise. Using HFSS is not trivially simple and producing a basic design is a good first step to learn the software. Based on intuitive estimation, the gain of a single element patch antenna can be predicted as approximately 6dB. Firstly, 3dB comes from the ground plane resulting in a hemisphere pattern. Secondly the rectangular patch is equivalent to two slot antennas, bringing additional directivity by acting as a two-element array. The simulation predicts even more gain at a maximum of 7.9dB, but this is not realistic to expect. The simulated gain pattern is shown in figure 39 and from the side in figure 40. As expected, the radiation pattern is roughly hemispherical.

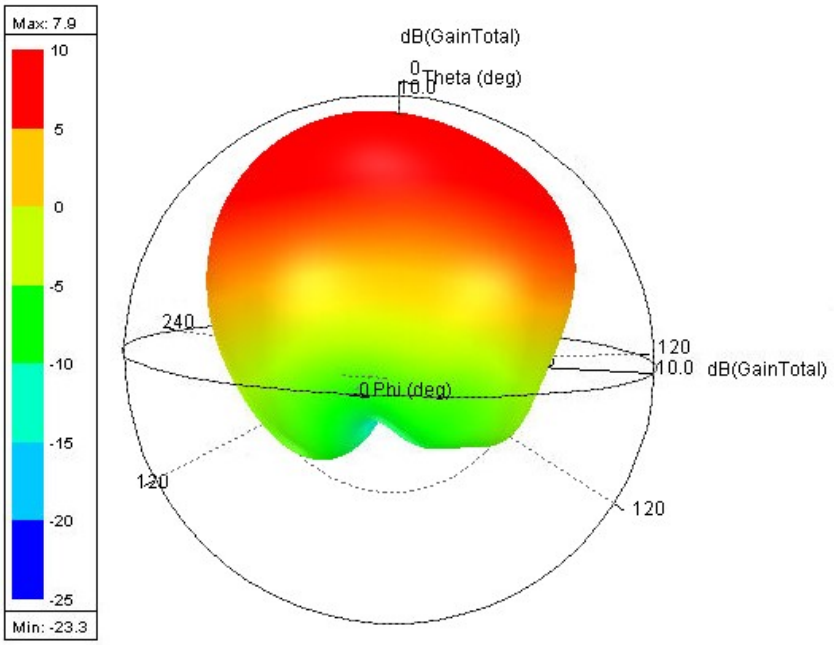

Figure 39 – Radiation Pattern of Single Patch Antenna 0º

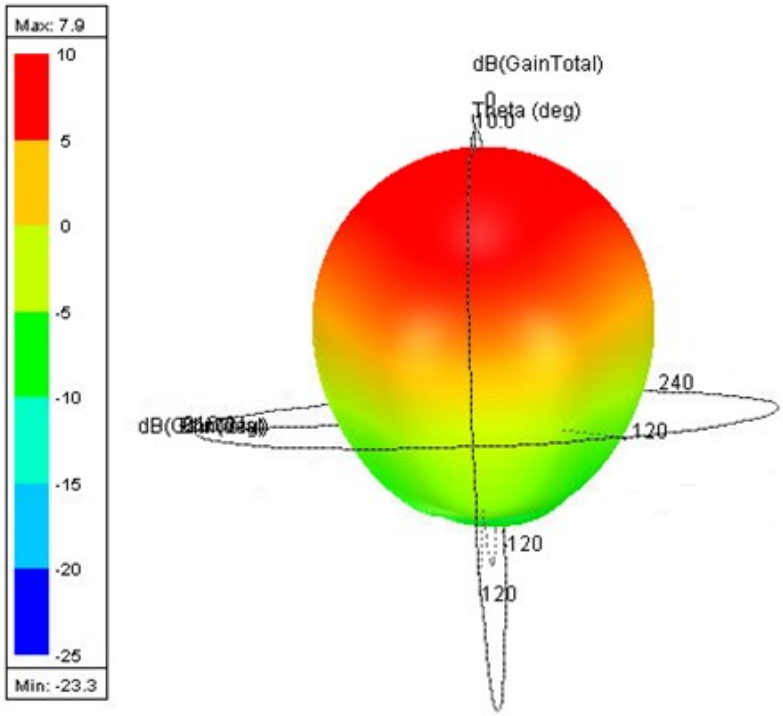

Figure 40 - Radiation Pattern of Single Patch Antenna 90º

The patch dimensions are designed to resonate at 3.4 GHz. The S parameter plot in figure 41 shows the predicted low impedance at the resonant frequency.

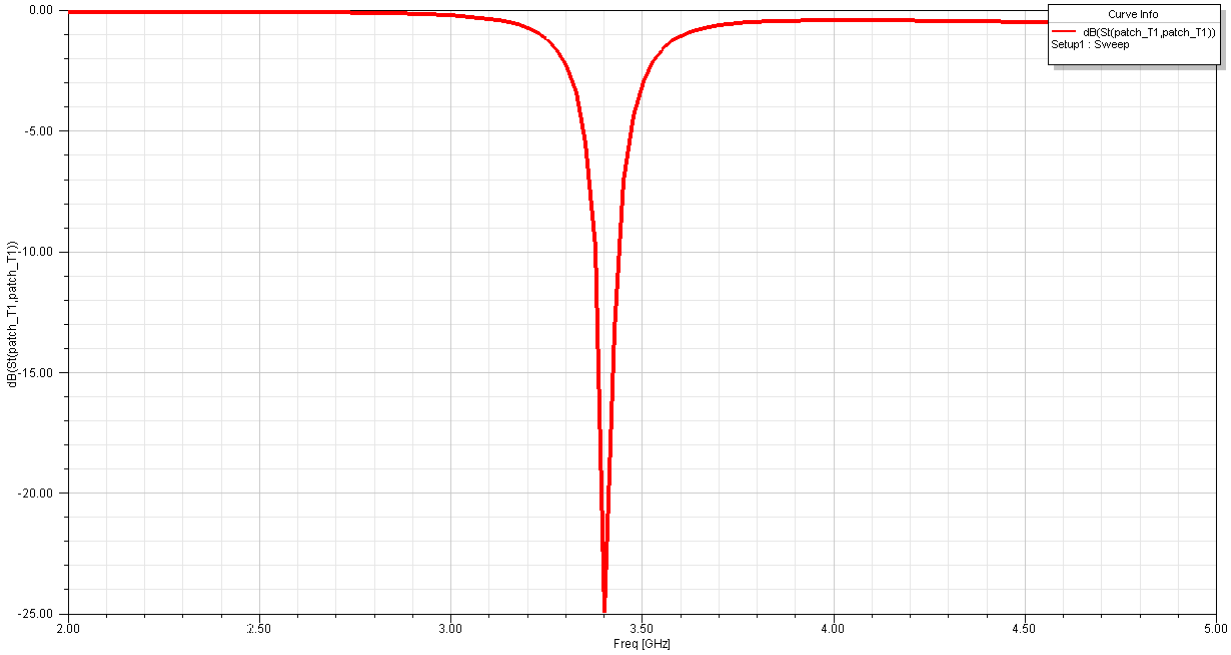

Figure 41 - S Parameter of Single Patch Antenna

The VSWR is shown in figure 42 and shows that the antenna will have low reflections at the target frequency

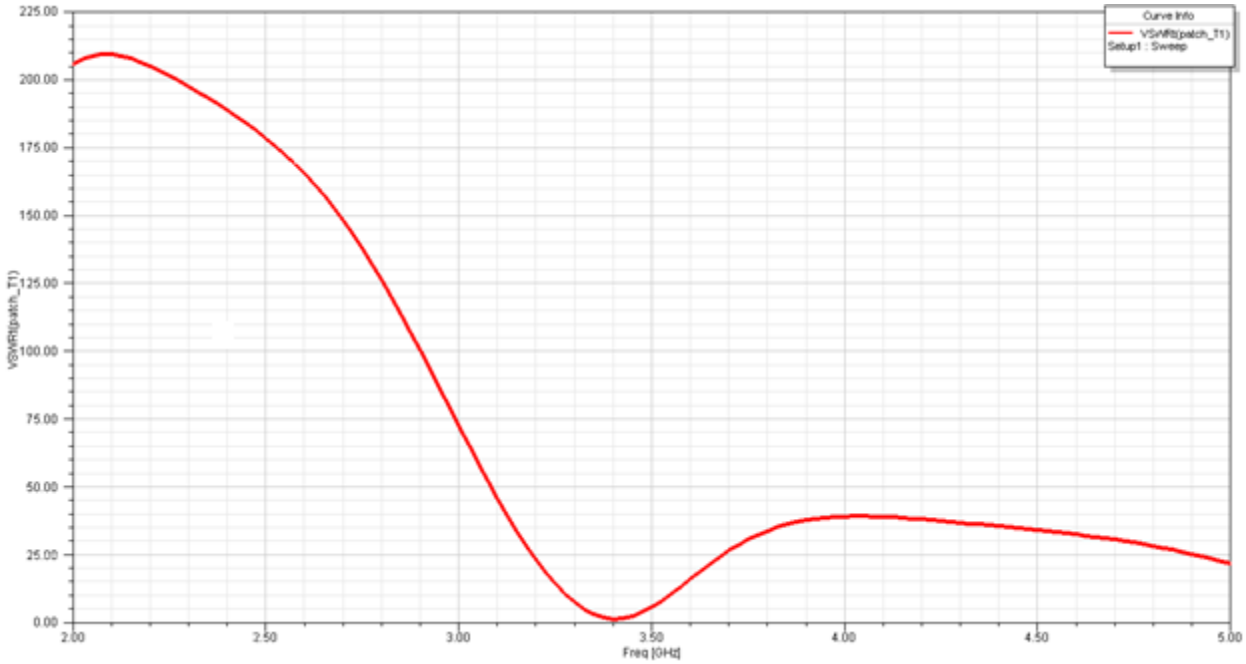

Figure 42 - VSWR of Single Patch Antenna

The following EAGLE (version 9.2.2) script will generate the 2-layer board layout which can be used to mill the antenna. The script can be run by entering “script” into the EAGLE command line and selecting the file by name.

```
GRID MM 0.1 10;
LAYER 20;
WIRE .1 (0 0) (0 56);
WIRE .1 (0 56) (40 56);
WIRE .1 (40 56) (40 0);
WIRE .1 (40 0) (0 0);
LAYER 16;
WIRE .1 (0 0) (0 56);
WIRE .1 (0 56) (40 56);
WIRE .1 (40 56) (40 0);
WIRE .1 (40 0) (0 0);
POLYGONIZE (0 0);
LAYER 1;
CHANGE WIDTH .1;
WIRE 'a' (17.61 0) (22.39 0);
WIRE 'a' (17.61 0) (17.61 34.5);
WIRE 'a' (17.61 34.5) (15.96 34.5);
WIRE 'a' (15.96 34.5) (15.96 25.4);
WIRE 'a' (15.96 25.4) (3.05 25.4);
WIRE 'a' (3.05 25.4) (3.05 53.4);
WIRE 'a' (3.05 53.4) (36.95 53.4);
WIRE 'a' (36.95 53.4) (36.95 25.4);
WIRE 'a' (36.95 25.4) (24.04 25.4);
WIRE 'a' (24.04 25.4) (24.04 34.5);
WIRE 'a' (24.04 34.5) (22.39 34.5);
WIRE 'a' (22.39 34.5) (22.39 0);
POLYGONIZE (17.61 0);
RATSNEST;
```

The board layout for the antenna is shown in figure 43. Antennas are fabricated on Rogers RT/duroid 5870 laminate with thickness 1.575 mm.

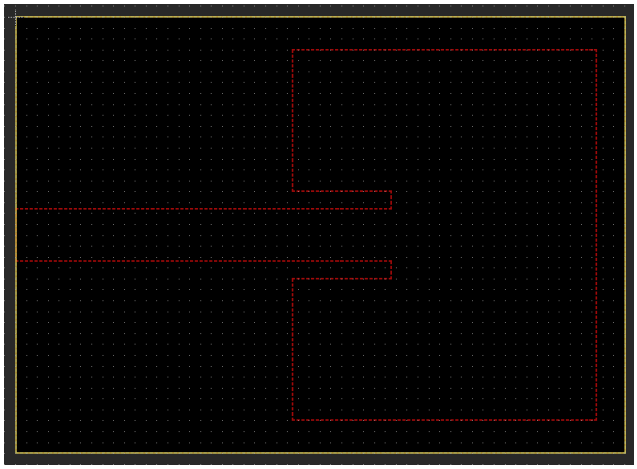

Figure 43 - EAGLE CAD Board Layout of Patch Antenna

After milling the antenna can be easily used with a side mount SMA adapter. The ground plane is soldered to the body of the adapter and the center pin is soldered to the microstrip transmission line. The antenna is shown in figure 44.

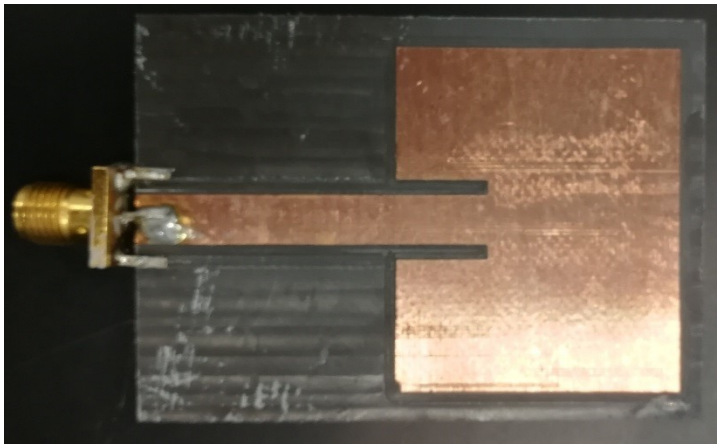

Figure 44 - Fabricated Single Patch Antenna

By measuring this antenna on a network analyzer, the realized impedance can be compared to the simulations. A measurement of S11 Parameter is shown in Figure 45. The measured Smith chart is shown in Figure 46. The measured VSWR is shown in Figure 47. The realized impedance is

an acceptable match and demonstrates that the characteristic impedance can be controlled by the geometry of the microstrip, inset feed, and patch.

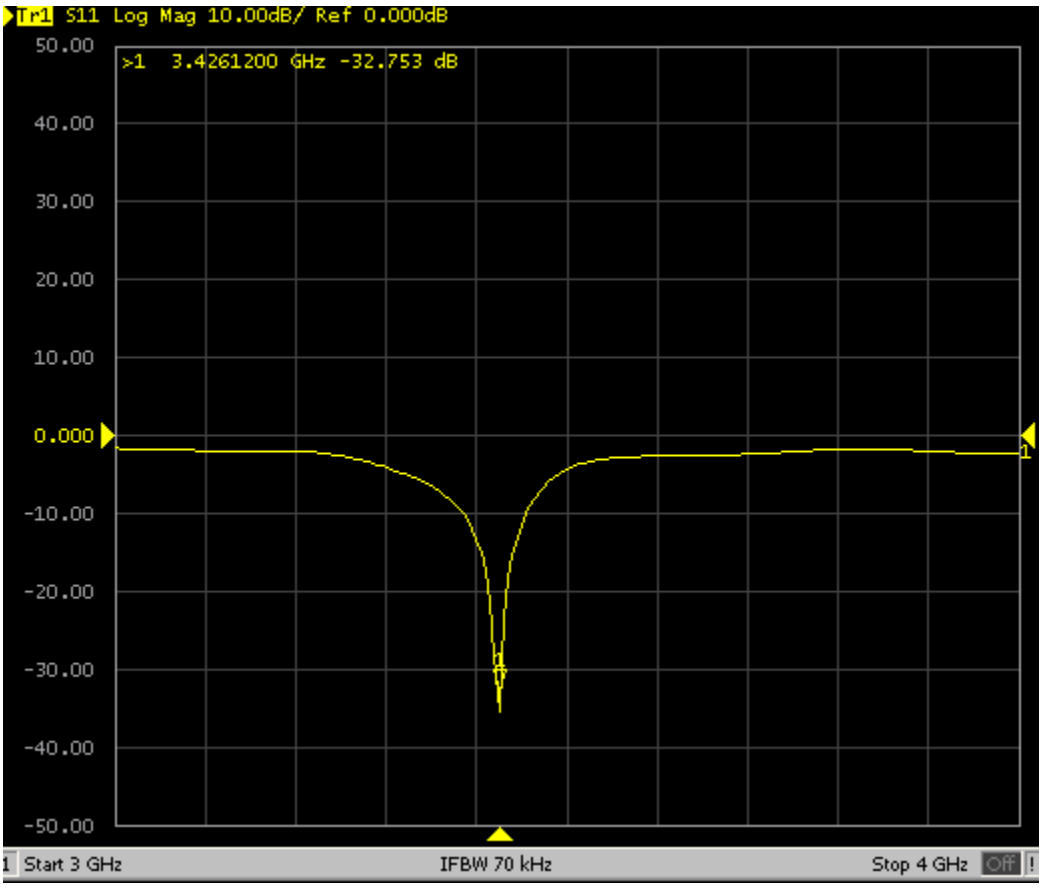

Figure 45 - Network Analyser S Parameter Measurement

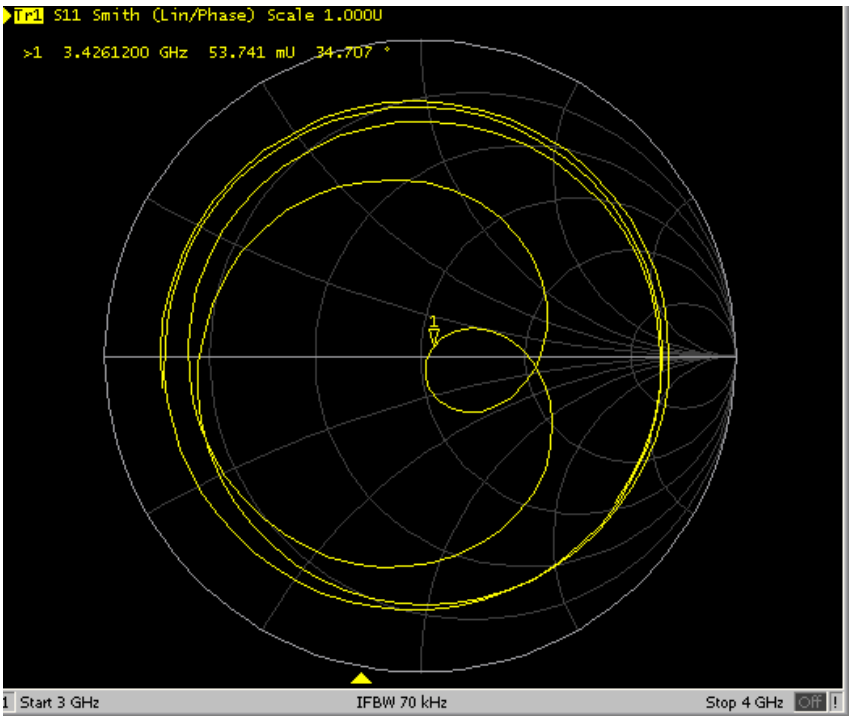

Figure 46 - Measured Smith Chart of Single Patch Antenna

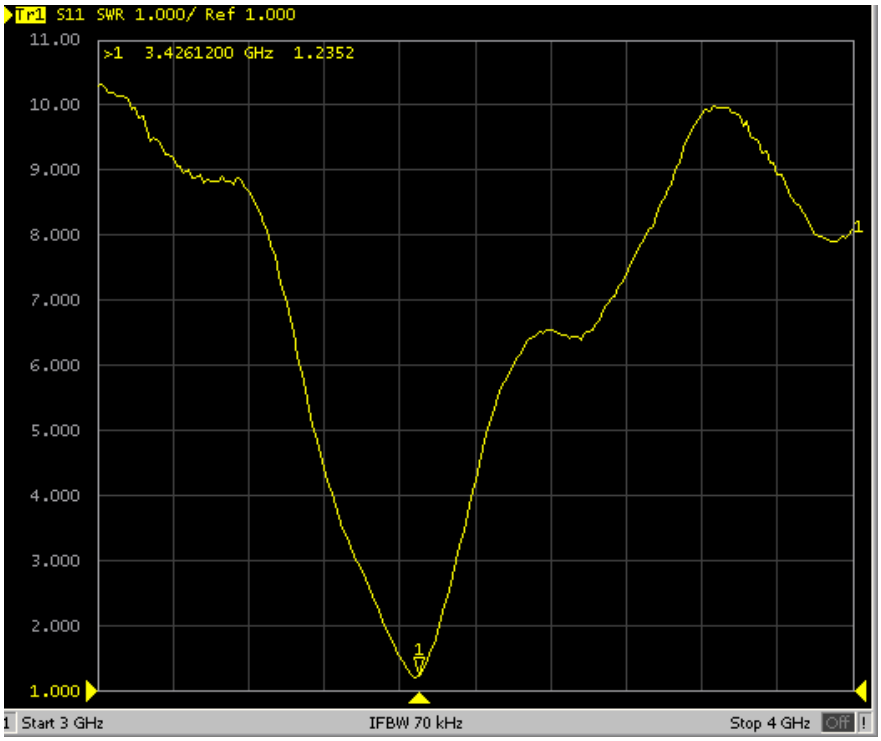

Figure 47 - Measured VSWR of Single Patch Antenna

Using the anechoic chamber, the radiation pattern of the antenna can be compared to the simulation. The near field horizontal cross section is shown in Figure 47. It confirms that the antenna radiates normal to the patch, and that the radiation pattern is very broad at 120^{o} HPBW. Figure 48 also shows that the power output of the network analyzer is unbalanced, since the right half is systematically 2 dB lower despite the fact that it is a symmetric antenna. The Tecom brand log periodic antenna acting as the probe has gain of 7.5dBi. The maximum output power of the Agilent brand 8722ES network analyzer is -5dBm or -25dBW. Losses such as line attenuation and insertion loss are unknown. By assuming no losses, we can use the link budget to estimate the gain of the antenna under test (AUT). Using equation (48):

$$R_{dB} = T_{dB} + G_{tX} + G_{rX} + Losses; \tag{48}$$

$$-5 = -25 + G_{tX} + 7.5 + Losses;$$

We can see that the AUT has gain of 12.5dB. Obviously, some unaccounted losses contribute to this large value. The gain of the patch antenna is supposed to be 8dB at most leaving 4.5dB for losses.

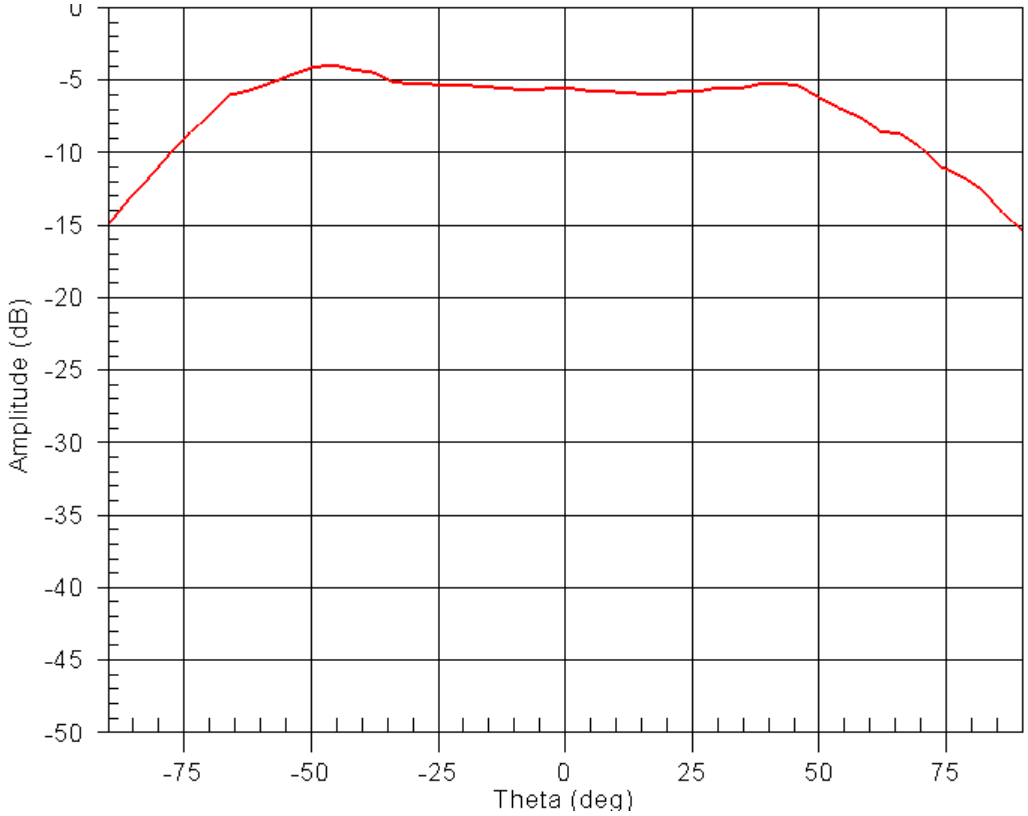

Figure 48 - Measured Radiation Pattern of Single Patch Antenna Theta Axis

The measured near field vertical cross section is shown in Figure 49. Due to the rotation limit of the phi axis of the test equipment, the vertical cross section shows limited information (90º instead of 180º). Where the equipment shows the antenna is at -45º it is in reality mounted at 0º. Where the equipment shows the antenna is rotated to 45º it is in reality rotated 90º in a cross polarized position. This measurement from the anechoic chamber adequately demonstrates that the antenna is linearly polarized and in a cross polarized position there is a severe signal fade of -43dB. The polarization loss factor is one which further designs will mitigate. Polarization loss comes from misalignment of linear polarization antennas. Linear polarization means that the E field component of the radiation is not rotating. If the E field is horizontal when transmitted from the linearly polarized antenna it propagates that way and arrives at the other antenna horizontally. If the receiving antenna is vertically polarized there is polarization loss factor (PLF)

due to cross polarization, which causes a severe signal fade such as the 43 dB loss demonstrated earlier. For antennas where the orientation can not be well controlled the circular polarization can be employed. Circular polarization occurs when the E field is rotating as it propagates. It can be thought of as two orthogonal EM waves of equal amplitude that are 90° out of phase. A technique can be seen in [36] whereby two or more orthogonal linear antenna elements can be fed with current phase shifted by 90° to produce CP. This technique is used later in this paper in rectangular patch antenna arrays to mitigate PLF.

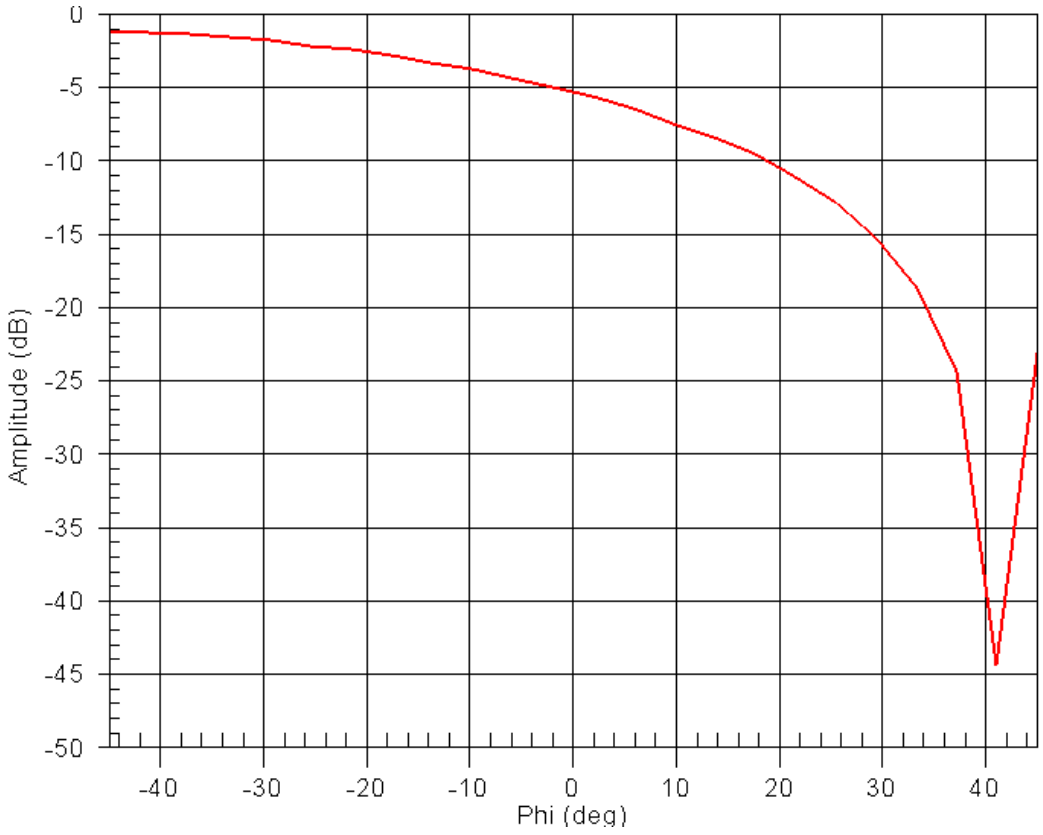

Figure 49 - Measured Radiation Pattern of Single Patch Antenna Phi Axis

5.7.4 Design of Four Element Array

By arranging multiple patch elements in an array, the directivity can be increased. In the second design quarter wave impedance transformers are utilized to allow the patch feed to be at 100 Ohms. This feed network presents 100 Ohm microstrip feed lines to the patches. It utilizes three power dividers and two quarter wave impedance transformers. By matching two 100 Ohm microstrip transmission lines in parallel to one 50 Ohm microstrip transmission line, the characteristic impedance is preserved, and the feed network can effectively carry a 3.4 GHz signal. The feed network and patch array are shown in figure 50. The expected size of the inset feed slots is much smaller than the size which delivered a matching impedance. However, based on the simulation results this geometry still yields a good impedance match.

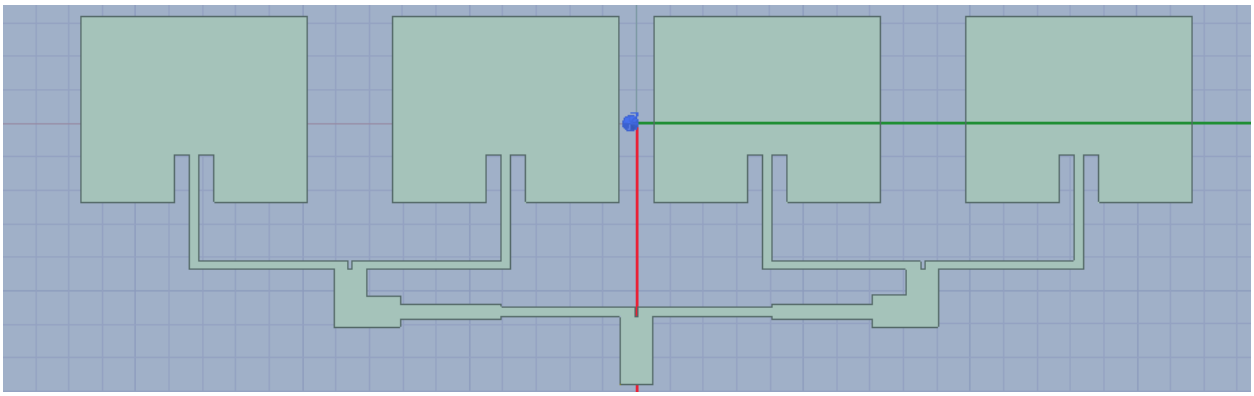

Figure 50 - Geometry of Linear Patch Array

The radiation pattern for the array is shown in figure 51. The maximum gain is simulated to be 11.8dB. Viewed from 0º Phi the radiation pattern can be described as narrow with small sidelobes. Rotated to the 90º Phi axis the radiation pattern is equally broad compared to the single patch.

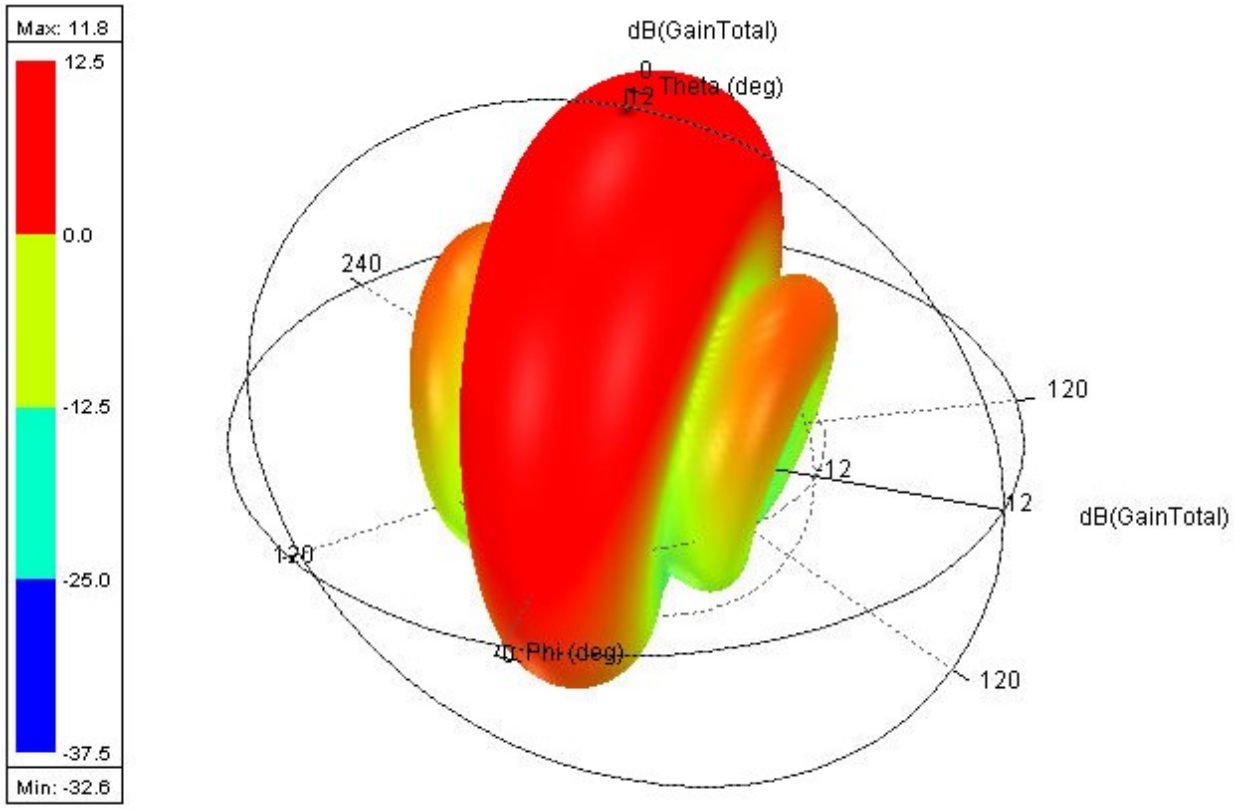

Figure 51 - Simulated Radiation Pattern of Linear Patch Array

The impedance characteristics are shown in figure 52, figure 53, and figure 54, which show the S11 parameter, VSWR, and Smith chart respectively. The patch array is well matched to the target frequency.

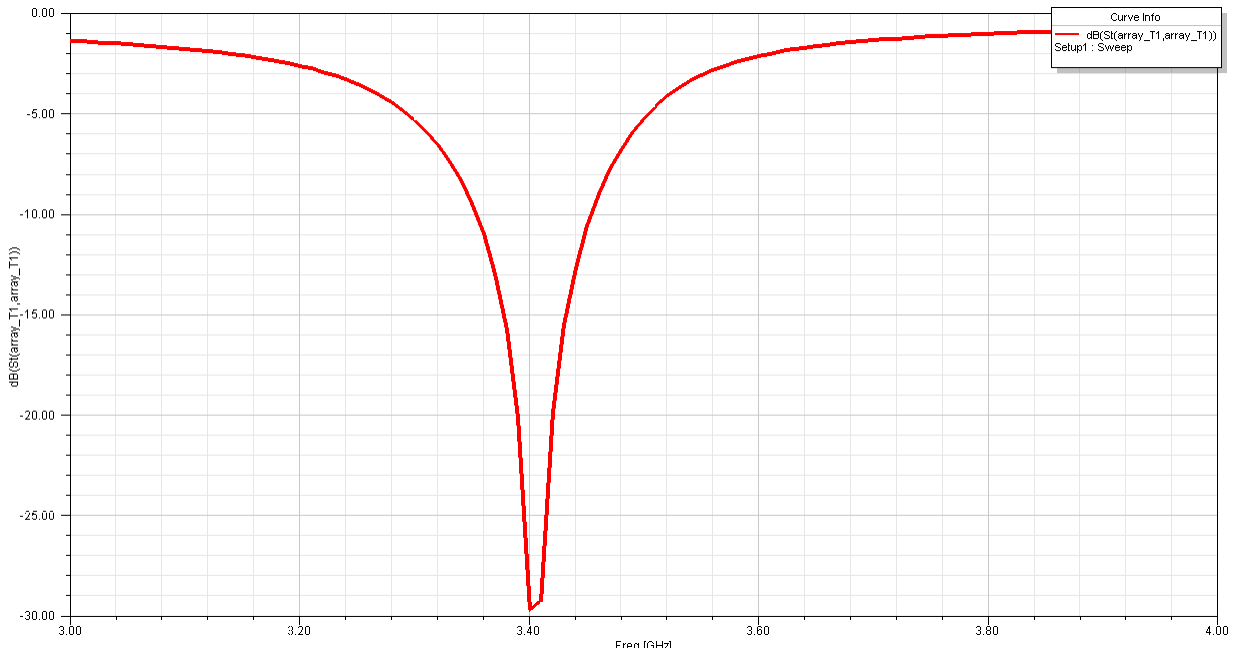

Figure 52 - Simulated S Parameter of Linear Patch Array

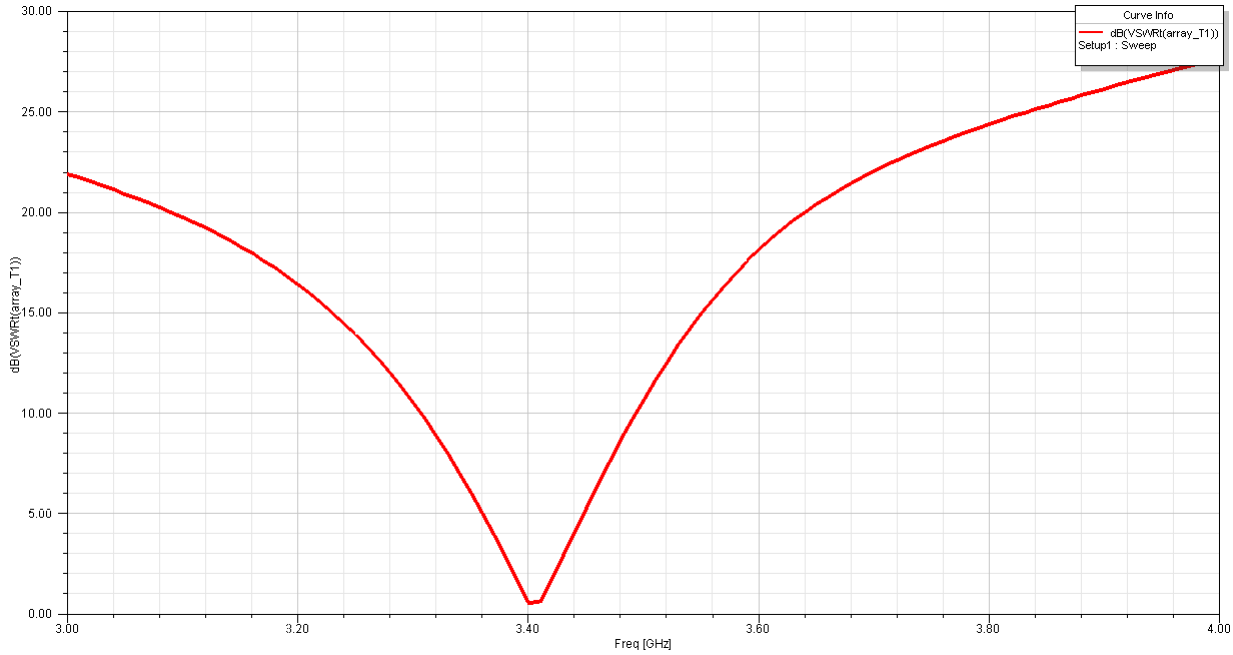

Figure 53 - Simulated VSWR of Linear Patch Array

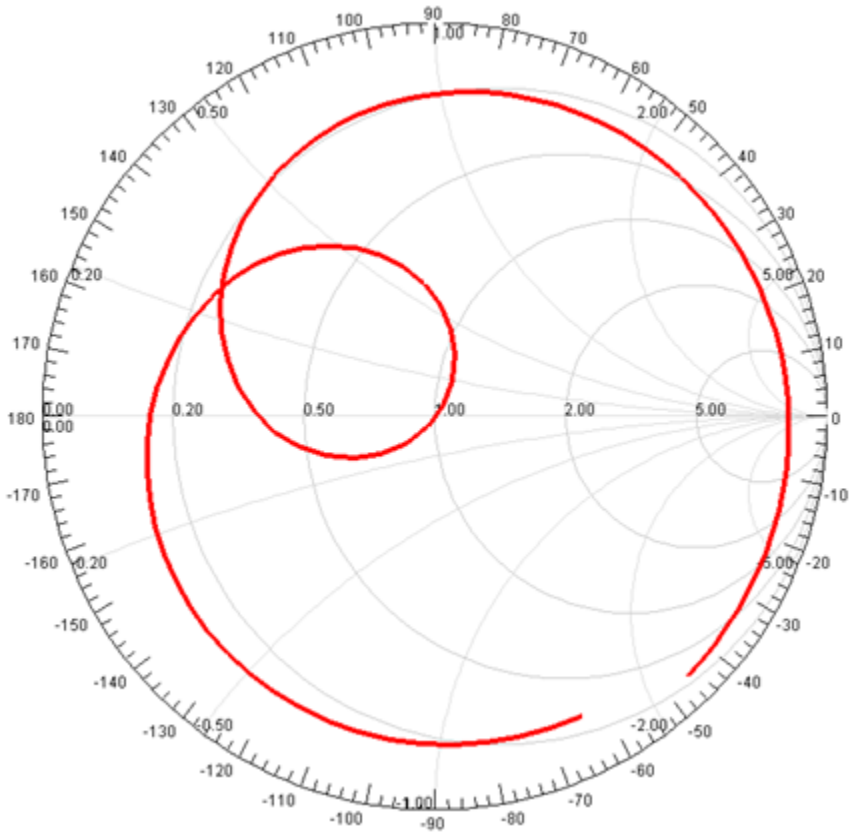

Figure 54 - Simulated Smith Chart of Linear Patch Array

Since this patch array is linearly polarized I did not fabricate it and moved on to the next iteration. This 4-element could have too much gain resulting in a narrow beamwidth for the intended application of LEO CubeSat communications. The narrow beamwidth would limit the communication window of the satellite. If the satellite could support two 4-element patch arrays at right angles the beam pattern issue could be mitigated. This would require additional mixing or switching to accomplish antenna diversity. An alternative strategy is to implement an array with circular polarization and a wider beamwith to tackle the issues of polarization loss and the potential for a short communication window. The next iteration of design incorporates rotated elements to achieve CP polarization and alters the element spacing for a wider beamwidth.

5.7.5 Design and Test of Circularly Polarized 4 Element Array

Linear arrays of patch antennas are still susceptible to deep fades caused by polarization loss. For applications where the relative orientation of antennas is not known it is preferable to utilize circular polarization on one or both ends of the radio link. The array geometry is shown in figure 55 and is fabricated using the same methods as the single patch described earlier. This array uses sequentially rotated feed network as described in [32] and [36]. This technique uses the angular relation between elements along with phase shift to generate CP. Two orthogonal elements generate orthogonally polarized fields, and a 90^{o} phase shift is added to delay one behind the other. Upon review of the geometry it can be seen that the vertical and horizontal elements are very close, which may result in undesirable mutual coupling between antennas. In addition, no inset feed slots are present which may reduce the radiated power of the patch because of impedance mismatch. While the characteristic impedance of the array as a whole is 50 Ohms, the feed point of each antenna may be mismatched leading to undesirable effects. Next, the antenna measurements are discussed in figures 56 to 60.

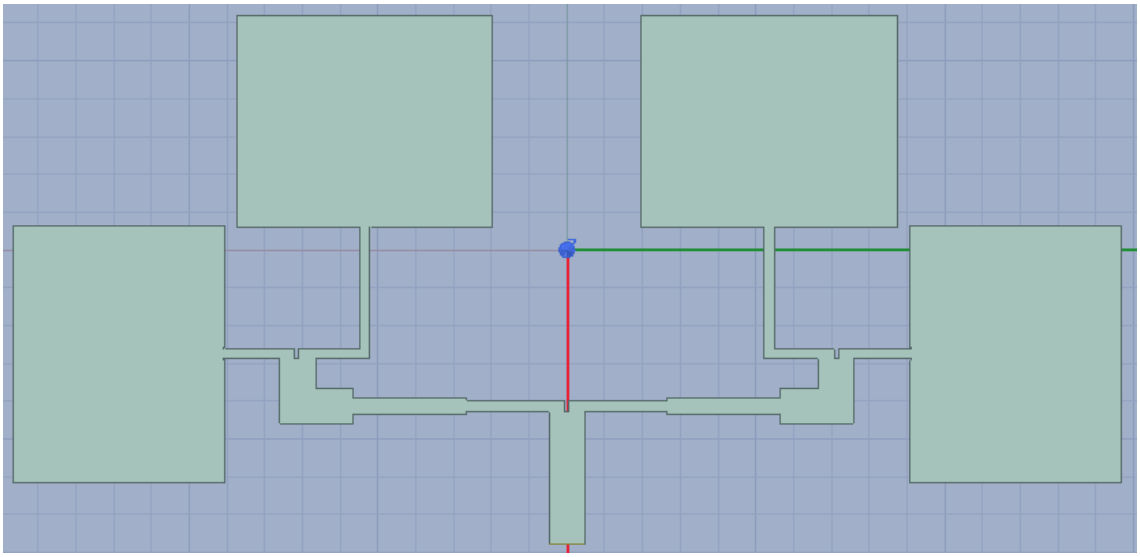

Figure 55 - Geometry of CP Patch Array

The radiation pattern consists of two main lobes. It appears to reach nearly 0dB in between. The beam width is wide but irregular. The gain is low for an array of 4 elements.

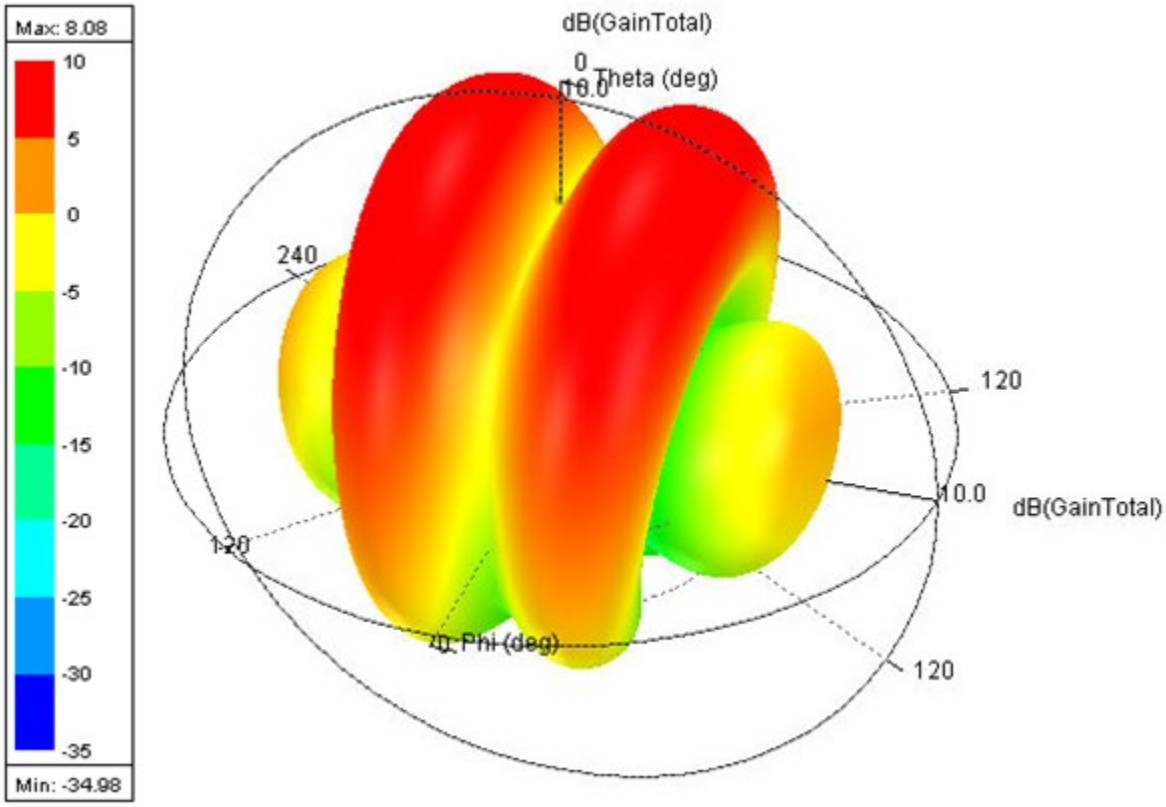

Figure 56 - Simulated Radiation Pattern of CP Patch Array

The next figure shows the RHCP radiation pattern. It is asymmetric but this is not concerning with regard to performance.

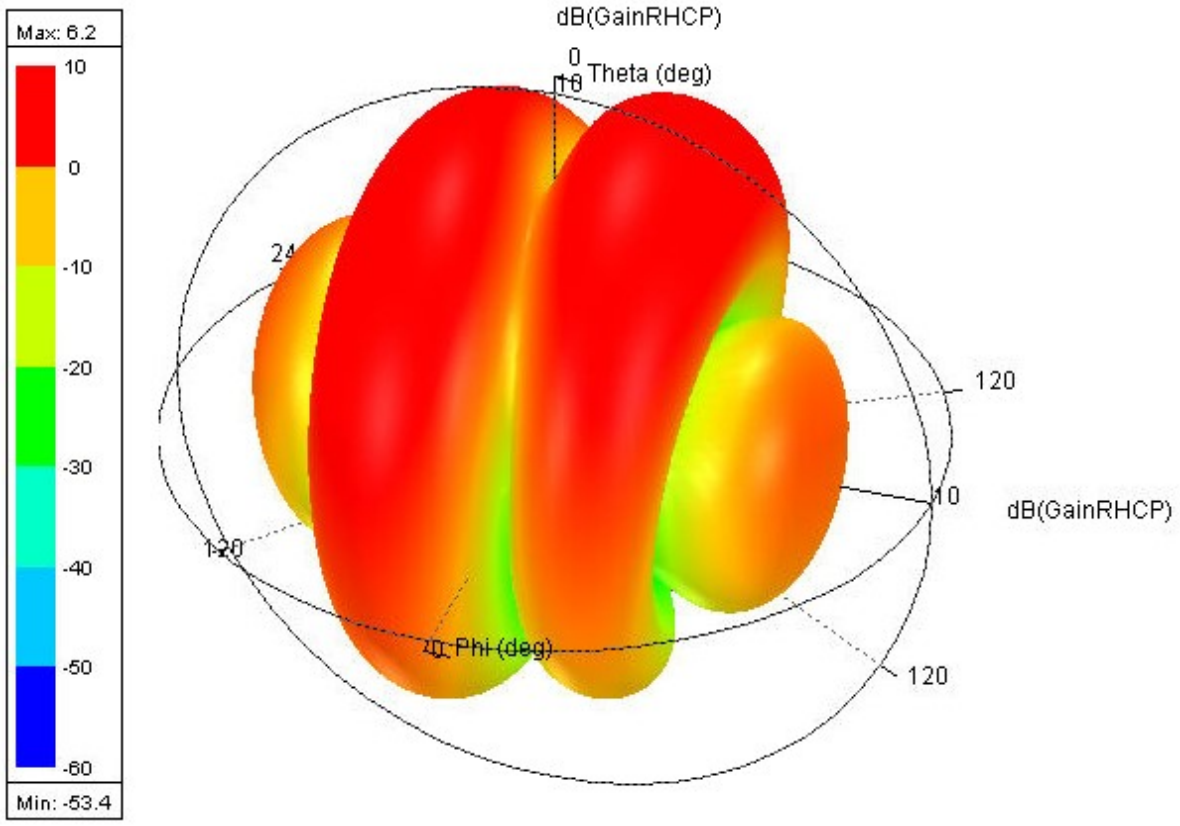

Figure 57 - Simulated RHCP Radiation Pattern of CP Patch Array

Because of the sequentially rotated feed network of the elements this antenna is dual polarized, both LHCP and RHCP. Only one handedness of CP is really required for this application.

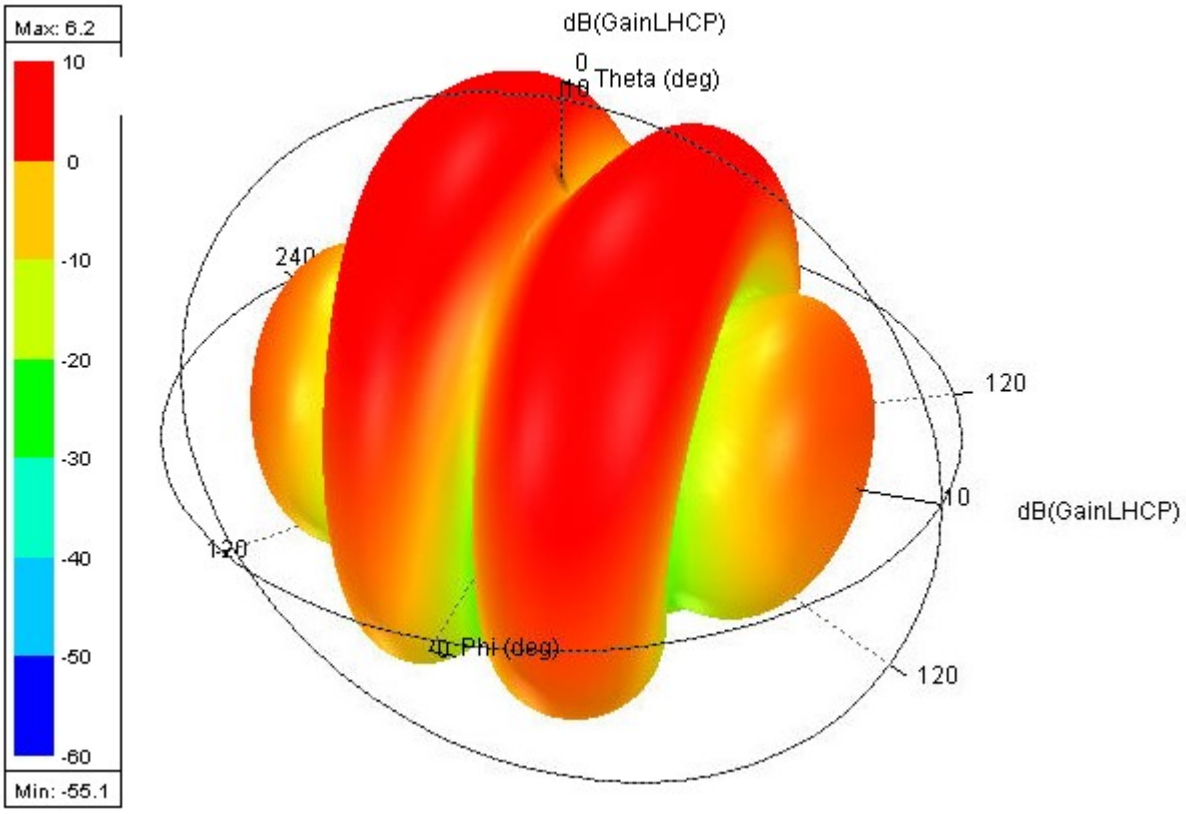

Figure 58 - LHCP Radiation Pattern of CP Patch Array

The array predicts a good impedance match in simulation which can be seen in figures 59 to 61.

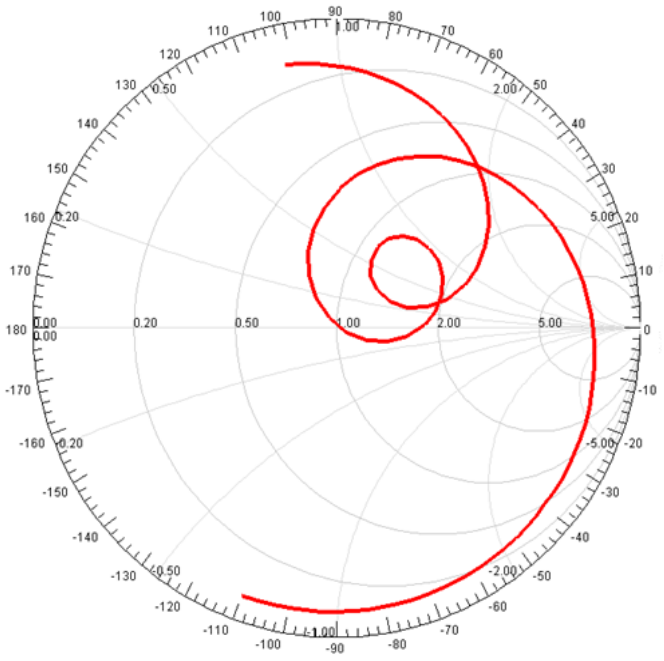

Figure 59 – Simulated Smith Chart of CP Patch Array

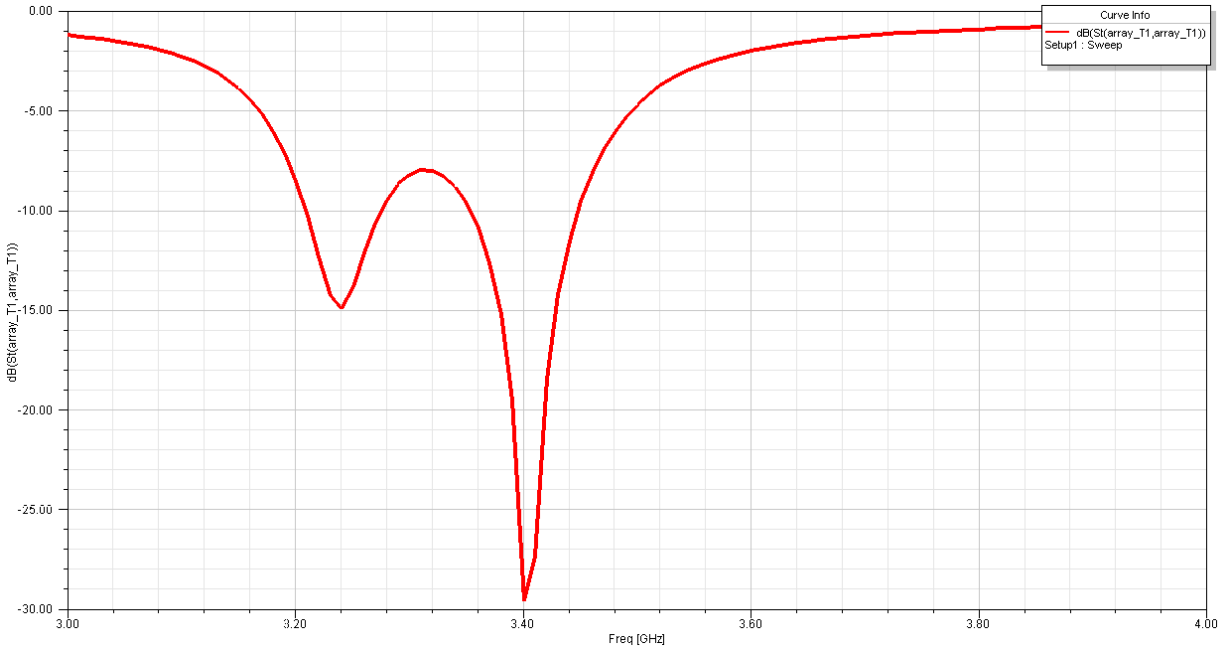

Figure 60 - Simulated S Parameter of CP Patch Array

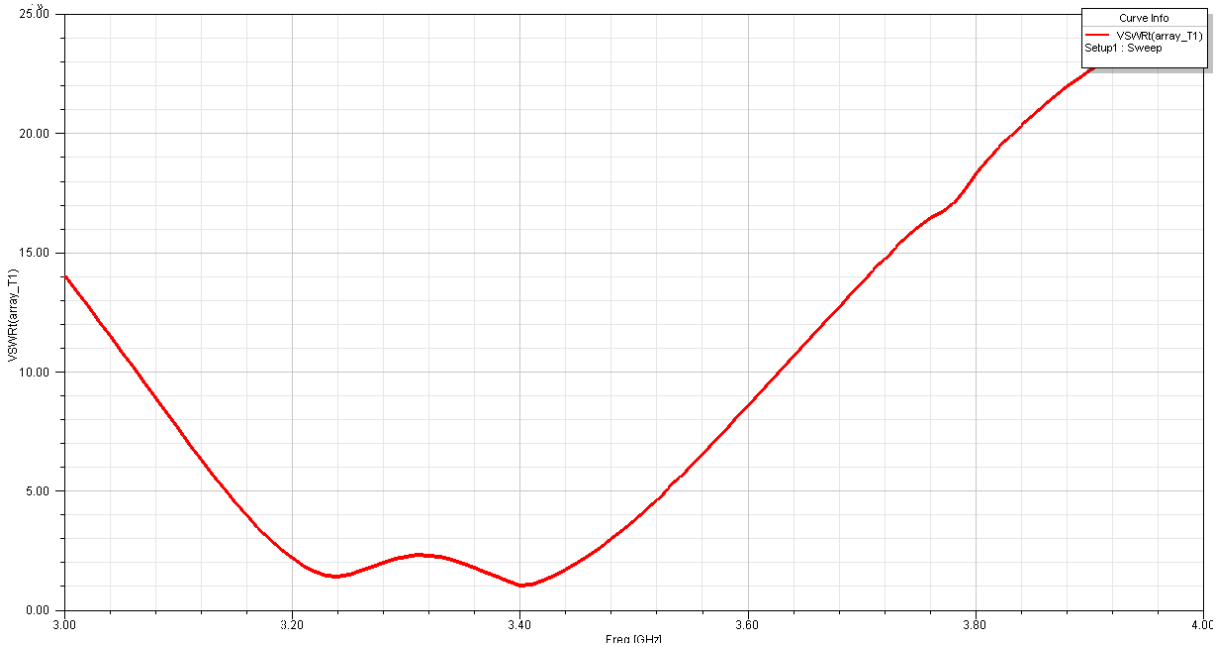

Figure 61 - Simulated VSWR of CP Patch Array

The measured impedance differs significantly from the simulated impedance. There is significant dual frequency band capability, which is interesting but unintended behaviour. This can be seen in figures 62 to 64.

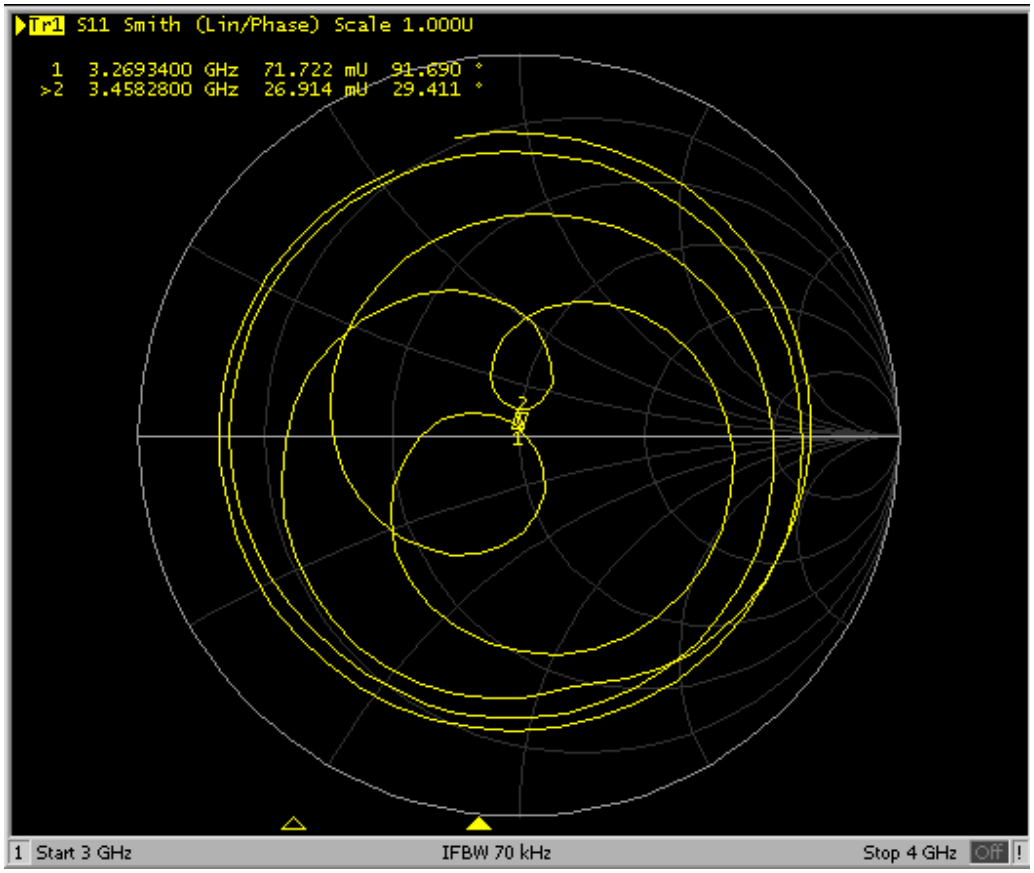

Figure 62 - Measured Smith Chart of CP Patch Array

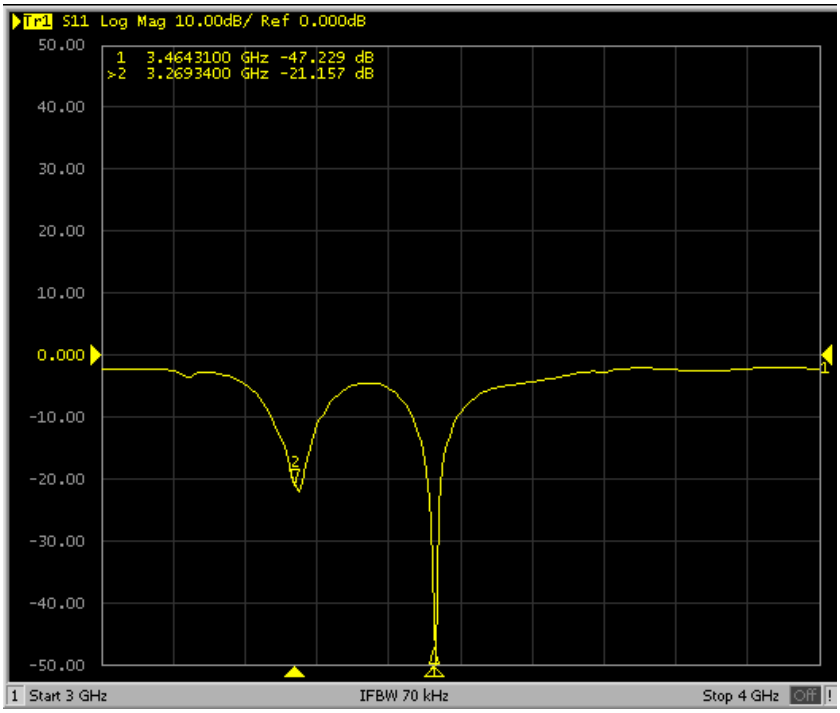

Figure 63 - Measured S Parameter of CP Patch Array

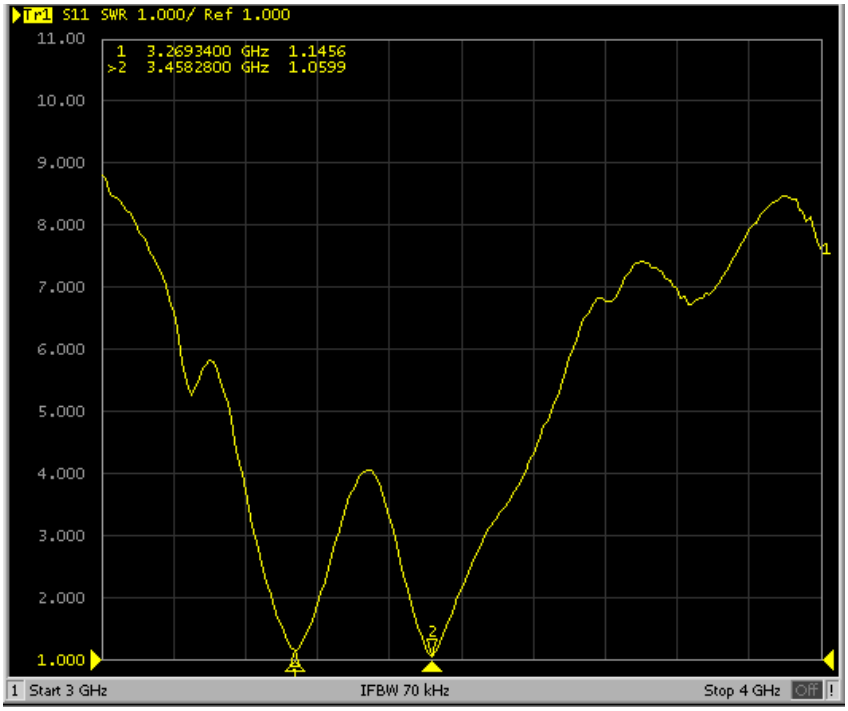

Figure 64 - Measured SWR of CP Patch Array

The radiation pattern of the antenna measured in the anechoic chamber matches the predicted shape. For LEO CubeSat application the wide beam pattern is desirable to increase the potential for long communication windows at low elevation angles. However, the deep signal fade resulting from the -19dB valley would be too extreme. This main lobe shape is suitable because when the satellite is directly overhead the slant range is low and high gain is not required to close the radio link. A similar shape with a shallower main lobe valley would be more suitable.

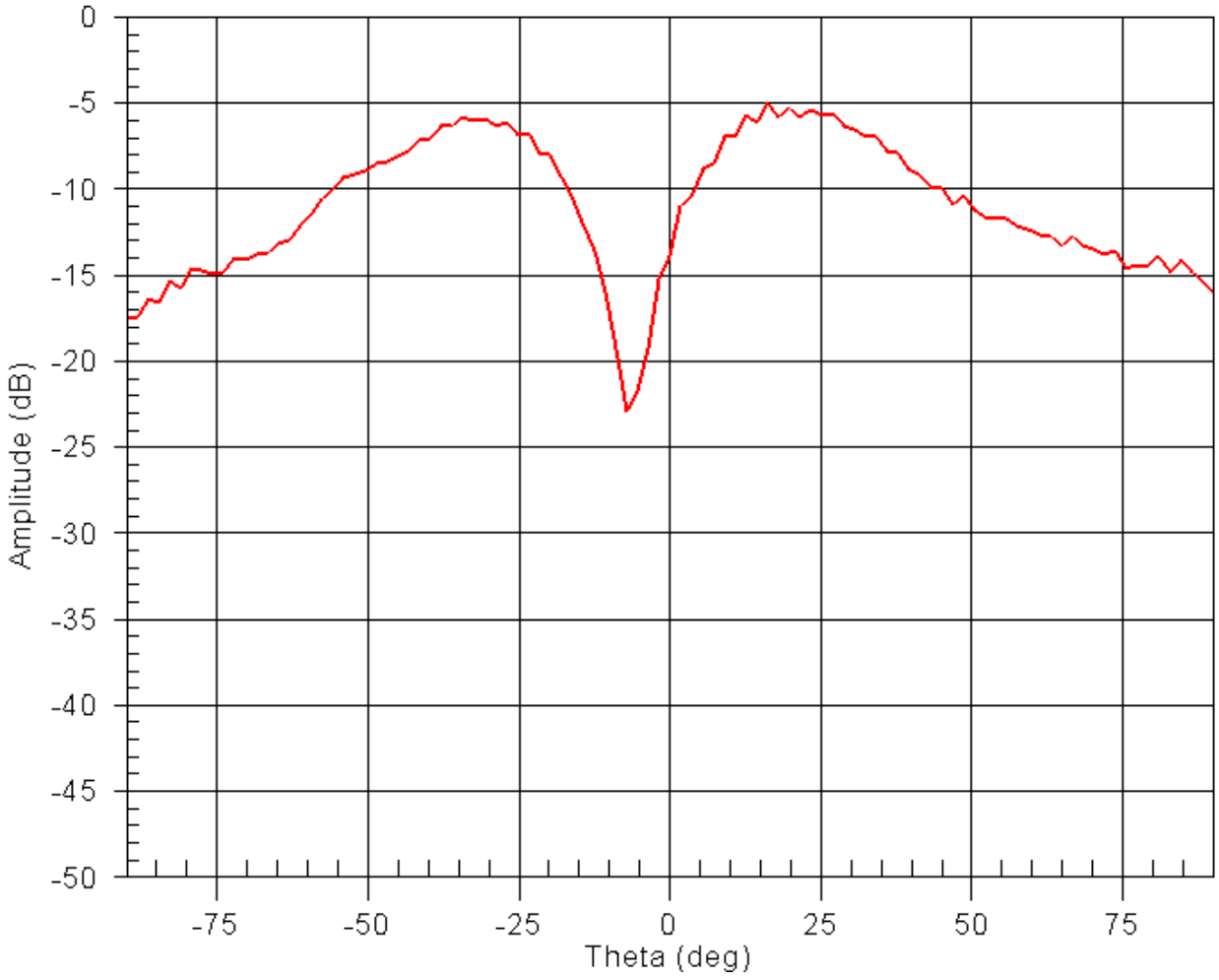

Figure 65 - Measured Radiation Pattern of CP Patch Array Theta Axis

As expected, there is no irregularity in the simulated Theta axis of the radiation pattern, here presented as the Phi axis of the anechoic chamber test measurement. The polarization loss factor has been successfully minimized using sequentially rotated feed network. The PLF was reduced from -42 dB to -3dB which is a 92% reduction.

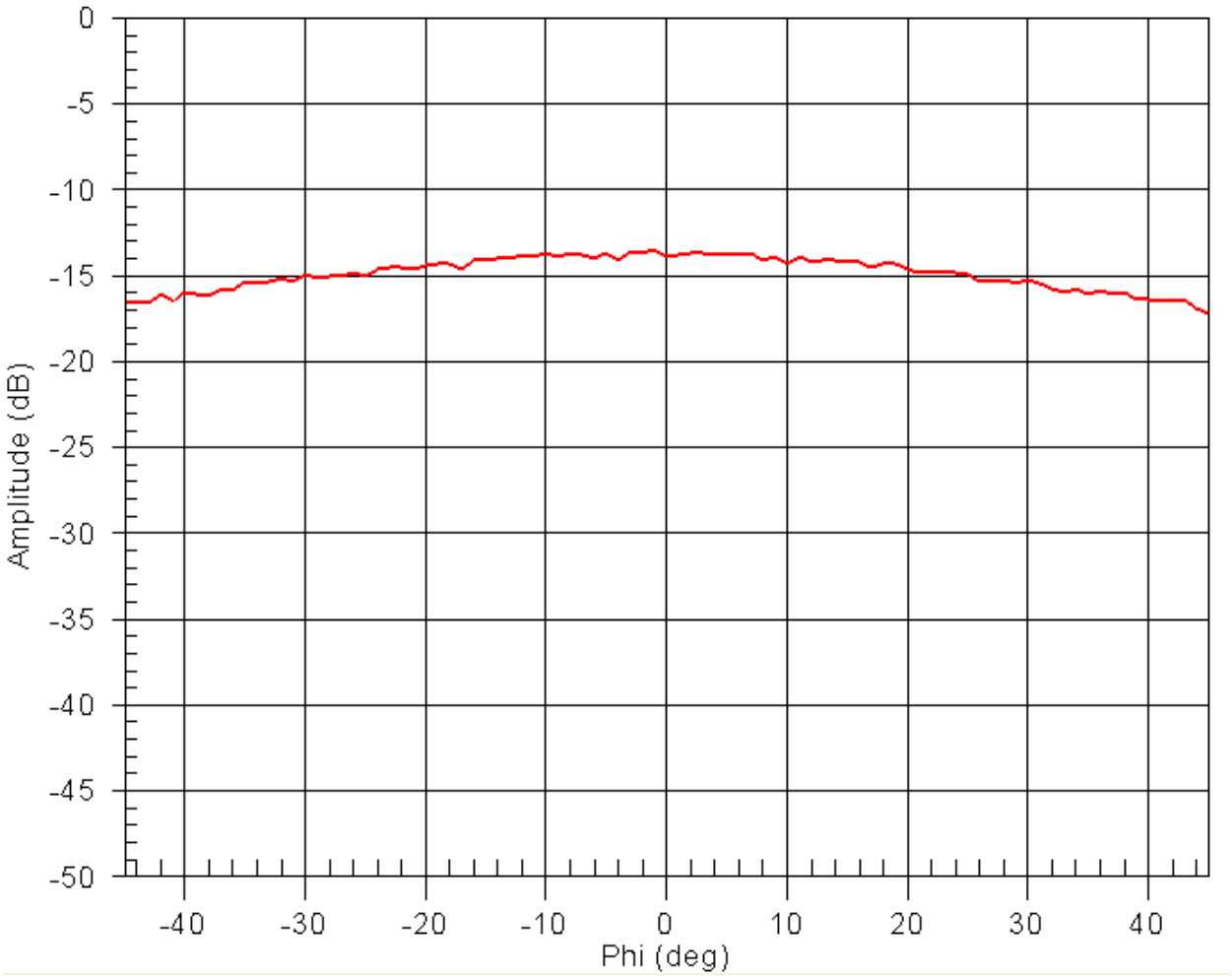

Figure 66 - Measured Radiation Pattern of CP Patch Array Phi Axis

5.7.6 Improvement of Radiation Pattern and Sequentially Rotated Feed

A novel patch antenna geometry is presented which combats PLF (polarization loss factor) using PSRF (partial sequentially rotated feed). In addition, it has wide usable bandwidth and does not require a matching network since it presents a natural characteristic impedance of 50 Ohms at the excitation port. The previous version of the SRF (Sequentially Rotated Feed) array is flawed in that it yields an impractical radiation pattern. In addition, both LHCP and RHCP senses of polarization were equally strong because the array was symmetric in geometry angle and phase shift. To alter this, we can move the array elements farther apart to reduce mutual coupling. We can also rotate the rightmost element by 180^{o} and phase shift the feed by the same amount to create a SRF array with the correct phase shift of the left and right elements [34]. This SRF technique uses a novel geometry to accomplish PLF reduction by using three phase shifts and corresponding angle shifts in the geometry. Figure 67 shows the new geometry of the improved array and the phase of each element.

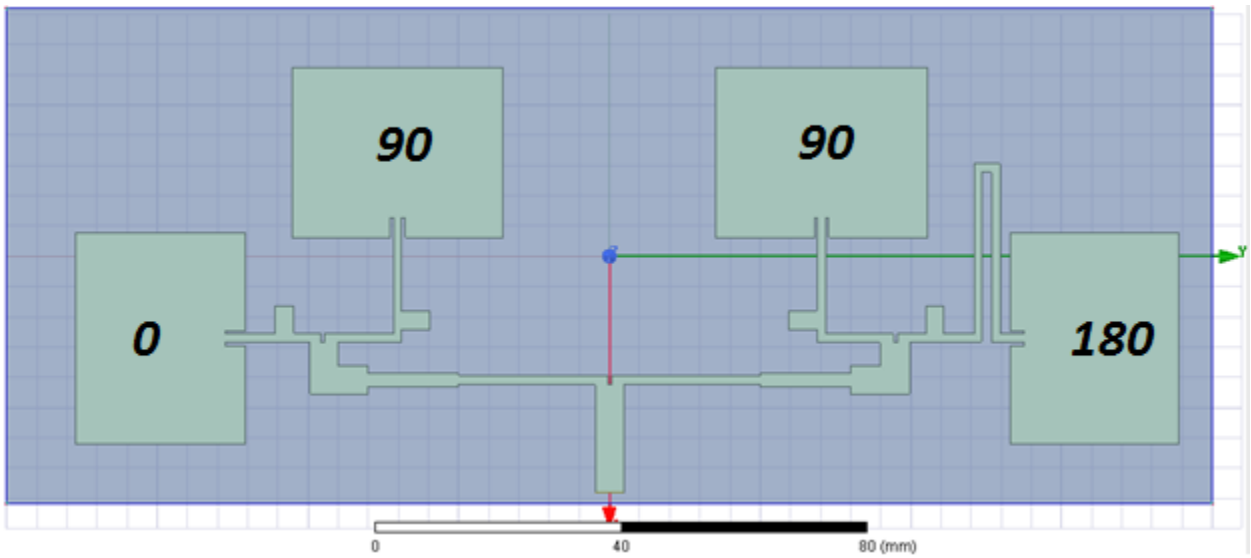

Figure 67 - Improved CP SRF Patch Array

The techniques used in this geometry are:

- Quarter wave impedance transformer
- T power splitter
- Tuning stubs
- Inset feed
- Partial Sequentially rotated feed network

This antenna is tuned to 3.405 GHz and is naturally matched to 50 Ohm impedance. Figures 68-69 show the impedance match of the antenna.

The following EAGLE script creates the geometry in a .brd (board layout) file which can then be used for fabrication.

```
GRID MM 0.01 10;
LAYER 20;
WIRE .1 (0 0) (0 74);
WIRE .1 (0 74) (190 74);
WIRE .1 (190 74) (190 0);
WIRE .1 (190 0) (0 0);
LAYER 16;
WIRE .1 (0 0) (0 74);
WIRE .1 (0 74) (190 74);
WIRE .1 (190 74) (190 0);
WIRE .1 (190 0) (0 0);
POLYGONIZE (0 0);
LAYER 1;
CHANGE WIDTH .1;
WIRE 'a'     (88.61 0)    (88.61 17.84);
WIRE 'a'     (88.61 17.84)(66 17.84);
WIRE 'a'     (66 17.84)   (66 17.365);
WIRE 'a'     (66 17.365)  (51 17.365);
WIRE 'a'     (51 17.365)  (51 16.13);
WIRE 'a'     (51 16.13)   (41.22 16.13);
WIRE 'a'     (41.22 16.13)(41.22 24.77);
WIRE 'a'     (41.22 24.77)(27.4 24.77);
WIRE 'a'     (27.4 24.77) (27.4 24.27);
WIRE 'a'     (27.4 24.27) (30.7 24.27);
WIRE 'a'     (30.7 24.27) (30.7 7.95);
WIRE 'a'     (30.7 7.95)  (2.7 7.95);
WIRE 'a'     (2.7 7.95)   (2.7 42.95);
```

```
WIRE 'a'     (2.7 42.95)  (30.7 42.95);
WIRE 'a'     (30.7 42.95) (30.7 26.63);
WIRE 'a'     (30.7 26.63) (27.4 26.63);
WIRE 'a'     (27.4 26.63) (27.4 26.13);
WIRE 'a'     (27.4 26.13) (35.5 26.13);
WIRE 'a'     (35.5 26.13) (35.5 30.68);
WIRE 'a'     (35.5 30.68) (38.5 30.68);
WIRE 'a'     (38.5 30.68) (38.5 26.13);
WIRE 'a'     (38.5 26.13) (43.2 26.13);
WIRE 'a'     (43.2 26.13) (43.2 24.77);
WIRE 'a'     (43.2 24.77) (43.8 24.77);
WIRE 'a'     (43.8 24.77) (43.8 26.13);
WIRE 'a'     (43.8 26.13) (55.14 26.13);
WIRE 'a'     (55.14 26.13)(55.14 45.43);
WIRE 'a'     (55.14 45.43)(54.64 45.43);
WIRE 'a'     (54.64 45.43)(54.64 42.13);
WIRE 'a'     (54.64 42.13)(38.32 42.13);
WIRE 'a'     (38.32 42.13)(38.32 70.13);
WIRE 'a'     (38.32 70.13)(73.32 70.13);
WIRE 'a'     (73.32 70.13)(73.32 42.13);
WIRE 'a'     (73.32 42.13)(57 42.13);
WIRE 'a'     (57 42.13)   (57 45.43);
WIRE 'a'     (57 45.43)   (56.5 45.43);
WIRE 'a'     (56.5 45.43) (56.5 29.93);
WIRE 'a'     (56.5 29.93) (61.25 29.93);
WIRE 'a'     (61.25 29.93)(61.25 26.93);
WIRE 'a'     (61.25 26.93)(56.5 26.93);
WIRE 'a'     (56.5 26.93) (56.5 24.77);
WIRE 'a'     (56.5 24.77) (46 24.77);
WIRE 'a'     (46 24.77)   (46 20.91);
WIRE 'a'     (46 20.91)   (51 20.91);
WIRE 'a'     (51 20.91)   (51 19.675);
WIRE 'a'     (51 19.675)  (66 19.675);
WIRE 'a'     (66 19.675)  (66 19.2);
WIRE 'a'     (66 19.2)    (90.7 19.2);
WIRE 'a'     (90.7 19.2)  (90.7 17.84);
WIRE 'a'     (90.7 17.84) (91.3 17.84);
WIRE 'a'     (91.3 17.84) (91.3 19.2);
WIRE 'a'     (91.3 19.2)  (116 19.2);
WIRE 'a'     (116 19.2)   (116 19.675);
WIRE 'a'     (116 19.675) (131 19.675);
WIRE 'a'     (131 19.675) (131 20.91);
WIRE 'a'     (131 20.91)  (136 20.91);
WIRE 'a'     (136 20.91)  (136 24.77);
WIRE 'a'     (136 24.77)  (125.5 24.77);
WIRE 'a'     (125.5 24.77)(125.5 26.93);
WIRE 'a'     (125.5 26.93)(120.75 26.93);
WIRE 'a'     (120.75 26.93)     (120.75 29.93);
WIRE 'a'     (120.75 29.93)     (125.5 29.93);
WIRE 'a'     (125.5 29.93)(125.5 45.43);
WIRE 'a'     (125.5 45.43)(125 45.43);
```

```
WIRE 'a'     (125 45.43)  (125 42.13);
WIRE 'a'     (125 42.13)  (108.68 42.13);
WIRE 'a'     (108.68 42.13)     (108.68 70.13);
WIRE 'a'     (108.68 70.13)     (143.68 70.13);
WIRE 'a'     (143.68 70.13)     (143.68 42.13);
WIRE 'a'     (143.68 42.13)     (127.36 42.13);
WIRE 'a'     (127.36 42.13)     (127.36 42.13);
WIRE 'a'     (127.36 42.13)     (127.36 45.43);
WIRE 'a'     (127.36 45.43)     (126.86 45.43);
WIRE 'a'     (126.86 45.43)     (126.86 26.13);
WIRE 'a'     (126.86 26.13)     (138.2 26.13);
WIRE 'a'     (138.2 26.13)(138.2 24.77);
WIRE 'a'     (138.2 24.77)(138.8 24.77);
WIRE 'a'     (138.8 24.77)(138.8 26.13);
WIRE 'a'     (138.8 26.13)(143.5 26.13);
WIRE 'a'     (143.5 26.13)(143.5 30.68);
WIRE 'a'     (143.5 30.68)(146.5 30.68);
WIRE 'a'     (146.5 30.68)(146.5 26.13);
WIRE 'a'     (146.5 26.13)(151.5 26.13);
WIRE 'a'     (151.5 26.13)(151.5 54.27);
WIRE 'a'     (151.5 54.27)(155.86 54.27);
WIRE 'a'     (155.86 54.27)     (155.86 26.13);
WIRE 'a'     (155.86 26.13)     (160.8 26.13);
WIRE 'a'     (160.8 26.13)(160.8 26.63);
WIRE 'a'     (160.8 26.63)(157.5 26.63);
WIRE 'a'     (157.5 26.63)(157.5 42.95);
WIRE 'a'     (157.5 42.95)(185.5 42.95);
WIRE 'a'     (185.5 42.95)(185.5 7.95);
WIRE 'a'     (185.5 7.95) (157.5 7.95);
WIRE 'a'     (157.5 7.95) (157.5 24.27);
WIRE 'a'     (157.5 24.27)(160.8 24.27);
WIRE 'a'     (160.8 24.27)(160.8 24.77);
WIRE 'a'     (160.8 24.77)(154.5 24.77);
WIRE 'a'     (154.5 24.77)(154.5 52.91);
WIRE 'a'     (154.5 52.91)(152.86 52.91);
WIRE 'a'     (152.86 52.91)     (152.86 24.77);
WIRE 'a'     (152.86 24.77)     (140.78 24.77);
WIRE 'a'     (140.78 24.77)     (140.78 16.13);
WIRE 'a'     (140.78 16.13)     (131 16.13);
WIRE 'a'     (131 16.13)  (131 17.365);
WIRE 'a'     (131 17.365) (116 17.365);
WIRE 'a'     (116 17.365) (116 17.84);
WIRE 'a'     (116 17.84)  (93.39 17.84);
WIRE 'a'     (93.39 17.84)(93.39 0);
WIRE 'a'     (93.39 0)    (88.61 0);
POLYGONIZE (93.39 17.84);
RATSNEST;
```

The simulated Smith chart from 3.15 GHz to 3.5 GHz shows that there will be resonance around 3.2 and 3.4 GHz. The dual band behaviour is captured by the simulation.

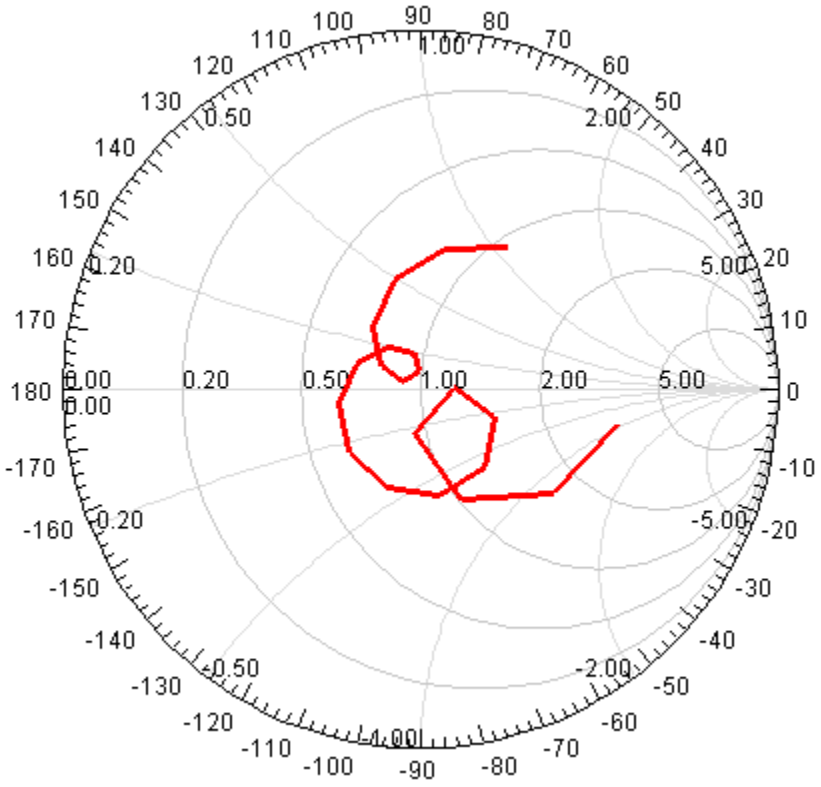

Figure 68 – Simulated S11 Parameter Smith chart of CP SRF Patch Array

This is an accomplishment in terms of wide band performance. The simulated VSWR shows the antenna is best used at 3.22 and 3.4 GHz, and with additional work this aspect could be improved.

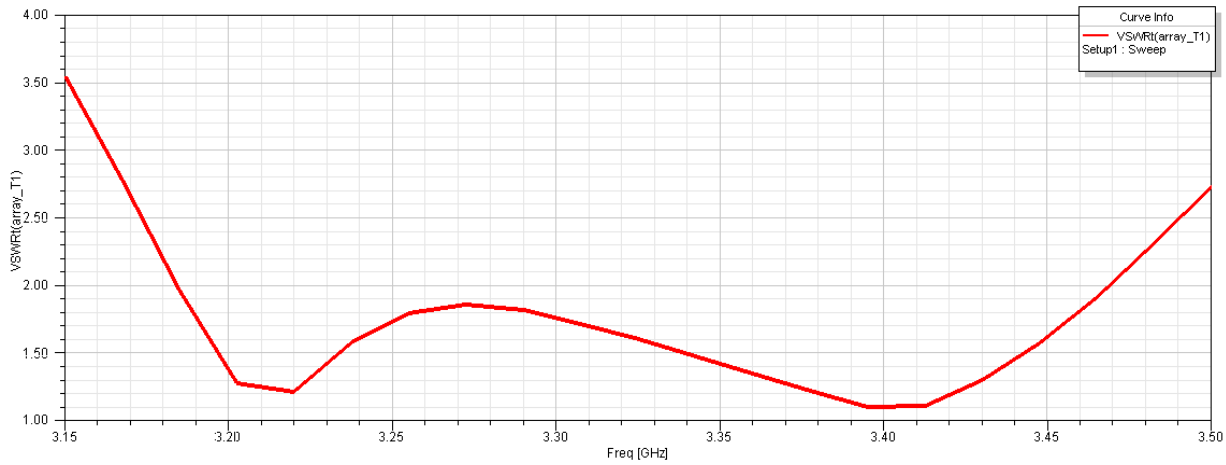

Figure 69 – Simulated VSWR of CP SRF Patch Array

The corrections to the antenna improve the radiation pattern. There is one main lobe of 9.9dB gain as shown in Figure 70 which shows the simulated radiation pattern. The peak gain is nearly 10dB, which is comparable to the linear 4 element array with a -2dB change.

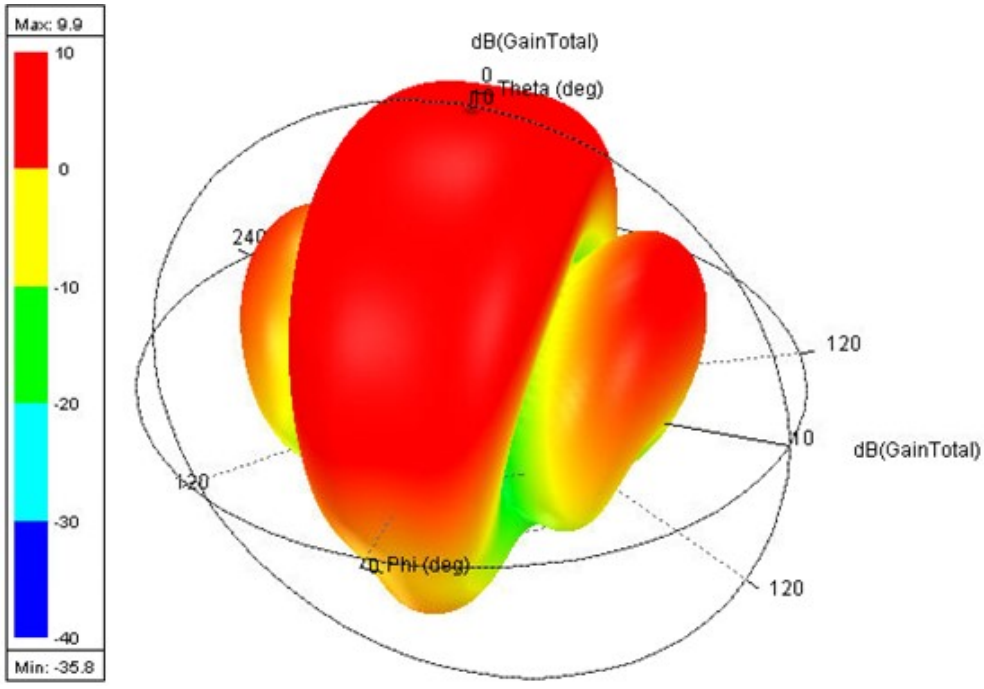

Figure 700 - Simulated Radiation Pattern of CP SRF Patch Array, Isotropic View

With this design the LHCP pattern has peak gain diminished by 2.1 dB. The simulated results are shown in Figure 717. In addition, Figure 72 shows the general gain characteristics in a 2D rectangular plot.

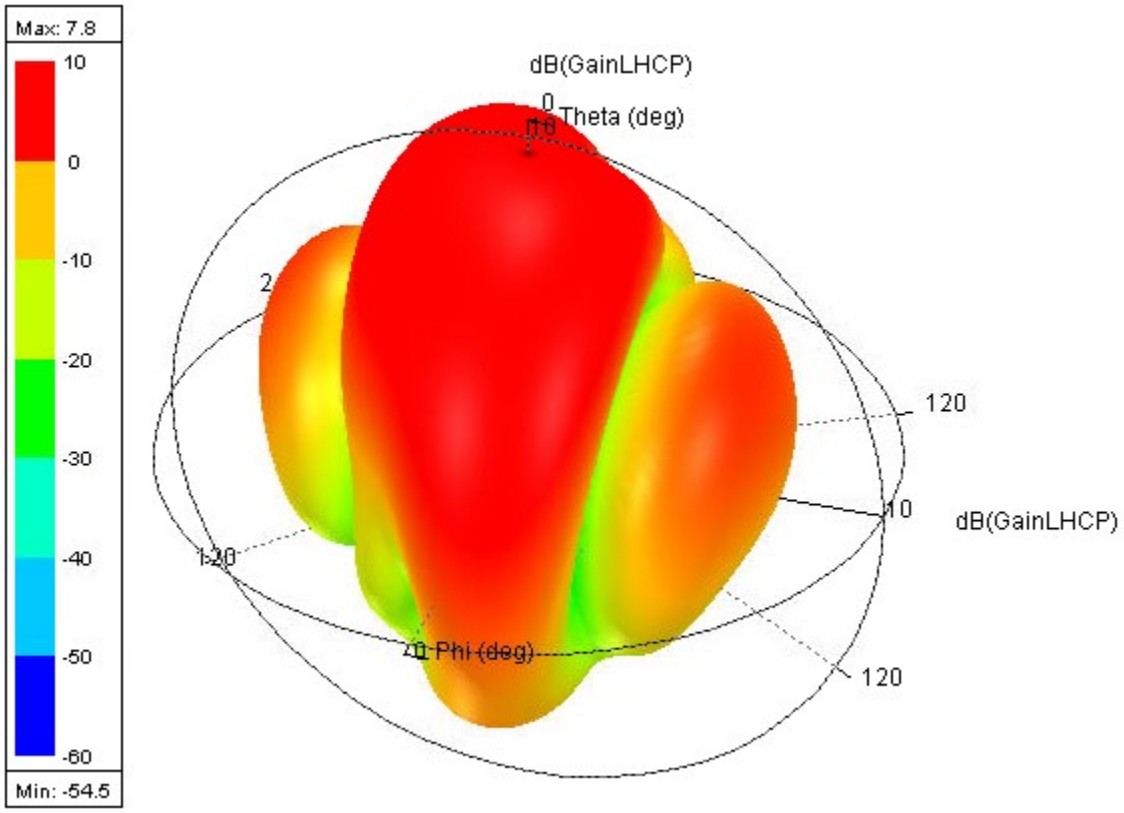

Figure 71 - Simulated LHCP Radiation Pattern of CP SRF Patch Array

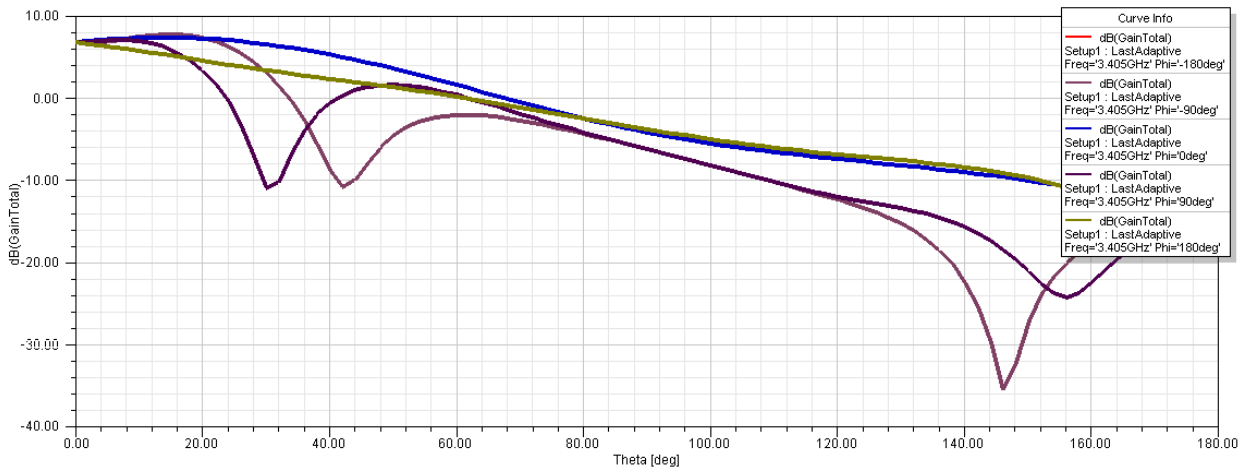

Figure 72 – Simulated Gain Pattern Summary for CP SRF Patch Array

The measured impedance shows that there is good resonance at 3.239 GHz and 3.454 GHz.

There is similarity in the predicted vs actual shape in that the actual appears rotated 90 degrees.

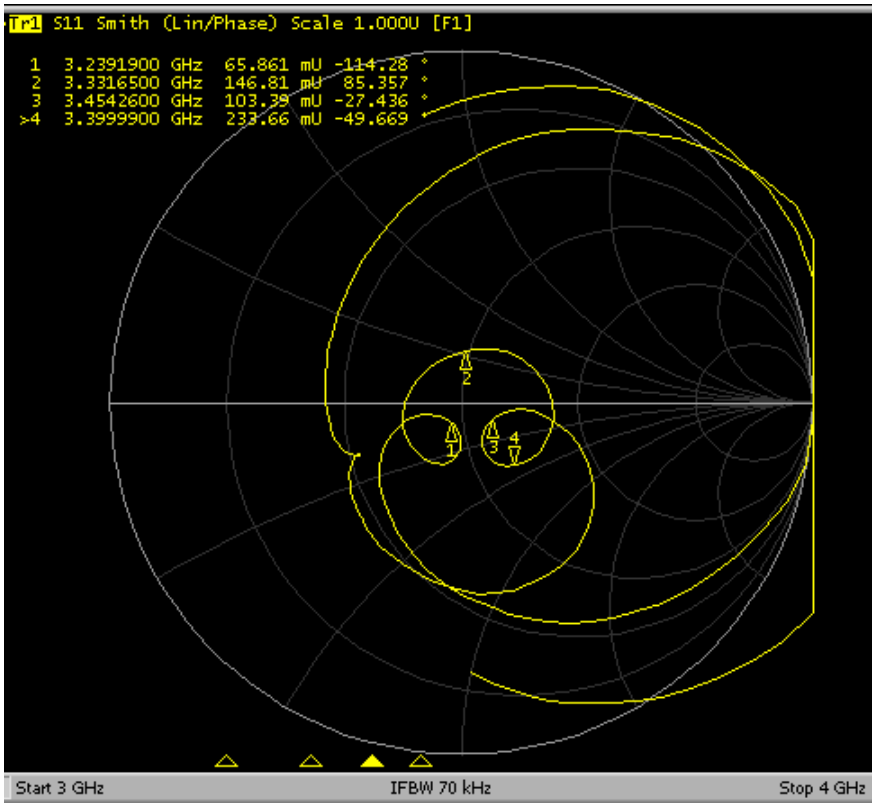

Figure 73 - Measured Smith Chart showing the impedance of the SRF patch array

The actual measured VSWR agrees in that there is a wide band under SWR of 2.

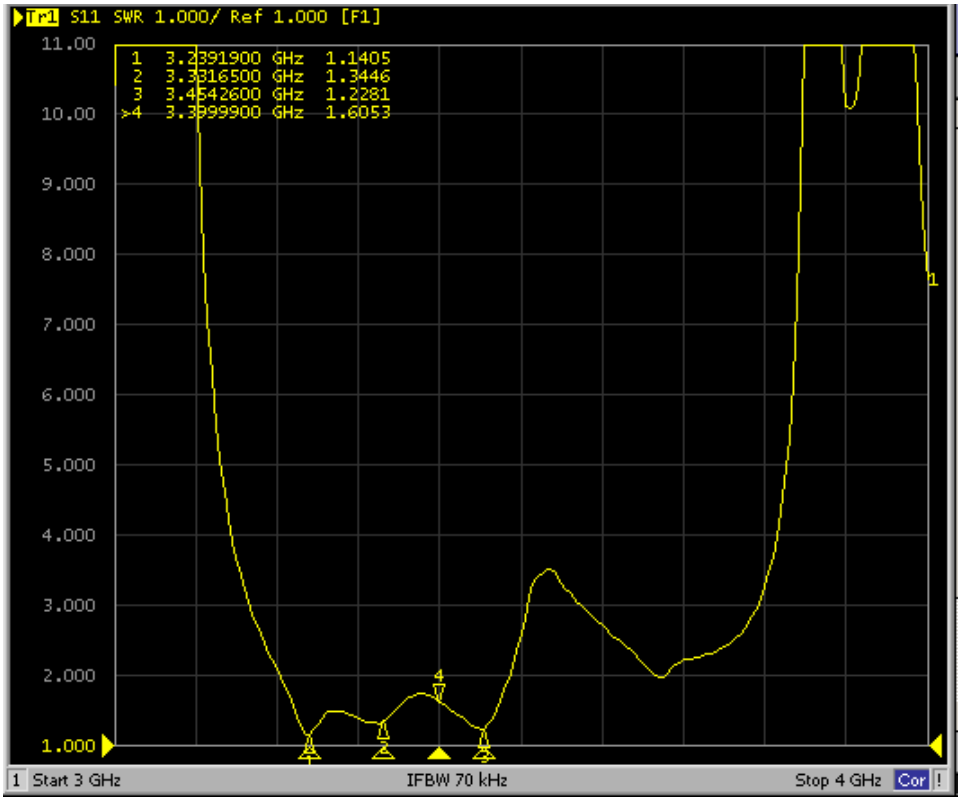

Figure 74 - Wide band performance of SRF patch array show by measured VSWR plot

Testing at 3.2 GHz in the anechoic chamber we can see that the overall radiation pattern has lots of variation in the range of -15 to -3 dB. However, the useful beam width is as wide as that of a single patch. We can say that the wideband behaviour comes at a cost of lower gain, while beam width is preserved. In addition, we see that fading due to cross polarization is greatly reduced compared to the linear antenna. For reference with the linear antenna the data shows fades around -45 dB. Here we see a fade of -12 dB. Thus, the PLF is reduced by 70%.

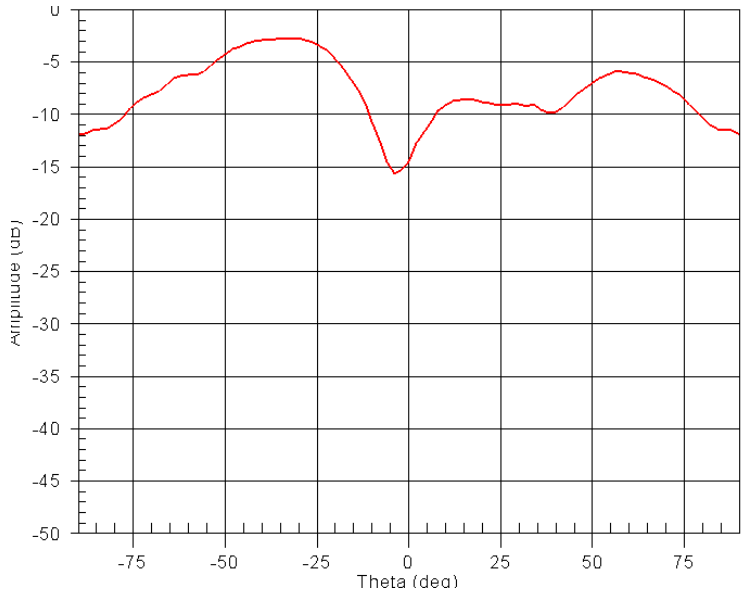

Figure 75 - Horizontal cross section of the SRF array's radiation pattern, showing signal amplitude along the theta axis of rotation. Test results are from 3.2 GHz measurement.

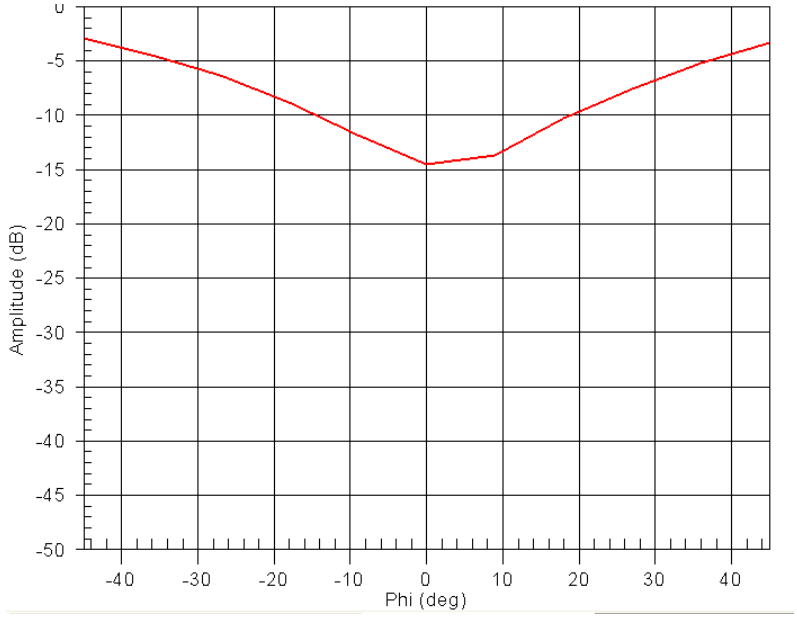

Figure 76 - Signal amplitude along Phi axis rotation. Test Results are from 3.2 GHz measurement.

Testing at 3.4 GHz in the anechoic chamber we can see that the overall radiation pattern has a useful main lobe and two side lobes. The power output appears unleveled and the

instrumentation needs re-calibration in between tests. The signal amplitude suddenly drops -3dB at 24 degrees and remains lower for the rest of the right side.

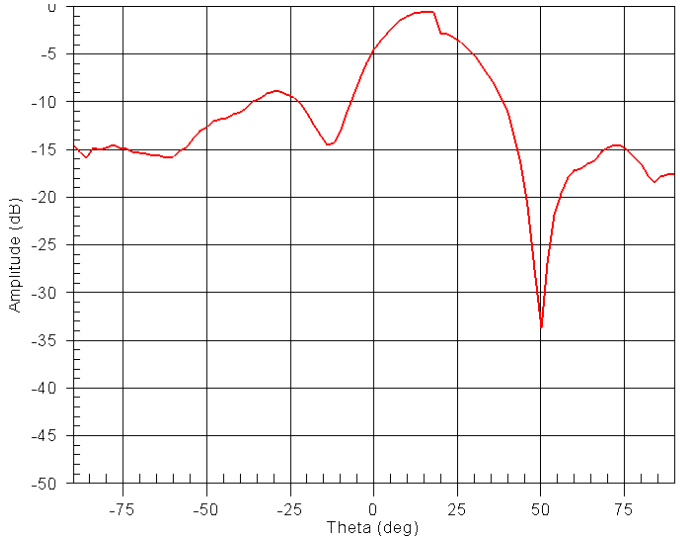

Figure 77 - Horizontal cut at 3.4 GHz

However, the PLF is once again reduced greatly. As the antenna rotates around the Phi Axis there is only -8dB loss. The Polarization Loss Factor is reduced by 81%.

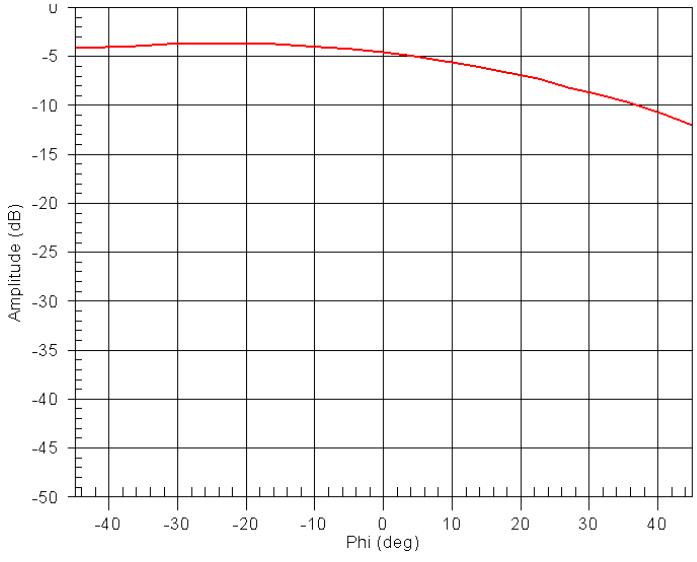

Figure 78 - Vertical cut at 3.4 GHz

Overall, the partial sequentially rotated feed successfully reduces the polarization loss factor. The antenna requires additional tuning to achieve higher performance at the target frequency. Wide band performance is another feature that this geometry can accomplish. Most CubeSats will use bandwidth under 500 KHz, so wide banding is not necessary if a good impedance match at the target frequency can be achieved. Achieving a more uniform radiation pattern is also desirable. The anechoic chamber also gives a live report of SNR while the equipment is on. With this feature we can take measurements manually by changing the frequency and position of the Phi and Theta axes.

Frequency (GHz)	Amplitude at Phi 0 Degrees (dB)	Amplitude at Phi 90 Degrees (dB)
3.2	44	44
3.36	37	37
3.4	35	40
3.45	42	24

Table 6 - Live SNR read outs with the SRF Patch Array under test

Table 6 shown above demonstrates that partial sequentially rotated feed can reduce polarization loss factor by as much as 100% based on readings from the anechoic chamber.

5.8 Novelty of Design

To see how novel this design is I checked for similar published designs using keyword search on IEEExplore and through Dalhousie's Novanet key word search bar. Using terms such as "rectangular patch antenna array" I was able to find designs using similar techniques. Five publications using related geometry or techniques were found in [32], [33], [34], [35], [36], but in over 300 search results there was no antenna design using partial sequentially rotated feed

(using 180º of rotation as opposed to a full 270º rotation in 4 elements). In addition, no published complete design was found for S band patch antenna array CubeSat S band communications.

5.9 Tuning

Further improvements to the antenna geometry are possible. Small alterations less than 1 mm can have a dramatic impact on the impedance and radiation pattern. For example, by making these changes:

- increasing patch length from 28 to 28.1mm
- decreasing stub thickness to 2.25mm
- increasing stub height to 6mm

the characteristic impedance of the antenna at 3.4 GHz can be brought closer to 50 Ohms. See Figure 79 for the smith chart and compare to figure 68 to see the effect of tuning. Still further small adjustments could continue to improve the antenna performance while utilizing the same fundamental geometry and techniques.

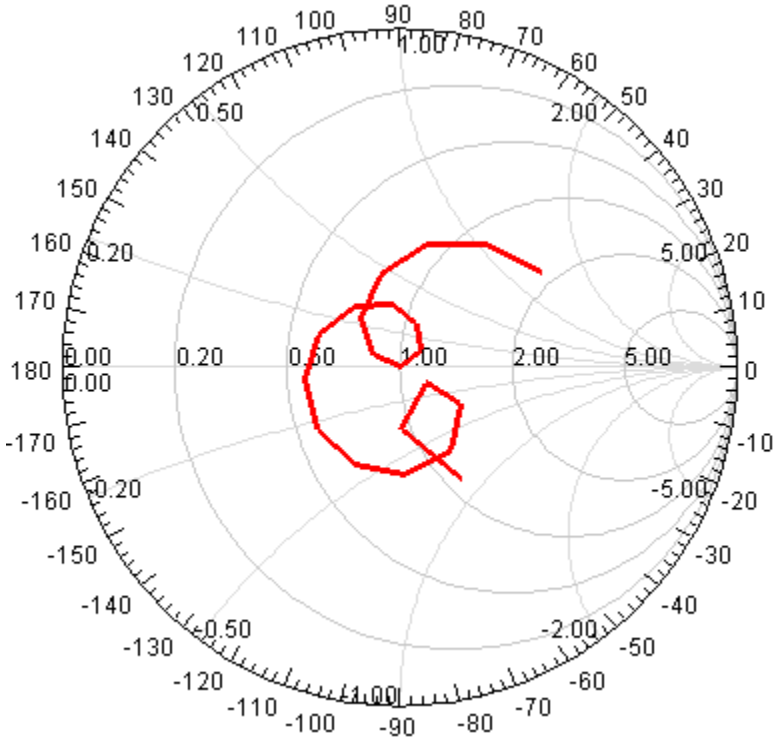

Figure 79 - Smith chart showing the results of tuning the antenna geometry

Chapter 6.0 Conclusion

Small satellites such as CubeSats provide a distinct advantage of low cost over their larger counterparts. They are becoming a popular platform for technological demonstrations and low earth orbit scientific research. Many CubeSats have used low date rate radio systems using UHF or VHF amateur satellite service. To help enable future small satellite designers this thesis has examined the challenges of high data rate CubeSat communication. Individual ground stations have limited LOS access to an individual satellite in LEO orbit approximately 1-2 hours per day. In addition, the orbital motion of the satellite introduces time varying doppler shift and slant range. The varying range between radio transceivers creates a time varying channel capacity. In order to utilize the channel efficiently a dynamic MCS is required. For a single CubeSat and single ground station the channel capacity is an average 2.61 bits/s per Hz. User congestion in sub-GHz bands is a real concern and acquiring wide bandwidth can be difficult and is unlikely. An S-band radio link could provide the additional bandwidth needed for high data rate communications, so an S-band transceiver was identified, and S-band patch antennas were presented. Due to the small size of the CubeSat and the low budget of the LORIS project, achieving a robust and high capacity radio system presents a design challenge. Low cost consumer grade S-band transceivers are not very common but several SDR products are available based on the AD9364 radio front end from Analog Devices. This type of direct conversion architecture radio could be leveraged for high performance in S band systems. Traditional super-heterodyning radios offer less flexibility but fit the requirements of the LORIS project better. Towards a high-performance S band radio link, the CubeSat antenna design is examined to provide a component with appropriate size, shape and performance for the application. It is found that the rectangular patch antenna is an excellent candidate. The design

software HFSS was used to simulate by finite element method several patch antenna geometries, some of which were fabricated and tested in anechoic chamber. It was found that an array of 4 elements in a partial sequentially rotated feed network can achieve peak directivity of 9.9 dB with a beam width of 50^{o}. The partial SRF technique reduces the polarization loss factor by introducing circular polarization to the RF waves. The anechoic chamber measurements show that the antenna geometry successfully reduced PLF by 70% to 90%.

In conclusion there are two main results which contribute toward high data rate CubeSat communications. Firstly, analysis of the orbital motion and the effect on channel capacity shows that channel capacity varies significantly in time. To utilize it efficiently a dynamic modulation coding scheme must be employed. Using just one modulation scheme and FEC encoding rate will always under utilize either the channel or the communication window. Secondly, several rectangular patch array designs are presented which could be mounted on the underside of a deployable CubeSat panel. They use a single layer of copper clad laminate and thus are very thin at only 1.575 mm. By using a sequentially rotated feed network, the array generates circular polarization and achieves immunity to polarization loss. Compared to measurements from a single linear patch antenna the partial SRF technique reduces PLF by 70-90%.

References

[1] H. Kramer, "OPAL (Orbiting Picosatellite Automatic Launcher)," *eoportal.org,* 2002. [Online]. Available: https://directory.eoportal.org/web/eoportal/satellite-missions/o/opal . [Accessed: October 24, 2019]

[2] M.A. Startwout, "CubeSat Database," *sites.google.com*, April 2019. [Online]. Available: https://sites.google.com/a/slu.edu/swartwout/home/cubesat-database . [Accessed: October 24, 2019].

[3] Author Unknown, "Developer Resources," *cubesat.org*, April 2015. [Online]. Available: http://www.cubesat.org/resources/ . [Accessed: October 24, 2019].

[4] NanoRacks, "Documents", nanoracks.com, Date unknown. [Online]. Available: http://nanoracks.com/resources/documents/ . [Accessed: October 24, 2019]

[5] J. Bouwmeester, J. Guo, "Survey of worldwide pico- and nanosatellite missions, distributions and subsystem technology," Acta Astronautica 67 (2010) 854-862

[6] Daniel Selva, David Krejci, "A Survey and assessment of the capabilities of Cubesats for Earth observation," Acta Astronautica 74 (2012) 50-68.

[7] Holli Riebeek, "Catalog of Earth Satellite Orbits," *nasa.gov*. Sept. 4 2009. [Online]. Available: https://earthobservatory.nasa.gov/features/OrbitsCatalog . [Accessed: October 24, 2019].

[8] National Geospatial-Intelligence Agency, "World Geodetic System 1984 (WGS 84)," *nga.mil*, Oct 18 2019. [Online]. Available: http://earth-info.nga.mil/GandG/update/index.php?dir=wgs84&action=wgs84 . [Accessed: October 24, 2019].

[9] C. Evans and J. Robinson, "Earth Sciences and Image Analysis," *nasa.gov*, date unknown. [Online]. Available: https://eol.jsc.nasa.gov/Tools/orbitTutorial.htm . [Accessed: October 24, 2019].

[10] R. Freeman, *Radio System Design for Telecommunications*, 3rd ed. Hoboken, New Jersey: John Wiley & Sons Inc., 2007. p. 308, 555, 5

[11] O. Breinbjerg, K. Kaslis, "On the accuracy of Friis' transmission formula at close range," In Proc. 2017 XXXIInd General Assembly and Scientific Symposium of the International Union of Radio Science (URSI GASS). 13 Nov. 2017. Available: https://ieeexplore.ieee.org/document/8105036 . [Accessed: October 24, 2019].

[12] SpaceX, "Starlink Mission: Mission Overview," May 2019. [Online]. Available: https://www.spacex.com/sites/spacex/files/starlink_mission_press_kit.pdf . [Accessed: October 24, 2019].

[13] D. Tse, P. Viswanath, *Fundamentals of Wireless Communication*. New York, New York, Cambridge University Press, 2005.

[14] Tektronix, "Wifi: Overview of the 802.11 Physical Layer and Transmitter Measurements," 2013. [Online]. Available: https://www.cnrood.com/en/media/solutions/Wi-Fi_Overview_of_the_802.11_Physical_Layer.pdf . [Accessed: October 24, 2019]

[15] Unknown Author, "CubeSat Litsat-1 First Lithuanian Space Mission," Date unknown. [Online]. Available: http://www.litsat1.eu/en/litsat-1-technical-overview/satellite-structural-scheme/ . [Accessed: October 24, 2019]

[16] International Telecommunication Union, "Article 22," *International Telecommunication Union*, ITU-R-REG-RR. [Online]. Available: https://www.itu.int/pub/R-REG-RR . [Accessed: October 24, 2019].

[17] A. Hutputtanasin, A. Toorian, "CubeSat Design Specification, Revision 9" May 2005. [Online]. Available: http://org.ntnu.no/studsat/docs/proposal_1/A8%20-%20Cubesat%20Design%20Specification.pdf . [Accessed: October 24, 2019].

[19] A. Gharagozli, "The LORIS Project – 2021," 2019. [Online]. Available: https://dalorbits.ca/index.php/2019/07/01/loris-2021/ . [Accessed: October 24, 2019]

[20] C. DeMartino, "Differences Between Receiver Types Part 1," Feb 23, 2016. [Online]. Available: https://www.mwrf.com/systems/differences-between-receiver-types-part-1 [Accessed: October 24, 2019].

[22] Texas Instruments, "Signal Chain Noise Figure Analysis," October 2014. [Online]. Available: https://www.ti.com/lit/an/slaa652/slaa652.pdf . [Accessed: October 24, 2019]

[23] National Instruments, "Super-Heterodyne Signal Analyzers: Descriptions and Applications," date unknown. [Online]. Available: http://download.ni.com/evaluation/rf/Super_Heterodyne_Signal_Analyzers.pdf [Accessed: October 24, 2019]

[24] G. Thiele, "Analysis of Yagi-Uda-type antennas," IEEE *Transactions on Antennas and Propagation,* Vol. 6, Issue 1, January 1969. Available: https://ieeexplore.ieee.org/abstract/document/1139356 [Accessed: October 24, 2019]

[25] B. Rulf, G. Robertshaw, *Understanding Antennas for Radar, Communications, and Avionics*. Springer Netherlands, Van Nostrand Reinhold Company Inc. 1987. p. 255, 13

[26] Author Unknown, "Antenna Introduction/Basics," date unknown. [Online]. Available: https://www.phys.hawaii.edu/~anita/new/papers/militaryHandbook/antennas.pdf [Accessed: October 24, 2019]

[27] Author Unknown, "VSWR (Voltage Standing Wave Ratio)," date unknown. [Online]. Available: http://www.antenna-theory.com/definitions/vswr.php [Accessed: October 24, 2019]

[28] R. Garg … [et al.], *Microstrip Antenna Design Handbook*. Artech House Inc. 2001. p. 266, 279-287

[29] M. Steer, *Microwave and RF Design: A Systems Approach, 2nd Ed.* Scitech Publishing, 2013.

[30] Rogers Corporation, "Width and Effective Dielectric Constant Data for Design of Microstrip Transmission Lines on Various Thicknesses, Types, and Claddings of TMM® Microwave Laminates". [Online]. Available: https://www.rogerscorp.com/-/media/project/rogerscorp/documents/advanced-connectivity-solutions/english/electrical-design-data/design-data-for-microstrip-transmission-lines-on-rt-duroid-laminates.pdf [Accessed: October 24, 2019]

[31] Rogers Corporation, "RT/duroid® 5870/5880 High Frequency Laminates," [Online]. Available: https://www.rogerscorp.com/acs/products/31/RT-duroid-5870-Laminates.aspx [Accessed: October 24, 2019]

[32] J. Jeong, Y. Kim, Y. Yoon, "Polarization tunable microstrip patch antenna for polarization loss compensation," In Proc. *2014 International Symposium on Antennas and Propagation Conference Proceedings*. Available: https://ieeexplore.ieee.org/document/7026660

[33] A. Efanov, H. Thim, "Corporate-fed 2/spl times/2 planar microstrip patch sub-array for the 35 GHz band," IEEE Antennas and Propagation Magazine, vol. 37, issue 5, Oct 1995. Available: https://ieeexplore.ieee.org/document/475865

[34] J. Huang, W. Lin, F. Qiu … [et al.], "A Low Profile, Ultra-Lightweight, High Efficient Circularly-Polarized Antenna Array for Ku Band Satellite Applications," IEEE Access, vol. 5, September 2017. Available: https://ieeexplore.ieee.org/document/8030059

[35] Z. Muludi, B Aswoyo, "Truncated microstrip square patch array antenna 2 × 2 elements with circular polarization for S-band microwave frequency," 2017 International Electronics Symposium on Engineering Technology and Applications (IES-ETA), December 2017. Available: https://ieeexplore.ieee.org/document/8240384

[36] J. Huang, "A technique for an array to generate circular polarization with linearly polarized elements," IEEE Transactions on Antennas and Propagation, vol. 34, issue 9, Sep 1986. Available: https://ieeexplore.ieee.org/document/1143953